GEOLOGICAL SURVEY OF CANADA

OPEN FILE 3514

Gravity and magnetic prospecting for massive sulphide deposits: a short course sponsored under the Bathurst Mining Camp EXTECH II Initiative

M.D. Thomas

1997

Natural Resources Canada | Ressources naturelles Canada

Canada

Geological Survey of Canada
Commission géologique du Canada

New Brunswick Department of Natural Resources and Energy

New Nouveau Brunswick

Contribution to 1994-1999 Bathurst Mining Camp, Canada-New Brunswick Exploration Science and Technology (EXTECH II).

Contribution aux Mesures Canada-Nouveau-Brunswick relatives au Programme de la science et de la technologie de l'exploration (EXTECH II) dans le camp minier de Bathurst (1994-1999).

TABLE OF CONTENTS

PREFACE

This set of notes results from a short course on the subject of gravity and magnetic prospecting for massive sulphide deposits presented at the Atlantic Geoscience Society Colloquium in Bathurst, New Brunswick, February 2nd 1996. The course, together with complementary courses on the electromagnetic and radiometric methods, was initiated in response to a major detailed airborne geophysical survey of the Bathurst mining camp, completed in 1995. Initial results of the survey were released in July, 1996. The survey was conducted as part of the EXTECH II program, a multidisciplinary initiative aimed at furthering the search for massive sulphides in the camp. The program is funded by the Canadian and New Brunswick governments and involves the participation of personnel from government, industry and academia. The short course was sponsored by EXTECH II.

Formatting a short course, on any subject, requires that a balance be maintained between the amount and detail of material presented and the length of the course. Too much detail may result in a report that is too voluminous, possibly discouraging a reader whose principal interest lies in other areas of geoscience. On the other hand, an incentive to seek a deeper understanding may not materialize if there is too little detail. Hopefully, this set of notes has achieved the right balance, providing a non-specialist with enough insight and confidence to extract meaningful information from gravity and magnetic maps, and to be aware of their advantages and limitations. The notes include an overview of the gravity and magnetic techniques in general, and a more specific examination of their roles in massive sulphide exploration. The interested reader may obtain additional knowledge from the many excellent text books, manuals and papers on the subject. Suggestions for further reading are provided.

Every effort has been made to ensure that the information presented herein is accurate. If any errors or inconsistencies come to light, the author would be grateful if these were brought to his attention.

M.D. Thomas
Geological Survey of Canada, 3 Observatory Crescent, Ottawa, Ontario K1A 0Y3

Phone: 613-995-5582
Email: mthomas@gsc.nrcan.gc.ca

INTRODUCTION

The Earth's gravity and magnetic fields are described as potential fields. Mathematically, they are expressed by a single function, the scalar potential, differentiation of which yields a vector quantity having magnitude and direction. Such vectors represent the gravitational or magnetic field strength (also called the force) at any point in space, arising from a system of bodies or magnetic poles (representing magnetizations), respectively. Generally, relatively short wavelength variations of both the gravity and magnetic fields are controlled by changes in rock properties residing in the upper part of the Earth's crust. Density is the critical physical property influencing the gravity field, and magnetic susceptibility and natural remanent magnetization (NRM) control the magnetic field. Sulphide bodies have physical properties that usually contrast sharply with those of host rocks. They can, therefore, exert considerable influence on the Earth's gravity and magnetic fields, thereby generating significant geophysical anomalies, which are prime targets for exploration. In favourable circumstances, such as where the bodies are close to the surface, of sizable dimensions and in a relatively homogeneous geological setting, such anomalies should be easily recognizable. Hence, geophysical surveys rank highly in most exploration strategies. Gravity and magnetic surveys can contribute to exploration programs in two principal ways. They can be applied in a focussed manner to the direct discovery of mineral deposits, and they can be used in a broader context to map geology and structure that may favour the presence of ore deposits. Before examining the role of gravity and magnetic investigations in mineral exploration, a general overview of the two disciplines is presented.

UTILITY OF GRAVITY AND MAGNETIC DATA

Gravity and magnetic data contribute to geoscientific studies in two principal ways. They provide a means of mapping geology and they can be modelled quantitatively to yield information on the shape, size and depth of geological bodies.

Mapping Application

When gravity or magnetic data are collected over a region of the Earth's surface, they define the respective potential field in that area, irregularities of which, known as anomalies, are related to geological causes. Trends of gravity and magnetic features mimic closely those of geology. Hence, structural trends are reflected quite accurately in potential field maps. Identification of lithology is more ambiguous, since the magnetic and density properties of different rock types can be very similar. Nevertheless, individual anomalies may signify the presence of a specific lithology or formation. Patterns of anomalies may also reflect certain lithologies, formations or geological domains. Consequently, gravity and magnetic maps are extremely useful in investigating geology that is obscured by water, glacial till, desert sands or younger sedimentary cover. In order to extract the maximum information from such maps it is desirable that they be 'calibrated' against an area where the geology is known. Unfortunately, calibration is not absolute, because anomalies of a particular amplitude or shape are not necessarily uniquely associated with a specific lithology. Such is the nature of potential field interpretations, which are inherently ambiguous. Nevertheless, a careful assessment of relationships where geology is exposed is prerequisite, and should result in enhanced geological interpretation. Potential field maps can be processed in a variety of ways to produce map images that assist lithological and structural mapping.

Modelling Application

Geological units that are characterized by mean densities and/or magnetic susceptibilities differing significantly from those of surrounding or adjacent units will generate distinct potential field anomalies. These can be modelled quantitatively to provide information on the size and shape of the units. Modelling may be enhanced if constraints are available to control the modelling process. Surface geological contacts and rock properties are probably the most readily available constraints. Borehole data and seismic images are less commonly available, but can play a critical role in modelling.

EARTH'S GRAVITY AND MAGNETIC FIELDS

As a precursor to examining gravity and magnetic fields on a relatively local scale, it is instructive to consider briefly the global context of the respective fields, and the derivation of commonly used fundamental gravity and magnetic maps.

Gravity Field

According to Newton's law of gravitation, every particle in the universe attracts every other particle with a force (**F**) which is directly proportional to the product of the masses (**m**) of the particles and inversely proportional to the square of the distance (**d**) between them. This may be expressed simply as:

$$F = Gm_1m_2/d^2$$

where **G** is the gravitational constant

Any body on Earth has **weight**. **Weight** of a body equals the **force** acting on it due to gravitational attraction of the Earth. If the body has a mass m_1 and the Earth has a mass m_2 and a radius **R**, then the force, $F = Gm_1m_2/R^2$. This force may be considered to be defined, also, by Newton's second law of motion, $F = m_1a$, where **a** is the acceleration due to the attraction of the Earth if the body m_1 were allowed to fall. This force on body m_1 is the same force it would experience if it had an acceleration $a = F/m_1$, which is equal to Gm_2/R^2. Thus the gravitational attraction of the Earth, as a force per unit mass, can be considered as equivalent to the acceleration of a freely falling mass.

An acceleration of 1 cm/s^2 is referred to as 1 Gal (1 cm/s^2 is a sub-multiple of the fundamental SI unit for acceleration which is 1 m/s^2: SI is the abbreviation for the Système international d'unités (International System of Units)). The Gal is a unit that is permitted for use with SI. This unit is too large for magnitudes of changes in gravitational attraction commonly encountered in geophysical work, and so a quantity one thousand times smaller, the milligal (mGal) is commonly employed. Gravitational attraction at the surface of the Earth is roughly 980 Gal. Gravity meters generally measure this attraction to a precision of 0.01 mGal, thus measuring approximately 1/100,000,000 of the Earth's total attraction. Gravity is sometimes measured in terms of a unit

that is one millionth of 1 m/s^2, and is known as the gravity unit (g.u.) in SI (Parasnis, 1973); 1 mGal = 10 g.u.

If the Earth were a homogeneous, stationary sphere, the force of gravitational acceleration at its surface would be the same everywhere, because the distance to the centre of mass would be constant. The Earth, however, is relatively flattened at the poles in comparison to its curvature at the equator, so that its shape is best approximated by an ellipsoid (Fig. 1). Furthermore, it spins about its polar axis, producing a centrifugal force in a direction opposite to that produced by its mass attraction. These two conditions result in a systematic variation of gravity with latitude at the surface of the Earth. The ellipsoid that best approximates the shape of the Earth is known as the reference ellipsoid, whose surface is fitted as closely as possible to the mean sea-level surface. It is assumed that the oceans would be filled with crustal material and that crust above the theoretical position of sea level in land areas would be removed. As thus defined, the surface of the reference ellipsoid is an equipotential surface with the force of gravity everywhere being perpendicular to the surface. The surface of the reference ellipsoid is the datum for the computation of the theoretical value of gravity (g_t), the formula for which is:

$$g_t = 978.03185\ (1 + 0.005278895 \sin^2\alpha + 0.000023462 \sin^4\alpha)\ \text{Gal}.$$

based on the geodetic reference ellipsoid of 1967 (Geodetic Reference System 1967, 1971), where α is latitude in degrees.

Hammer (1943) discussed the sources that contribute to the systematic variation of gravity with latitude. Flattening at the poles causes the field at the poles to be 6.63 Gal greater than at the equator, because the polar radius is smaller and the pole is closer to the theoretical mass concentration at the Earth's centre. Outward centrifugal force related to rotation results in the field at the pole being 3.39 Gal larger than at the equator. The mass-shape effect, which is the relative bulge at lower latitudes producing an additional mass attraction, results in the field at the pole being 4.85 Gal lower than at the equator. The net effect is that gravitational attraction is about 5.17 Gal greater at the pole than at the equator.

Bouguer Gravity Anomaly Maps: The preceding discussion deals with theoretical aspects of the Earth's gravity field, relating in particular to variations associated with latitudinal positioning. On a more practical level, the derivation of Bouguer gravity maps, which have long been regarded as standard products for geological investigations, is now examined. The value of gravity to geological studies is that it is sensitive to spatial variations in rock density. Unfortunately, it is also effected by changes in elevation. As a result, variations in gravity from the latter source must be eliminated. This is accomplished by computing Bouguer gravity anomalies. In Figure 2 a series of gravity observations (G_{obs}) has been made on the land surface at various elevations above sea level. The geology is variable across the corresponding section, and hence, in addition to any changes relating to latitudinal variation, gravity is influenced by changes in density and elevation. Variations due to elevation are eliminated by "reducing" the observed data to a common datum, which in many surveys is taken to be sea level. Effectively, the reduction procedure produces gravity values, known as Bouguer anomalies, which are equivalent to the gravity values that would have been observed had it been possible to remove the topography and make the observations at sea level. The reduction to sea level involves two separate corrections, known as the free air and the Bouguer corrections.

The free air correction compensates for the height of the observation above sea level (the additional distance of the observation point from the centre of the attracting Earth's mass). It is added to G_{obs} and is equal to 0.3086 mGal/m. The Bouguer correction is applied to remove the additional component of attraction produced by the rock mass lying between the observation point and sea level. This correction is effected by assuming that the mass is approximated by an infinite slab of rock, whose lower surface coincides with sea level and upper surface passes through the observation point. In many cases a rock density of 2.67 g/cm^3 is assumed for the slab resulting in a correction equal to 0.1119 mGal/m, which is subtracted from G_{obs}. This approximation introduces little error into Bouguer anomalies where the terrain is reasonably flat, but where terrain is rugged additional corrections known as terrain corrections should be applied. Terrain above the observation point exerts an upward attraction, thereby reducing the gravitational attraction. Hollows in the terrain below the observation point are considered to be occupied by rock in the Bouguer correction, and thus the Bouguer correction is too large. Terrain corrections for hollows and positive relief are added to the Bouguer anomaly. Further details on terrain corrections are provided by Hammer (1939) and Bible (1962). The Bouguer anomaly at a station is obtained by subtracting the theoretical value of gravity on the reference ellipsoid (g_t) at the station from the corrected value of G_{obs}.

Magnetic Field

The source of the magnetic field of the Earth can be approximated by a bar magnet aligned along an axis joining the north and south magnetic poles (Fig. 3), which makes a small angle of about 10° with the axis joining the geographical poles. The pole of the bar magnet nearest the north geographical pole is actually a south pole, yet conventionally it is referred to as the north magnetic pole (Breiner, 1981). This disparity arises because the north-seeking end of a compass needle, which is effectively the north pole of the needle, must be attracted to a pole of the opposite sense. By convention, a north-seeking pole is a positive pole, and a south-seeking pole is a negative pole. The magnetic field of the Earth simulates the field produced by a theoretical bar magnet, and can be visualized in terms of the lines of force produced by that magnet (Fig. 3). A line of force represents the path that a single free north (= positive) pole would follow. The inclination of these lines with respect to the Earth's surface varies from 0° at the magnetic equator to 90° at the poles. The concentration or density of the lines, which reflects the strength of the field, also varies with latitude. At the poles it is approximately twice that at the equator, the corresponding field strengths being about 60,000 gammas (γ) and 30,000 γ, respectively (Breiner, 1981).

At this point it is appropriate to comment on the use of terminology and units in magnetism. Increased use of the SI system of units in science, at the expense of the traditional Gaussian centimetre/gram/second (cgs) system, seems to have caused confusion regarding the meaning of terms and equations used in magnetism (Payne, 1981; Shive, 1986). For example, considering terminology, there does not seem to be agreement as to whether **B** (magnetic induction) or **H** (magnetic field strength or intensity) is the fundamental magnetic field (Payne, 1981). Gauss is a unit of magnetic induction, and oersted is a unit of magnetic intensity. Both are units in the cgs system, and they are numerically equal in free space. The subject of units is not pursued in depth in these notes, but rather both cgs and SI units, and respective conversion factors, are provided for the various magnetic parameters.

1 gamma (γ) (cgs) = 10^{-5} gauss (G) (cgs) = 10^{-5} oersted (Oe) (cgs) = 10^{-9} nanotesla (nT) (SI)

The magnetic field at any point on the Earth's surface may be defined in terms of three parameters. Inclination (I), declination (D), which is the angle between the magnetic meridian and geographic north, and intensity (H), already defined (Fig. 4). Lest there be any confusion, note that the Earth's total field intensity is identified with F in Figure 4 (instead of the traditional H), since H is used for the horizontal component of total intensity.

Total Magnetic Field Maps: Both ground and airborne magnetic surveys commonly use cesium or proton precession magnetometers to measure the Earth's total magnetic field. Long wavelength components of the Earth's field are generated mainly by the Earth's core, as observed in Figure 3 (core is simulated by a bar magnet), and by the Earth's crust. These long wavelength components combine to produce a single long wavelength component, conventionally referred to as a geomagnetic reference field. In Canada, the reference field ranges in intensity from roughly 53,000 nT to 61,000 nT (Newitt and Haines, 1990). Short wavelength components of the magnetic field originating from the crust, the focus of interest in most geological applications, are superposed on the long wavelength component of the Earth's field. Therefore, although magnetic surveys measure the total field, the production of total field magnetic maps often involves an intermediate step of removing a reference field, such as the International Geomagnetic Reference Field, which represents mainly the magnetic field produced by the Earth's core. The result is a magnetic map that displays both negative and positive values, instead of absolute total field values. These are referred to as residual total field magnetic maps, but for conciseness they will be referred to as total magnetic field maps in this report.

UNDERSTANDING POTENTIAL FIELD MAPS

Typically, when a gravity and magnetic map of the same region are viewed side by side, the magnetic map appears to contain significantly more detail (Fig. 5). True comparison is difficult, because different parameters are measured, and it is rather like comparing apples and oranges. Nevertheless, some factors, common to both types of map, can affect the amount of detail. Principally, these are the range of the data, the contour interval used in displaying the data, sensitivity of measurements and data spacing. Another important factor, common to both maps, is mineralogical control, which leads to the overall range of magnetic susceptibilities in rocks being orders of magnitude larger than the range of rock densities. The controlling minerals are usually different. In aeromagnetic maps, flight elevation is another critical factor influencing detail. A discussion of these factors follows, some of which are grouped since they are inter-related. In making the comparisons, regional gravity and magnetic data archived in the National Geophysical Data Centre maintained by the Geological Survey of Canada are used.

Range and Contour Interval of Data, and Sensitivity of Measurements

The range of Bouguer gravity anomalies over the Canadian landmass is about 360 mGal. Gravity meters routinely measure with a precision of 0.01 mGal, but in practice the accuracy of the derived Bouguer anomaly is probably less, mainly as a result of error in determining elevation. This applies particularly to regional surveys in which elevations have been determined by

altimetry, and which may be in error by up to 3 m. The corresponding error in Bouguer anomaly is about 0.6 mGal. If one place of decimal (0.1 mGal) is accepted as a practical estimate of the precision of measurement of Bouguer anomalies, it is equivalent to 1/3,600th of the range of Bouguer anomalies in Canada.

The range of magnetic anomalies in Canada for surveys flown at 305 m mean terrain clearance, based on values in the National Geophysical Database interpolated to a 2 km grid, is about 23,000 nT. The actual range could be many thousands of nanoteslas greater. Magnetometers routinely measure the Earth's magnetic field with a precision of 0.01 nT, although when the noise envelope is considered this value is probably more realistically 0.05 nT. If 0.1 nT is accepted as a practical value for the precision of measurement, then magnetometers measure approximately 1/230,000 of the range.

On the basis of the aforementioned values, the precision of measurement of magnetic anomalies, with respect to the total range of anomalies, is two orders of magnitude finer than that for Bouguer anomalies. This is an important factor controlling the respective degrees of detail in the two types of map. It should be recognized, however, that any potential increase in detail resulting from increased precision, could be negated by the choice of contour interval. The contour interval acts as a filter. The smaller the interval, the more detail becomes apparent. The influence of contour interval is illustrated in Figure 6. Here, an array of 21 x 21 point Bouguer anomaly values are contoured at 0.5 and 2 mGal intervals. Significant features of the gravity field are several linear highs oriented NE-SW, which characteristically might represent a series of mafic intrusions. The extents of the intrusions are readily appreciated in the gravity map of Figure 6a, but are more uncertain in Figure 6b. In the latter figure, the highs H1 and H2, and the lows L1 and L2, which are clearly defined in Figure 6a, are essentially eliminated.

Considering that magnetic anomalies are determined to 1 part of a range of 230,000 and Bouguer anomalies to 1 part of a range of 3,600, it is evident that a greater number of contour intervals is required in magnetic maps to display variations over the range. In the discussion of mineralogical controls it will be become apparent why the range of magnetic anomalies is two orders of magnitude larger than that of Bouguer anomalies.

Data Spacing

Spacing of data is an important control on the amount of detail portrayed in a potential field map. This point is well illustrated by gravity and magnetic maps for the margin of the Canadian Shield in the Trans-Hudson Orogen (Fig. 5), displaying data collected under Canada's national gravity and magnetic mapping programs. The distributions of data in the two maps are significantly different. Gravity data are spaced about 10-15 km apart, observation points being arranged in an irregular grid pattern. On the other hand, aeromagnetic data were collected along flight lines spaced 805 m apart. Modern magnetometers sample the magnetic field every tenth of a second along each flight line, providing a point magnetic value roughly every 3 to 10 m, depending on the aircraft's speed. The magnetic surveys covering the region of Fig. 5 were done mainly in the 1960s, when the magnetic field was sampled approximately every 1 second. Hence point values may have been spaced about 100 m apart. The much closer spacing of aeromagnetic data clearly results in improved resolution and detail of the magnetic field compared to the gravity field.

A full understanding of potential field maps requires an awareness of the spacing and distribution of data, as illustrated by an example of a gravity map covering an area near Flin Flon, Manitoba. The map spans the boundary between the Flin Flon - Snow Lake Belt and the South Flank of the Kisseynew Gneiss Belt (Fig. 7). The boundary is linear and separates mainly mafic volcanics of the Amisk Group to the south, from a variable assemblage of mixed gneisses and metasediments to the north. Gravity data available prior to the summer of 1993 outlined a prominent high over the Amisk Group, which, based on the data distribution at that time, appeared to extend about 8 km north of the boundary, suggesting that the volcanics dipped northward beneath the South Flank. The possibility of a thrust contact was considered. Additional gravity observations were made in the summer to investigate the boundary. These were located on the shores and islands of Kisseynew Lake, immediately north of the boundary, and the only means of ready access to the area. The new data indicated that the gravity anomaly is restricted to the Flin Flon - Snow Lake Belt, suggesting that Amisk volcanics do not dip northward under the South Flank.

Distinct circular anomalies may be an artifact of data distribution, and should be treated with caution. Often, they may be defined on the basis of a single point. In such cases, the validity of the point itself may be called into question, or the particular method of contouring may be the fundamental reason. In some automatic contouring packages, a prelude to contouring randomly distributed data is the computation of values on a regular grid. If the size of the grid cell specified by the user is much smaller than the average distance between data points, circular anomalies may be generated around observation points. These may be interpreted to signify the presence of discrete geological bodies. This aspect of the contouring process is illustrated using a gravity data set in the region of the Canoe Landing Lake massive sulphide deposit in the Bathurst mining camp (Fig. 8). Here, detailed gravity observations at 25 m intervals were made along six lines crossing the deposit. Additional observations spaced roughly 0.5 to 3 km apart were made around the deposit to define the background gravity field. Automatic contouring of the data using a grid size of 10 m produced a map with several 'bull's eyes' anomalies (Fig 8a), which have no geological significance. When the grid size is increased to 100 m, the 'bull's eyes' disappear (Fig. 8b), and the gravity field is much smoother and probably more representative of reality.

Mineralogical Controls

The fundamental factor influencing potential field anomalies is the mineralogy of the rocks, which controls density and magnetic susceptibility. The gravity field reflects the bulk or whole-rock mineralogy, i.e. the principal rock-forming minerals that constitute and define a particular rock type: e.g. quartz, feldspar and biotite. Within a given rock type the defining mineralogy is not likely to vary substantially, hence the density characteristics tend to remain fairly uniform. The magnetic field is controlled by the accessory minerals in a rock, principally magnetite, which is reported to constitute about 1.5% of crustal minerals (Clark and Emerson, 1991). Accessory minerals are generally ignored in petrological classifications, and specific lithologies may exhibit a wide range of magnetic susceptibility. Distribution of accessory magnetic minerals may not be uniform for various reasons: concentration in distinct layers; uneven hydrothermal alteration, e.g. serpentinization of ultramafic rocks releases iron atoms from olivine and pyroxene, which are oxidized to produce magnetite; variable conditions of differentiation in plutonic rocks, e.g. oxygen fugacity, CO_2 content.

The density of common rock types ranges generally from about 2.00 g/cm^3 to 3.2 g/cm^3, and so relative differences are usually not more than a few tens percent. On the other hand, magnetic susceptibility of common rocks ranges from practically zero to about 300 x 10^{-3} SI; the susceptibility of magnetite itself ranging from about 1000 to 5700 x 10^{-3} SI. Relative variation of susceptibility is therefore orders of magnitude greater than relative variation of rock density, a difference which is reflected in the respective potential field. Such differences between gravity and magnetic maps may be enhanced by the fact that the density of a specific rock type is likely to be fairly uniform, whereas its susceptibility may vary significantly. It is possible, therefore, that even if gravity and magnetic data are collected at the same points, the magnetic field would be more variable than the gravity field.

Flight Elevation: Aeromagnetic Surveys

Another factor influencing detail in the case of aeromagnetic maps is flight elevation. In measuring a magnetic field the distance between the magnetometer and the source of the field will influence the amplitude of the measured anomaly. The fall-off rate is dependant on whether the magnetic source can be approximated by a monopole or dipole, which have fall-off rates that vary as $1/d^2$ and $1/d^3$, respectively (d = distance between magnetometer and source). In practice, the exponents are not so exactly defined, since various configurations of dipoles, monopoles, lines of poles, and sheet-like distributions of poles associated with the particular shape of the source will generate a spectrum of exponential values that may vary from 0 to 3 (Breiner, 1981). The increased resolution of anomalies with decreasing distance from source to sensor is illustrated through comparison of an aeromagnetic survey flown at 305 m elevation and a ground magnetic survey across a section of Lower Palaeozoic sedimentary and igneous rocks in the Bathurst mining camp (Fig. 9). This figure illustrates, also, the suppression of a signal as a body becomes more deeply buried.

ROCK DENSITY

Rock density is essentially a function of the major rock-forming minerals, which themselves define a rock. In igneous and metamorphic rocks, quartz and feldspar are important constituents. Mafic minerals such as biotite, hornblende and pyroxene may be present in significant amounts also. A classification of igneous rocks based on quartz content, feldspar composition and content of mafic minerals is shown as Figure 10. Mafic minerals are invariably more dense than felsic ones and quartz, so that an increase in these results in an increase in density. Densities of some common rock-forming minerals are presented in Table 1. In the plagioclase series of feldspars, density increases with increasing calcium content at the expense of sodium in going from albite to labradorite. Mafic minerals have densities well above the maximum 2.70 g/cm^3 value for feldspars. The influence of these heavier minerals on rock densities is illustrated by the gradual increase in density of igneous rocks in going from felsic rich granite to mafic rich ultramafics (Table 2), and in Figure 11, which shows an increase in density of the anorthosite-troctolite series as the percentage of olivine increases. A 10% increase results in a significant increase of about 0.1 g/cm^3 in density. Among sedimentary rocks there is a wide range of density for sandstones and shales. In such rocks, age and depth of burial are a major control on density. In the case of sandstones, porosity can also be a significant factor. Table 2 provides a general guide to rock densities, but since there can be regional differences in rock types, density may vary from area to area. For this reason it is recommended that measurements of density be conducted wherever possible to establish local values.

Table 1 - Mineral Densities (g/cm^3)	
Quartz	2.65
Feldspars	
Albite	2.62
Oligoclase	2.65
Andesine	2.67
Labradorite	2.70
Microcline	2.54 - 2.57
Orthoclase	2.57
Mafic Minerals	
Chlorite	2.60 - 2.90
Biotite	2.80 - 3.20
Hornblende	3.20
Augite	3.20 - 3.40
Olivine	3.27 - 4.37
Garnet	3.50 - 4.30

Table 2 - Rock Densities (g/cm^3)	
Plutonic Rocks	
Granite	2.60 - 2.67
Granodiorite	2.70
Diorite	2.77
Gabbro	2.90 - 3.00
Ultramafics	3.00 - 3.30
Anorthosite	2.72
Volcanic Rocks	
Rhyolite	2.60 - 2.65
Andesite	2.85
Basalt	2.90 - 3.00
Metamorphic Rocks	
Quartzo-feldspathic Gneisses	2.70 - 2.75
Argillites/Slates	2.70 - 2.75
Sedimentary Rocks	
Sandstones	2.00 - 2.65
Shales	2.00 - 2.70
Greywackes	2.65 - 2.75
Limestones	2.70

ROCK MAGNETISM

Magnetic anomalies produced by the Earth's crust are controlled by two principal sources: magnetization induced by the Earth's present magnetic field and natural remanent magnetization (NRM), which is a fossil magnetization acquired under the influence of a magnetic field some time in the past. Magnetite is probably the most common host of magnetization. According to Clark and Emerson (1991) ferrimagnetic magnetite accounts for about 1.5% of crustal minerals. The two magnetizations can reside together in a rock because they can occupy different magnetic grains or elements of a grain known as magnetic domains. The size of magnetic grains is an important control on the nature of magnetization. Grains smaller than the size of a domain are known as single domain (SD) grains. SD grains are the principal magnetic grains in a rock that contains remanent magnetizations. Grains larger than the size of a single domain contain more than one domain and are known as multidomain (MD) grains. Larger MD grains are readily demagnetised (Piper, 1987), and therefore are less likely to retain remanent components. Some MD grains containing only a few domains exhibit characteristics similar to those of SD grains. These are referred to as pseudo-single domain (PSD) grains, and they too can contain significant remanent magnetizations. Extremely small SD grains cannot retain a stable magnetization, and they are described as superparamagnetic (SPM). For magnetite, Piper (1987) documents the SPM/SD boundary as occurring at a grain size ranging from 0.025 to 0.030 μm, and the SD/MD boundary at a

grain size ranging from 0.05 to 0.08 μm. Carmichael (1982) presents similar numbers, but indicates additionally that the PSD/MD transition occurs at a grain size of 15 to 17 μm.

Induced Magnetization

An external magnetic force or field can induce a magnetization within a material coming under its influence. The degree to which the material may be magnetized is quantified by a parameter known as the magnetic susceptibility (k). A schematic representation of induced magnetization is portrayed in Figure 12. Here, an external magnetic field (H) acts on a material having a magnetic susceptibility equal to k. Within the material an induced magnetic field (H') is created, which is equal to $4\pi kH$. The quantity kH is equal to the induced magnetization (M). Therefore, susceptibility (k) is simply the ratio of the induced magnetization (M) to the magnetizing force (H) producing it. Following are some notes on units associated with induced magnetizations.

- Earth's magnetic field strength ≈ 0.5 oersted (Oe) (cgs) [1 Oe (cgs) ≈ 79.6 A/m (SI)].
- 0.5 Oe = 50,000 γ (cgs) = 50,000 nT (SI).
- Susceptibility (k) is a dimensionless quantity, but is of different magnitude in the SI and cgs systems of units: $k_{SI} = 4\pi k_{cgs}$.
- The unit of magnetization in the SI system is ampere/metre (A/m).
- The unit of magnetization in the cgs system is electromagnetic units per cubic centimetre (emu/cc).
- To convert SI magnetization to cgs magnetization multiply by 10^{-3}.
- In the SI system: magnetization (A/m) = k x field strength (A/m).
- In the cgs system: magnetization (emu/cc) = k x field strength (Oe).

Types of Induced Magnetization: A magnetic field is generated by movement of electrical charge, which at an atomic level can be related to the spin of electrons about their axes or to orbital motion of electrons around atomic nuclei (Piper, 1987). In the absence of an external field the individual magnetic effects are randomly oriented. When an external field is applied, the electrons respond in a variety of ways, that depend on the electrical configuration of the atoms and on the atomic structure of the material. Depending on the material, one of three principal types of magnetization will be induced. These are diamagnetism, paramagnetism and ferromagnetism. The following brief descriptions are taken from Thompson and Oldfield (1986).

- Diamagnetism: arises from interaction of magnetic field with orbital motion of electrons, producing a very weak negative magnetization, which is lost when the field is removed. Quartz, feldspar and calcite are diamagnetic.

- Paramagnetism: occurs when individual atoms, ions or molecules possess a permanent elementary dipole moment. Dipoles tend to align along the direction of applied field producing a very weak positive magnetization, which is lost when field is removed because of

thermal effects. Iron is incorporated into paramagnetic silicate minerals, mainly as Fe^{2+}. Iron-rich garnets, micas, olivines, pyroxenes and amphiboles are paramagnetic, having susceptibilities that range up to about 3×10^{-3} SI.

- Ferromagnetism: diamagnetism and paramagnetism are dependant on the presence of an external field, and are removed from a material when the field is removed. Ferromagnetic materials differ in that they retain a magnetization when the field is removed. They have significantly larger susceptibilities, which are dependant on the strength of the applied field. Of particular importance for rock magnetism is a type of ferromagnetism known as ferrimagnetism. Ferrimagnetic materials undergo a dramatic change at a temperature known as the Curie temperature. Below this they have a permanent (= remanent) magnetization, and above it they are paramagnetic. Ferrimagnetic minerals are the principal sources of magnetic anomalies, and include magnetite and pyrrhotite.

Remanent Magnetization:

Remanent magnetizations are "fossil" magnetizations acquired under the influence of an ancient magnetic field, and these reside in ferrimagnetic minerals such as magnetite.

Types of Remanent Magnetization: There are several types of natural remanent magnetization (NRM). The main types are listed below.

- Thermoremanent magnetization (TRM): geoscientists are probably most familiar with TRM, which is present in most igneous rocks, and is acquired by a magnetic mineral as it cools through the Curie temperature. Intensity of TRM is much greater for single domain grains than for multidomain ones.

- Chemical remanent magnetization (CRM): may be developed when a magnetic mineral is produced by chemical changes at temperatures below its Curie temperature. A CRM is locked into the magnetic grain when it grows larger than a critical size called its blocking volume.

- Detrital remanent magnetization: occurs for detrital magnetic particles with TRM or CRM which align parallel to the applied field, while falling though water, or more likely rotate into parallelism in water-filled interstices after coming to rest on substrate.

- Viscous remanent magnetization (VRM): is produced over time by thermal vibrations of the material's lattice, which cause domain walls to move slightly and irreversibly. Domains oriented close to the direction of the ambient Earth's field will expand at the expense of those having markedly different orientations (Piper, 1987). The net result of VRM is a magnetization oriented close to the orientation of the Earth's present field.

It is essential to consider the potential contribution of remanent magnetizations to the Earth's magnetic field when examining magnetic maps. For example, remanent magnetizations in directions opposing that of the Earth's field, called reversed magnetizations, can produce negative

anomalies. Quantitative modelling of anomalies in terms of shapes and sizes of geological bodies also needs to recognize the influence of remanent magnetizations, which can dominate in many rocks. The ratio of the remanent magnetization to induced magnetization is referred to as the Koenigsberger ratio (Q). Clark (1983) points out that Q values greater than 1 are predominant in most rock types. This property is depicted in Figure 13, adapted from Clark and Emerson (1991). The following list of facts relating to remanent magnetization is based on Clark (1983) and Clark and Emerson (1991).

- NRM: is often multicomponent, each one carried by a different subpopulation of magnetic grains. Hence, variations in relative proportions of the different NRMs within a rock unit can produce scatter in the remanent direction and variations in intensity.
- Smaller magnetite grains (SD grains <0.06 μm, in particular, and also MD grains up to ~0.20 μm that exhibit SD-like properties, the so-called PSD grains) have intense remanent magnetizations and are the dominant carriers of remanence in many rocks.
- Larger MD magnetite grains have relatively weak remanences with Q values < 1.
- Generally, plutonic and metamorphic rocks with secondary magnetite have low Q values, because the magnetite is relatively coarse and MD.
- Young rapidly chilled basaltic rocks exhibit very high Qs because of the fine grain size of magnetites (titanomagnetites).
- NRM carried by hematite and pyrrhotite is characteristically high with attendant high Q values (Fig. 13). Since hematite is weakly magnetic, hematite-rich rocks normally do not generate large magnetic anomalies. Pyrrhotite often has a strong NRM that differs in direction from the Earth's present field and can produce prominent anomalies. Commonly, anomalies related to pyrrhotite are negative.
- Magnetically soft MD magnetite, which is the principal magnetic carrier in many rocks, is dominated by VRM. Since VRM often has a direction similar to that of the Earth's ambient field, the VRM tends to enhance the induced magnetization. In essence this increases the effective susceptibility of a rock. It follows that, in some situations, magnetic anomalies may be modelled in terms of an induced magnetization only. Nevertheless, it should be noted that a modelled source based on an induced magnetization calculated on the basis of measured susceptibilities would be larger than reality, because the total magnetization would be underestimated in the absence of data on the VRM component.

Magnetic Minerals

Some of the most important magnetic minerals are iron oxides and solid solution series of these oxides with titanium oxides. They plot within the ternary system FeO-TiO_2-Fe_2O_3 (Fig. 14). The most important group of magnetic minerals producing magnetic anomalies are those of the magnetite-ulvospinel solid-solution series (Reynolds et al., 1990), known as titanomagnetites. The susceptibility of titanomagnetites is effectively zero for ulvospinel contents greater than about 70% (Reynolds et al., 1990), but is significant and fairly uniform for the rest of the series (Thompson and Oldfield, 1986). Second in importance to the titanomagnetites are the titanohematites (Clark and Emerson, 1991), which represent the ilmenite-hematite solid-solution series. Titanohematites composed of between 50 mole% and 80 mole% ilmenite are strongly

magnetic and effective carriers of NRM. More ilmenite-rich varieties are paramagnetic at room temperature, and hematite-rich ones are relatively weakly magnetic. Piper (1987) points out that natural titanomagnetites tend to be oxidized towards the titanohematite trend (Fig. 15), and are more correctly termed titanomaghemites. However, the term titanomagnetite is generally used for both pure and oxidized varieties.

Magnetite (Fe_3O_4) is a common magnetic mineral found in igneous, metamorphic and sedimentary rocks. Hematite (αFe_2O_3) is common in oxidized igneous rocks and sediments formed in oxidizing conditions. Maghematite (γFe_2O_3), with the same composition as hematite, is formed by low temperature oxidation of magnetite in subaerial and submarine environments. It is found in oceanic basalts and laterites.

The second most important group of magnetic minerals is one comprising iron sulphides, the most magnetic of which is ferrimagnetic pyrrhotite. A common type of pyrrhotite occurring in nature is monoclinic pyrrhotite having the composition Fe_7S_8. Pyrrhotite is found in basic igneous rocks, low to medium grade metamorphic rocks and sedimentary rocks (Piper, 1987).

Magnetic Susceptibilities of Minerals and Rocks

Magnetic susceptibilities of some paramagnetic and ferrimagnetic minerals are given in Tables 3 and 4, respectively. It is noticeable that the ferrimagnetic minerals have susceptibilities which are generally two or three orders of magnitude larger than paramagnetic susceptibilities.

Table 3 Magnetic Susceptibilities of Paramagnetic Minerals (x 10^{-3} SI)	
Amphibole	0.2^S - 0.9^S
Biotite	0.7^S - 2.9^H
Garnet	0.4^S - 2.7^H
Olivine	1.3^S - 1.6^H
Pyroxene	0.9^S - 3.6^C
Pyrite	0.03^H - 5.3^C
Chalcopyrite	0.02^H - 0.4^H
Sources: C, Carmichael (1982); H, Hunt et al. (1995); S, Strangway (1981).	

Table 4 Magnetic Susceptibilities of Ferrimagnetic Minerals (x 10^{-3} SI)	
Ilmenite	2 - 3800
Hematite	0.5 - 40
Maghemite	2000 - 2500
Magnetite	1000 - 5700
Titanomagnetite	130 - 620
Titanomaghemite	2800
Pyrrhotite (Fe_7S_8)	3200
Source: Hunt et al. (1995)	

$k_{SI} = 4\pi k_{cgs}$: To obtain susceptibilities in cgs units divide values in tables by 4π (= 12.566)

An illustration depicting the range of susceptibilities in common rock types is featured in Figure 16, modified from Clark and Emerson (1991). Some key points relating to the information in this diagram are listed following:

- Every rock type of sedimentary, igneous or metamorphic origin has a wide range of magnetic susceptibility; the ranges overlap significantly, thus susceptibility alone generally is not diagnostic of lithology.

- Many rock types have a bimodal distribution of susceptibility values; generally these represent distinct populations within each rock type for which ferrimagnetic minerals are absent or present. In the weakly magnetic subpopulation Fe is incorporated into paramagnetic silicates mainly as Fe^{2+}. Iron-rich garnets, olivines, pyroxenes, amphiboles and micas may exhibit values ranging up to about 4×10^{-3} SI.

- Within each magnetic subpopulation, susceptibility tends to increase with basicity.

- The bimodal pattern in granite reflects two distinct categories:
  magnetite series - relatively oxidized = I-Type
  ilmenite series - more reduced = S-Type
  Recognition of the two types has important petrogenetic and metallogenetic implications, and has had an influence in developing concepts of mapping granitoid terrains using a hand held susceptibility meter or magnetometer.

- In the metamorphic group, different grades of metamorphism have a considerable impact on the susceptibility of basic igneous rocks such as basalt/diabase. Regional metamorphism to greenschist or amphibolite grade tends to lower susceptibility, but further increase up to granulite grade may produce secondary magnetite. Eclogite grade destroys all magnetite and partitions iron into paramagnetic silicates.

- Sedimentary rocks typically have very low susceptibilities, although some immature clastics may contain significant amounts of magnetite.

- The Fe content of sediments and the Fe^{3+}/Fe^{2+} ratio, which reflects redox conditions during sedimentation, are critical factors controlling development of secondary magnetite during metamorphism. Thus, magnetic patterns over metasediments tend to reflect variations in sedimentary facies as well as metamorphic conditions. Pyrrhotite is the principal magnetic mineral in many metasedimentary rocks, especially in mineralized areas.

- Ultramafic rocks, such as pyroxenites, hornblendites and serpentinized dunites in zoned Alaskan-type complexes are generally highly magnetic.

- Serpentinization creates abundant magnetite. Dunite, peridotite and pyroxenite yield Fe atoms from paramagnetic olivine and pyroxene, which are oxidized to produce ferrimagnetic magnetite.

Magnetite produced by serpentinization is generally multidomain, well crystallized, almost pure Fe_3O_4, which is magnetically soft and carries relatively weak remanence. Prograde metamorphism of serpentinized ultramafics produces increased substitution of Mg and Al into the magnetite, eventually shifting the composition into the paramagnetic field.

EXAMPLES OF POTENTIAL FIELD MAPS

Gravity Maps

Bouguer Anomaly Maps: The Bouguer gravity anomaly map is the most common form of gravity map, whose derivation has been described previously. To reiterate, a Bouguer map is a representation of the gravity field as it would appear if measured on a surface having a constant elevation above sea level. Conventionally, in national and regional surveys this surface is sea level itself. The utility of the Bouguer map may be appreciated from Figure 5, which illustrates the mapping capabilities of such maps. Structures and lithological units can be traced, with considerable confidence, from the exposed geology of the Trans-Hudson Orogen under adjacent Phanerozoic sedimentary cover. Granitic rocks typically produce negative anomalies, whereas mafic and ultramafic rocks are associated with positive anomalies. Consequently, in many cases, distinct anomalies can be linked to such rock types, particularly in crystalline terrains where these rocks generally represent end members in terms of the density spectrum. Naturally, many other rock types, having intermediate density characteristics, may produce anomalies that are not as distinct or prominent and may be more difficult to tie to a particular lithology without first "calibrating" the anomalies in an area of good exposure.

Isostatic Anomaly Maps: Bouguer gravity anomaly maps are relatively easy to decipher in regions where terrain varies little in elevation. Complications may arise where relatively rugged and elevated terrain, for example, a mountain or plateau, is present within a region. Such terrain is usually isostatically compensated by a root at the base of the crust. Compared to laterally adjacent mantle, such roots represent mass deficiencies. These produce relatively negative, long wavelength gravity signals that may obscure or interfere with shorter wavelength features related to intra-crustal geology. This type of complication is illustrated in Figure 17. When the topographic load is not compensated by a root (Fig. 17a), the gravity signature would be interpreted correctly in terms of two intra-crustal masses (having positive density contrasts). When a root is introduced (Fig. 17b), its associated long wavelength, negative anomaly transforms the gravity profile into a signature that could be interpreted to signify the presence of near-surface bodies having both positive and negative density contrasts. The effect of topography on a Bouguer gravity map is further illustrated with an example from a broad region of southwestern Alberta, where the ground rises southwestward towards the Rocky Mountains. The progressive increase in elevation is complemented by a decrease in the Bouguer gravity field (Fig. 18), an inverse relationship that is characteristic of most Bouguer maps, though sometimes not easily recognized if changes in elevation are not dramatic. The Bouguer map of Figure 18 tends to be dominated by contours oriented north-northwest to northwest, although northeast trends are prominent in some places. The latter reflect the trends of Precambrian basement geology, which are manifested in aeromagnetic maps. When isostatic corrections are applied to the Bouguer anomaly map, the isostatic gravity map of Figure 19 is produced. On this, contour trends oriented northeast predominate and provide a more representative picture of geological trends in the basement.

Residual Gravity Anomaly Maps: Not all long wavelength features of gravity maps are necessarily related to topography. Phenomena such as variations in depth to intra-crustal

discontinuities, and changes in sedimentary facies and metamorphic grade can produce regional signals. These can be removed by a variety of mathematical or graphical methods, in a process known as filtering. The remaining gravity field is termed the residual gravity field. A section on regional-residual separation is included later in the report, but the subject is introduced at this point so that a comparison of isostatic and residual gravity maps for southwestern Alberta can be facilitated. Superimposed on the Bouguer gravity map of Figure 18 is a regional gravity field derived by applying polynomial regression using an algorithm available in a software package called "Surfer" (Keckler, 1994). When the regional is subtracted from the Bouguer map, the residual anomaly map (Fig. 20) is obtained. This displays a series of distinct anomalies having northeast trends, and there are similarities with the isostatic gravity map of Figure 19.

Horizontal Gradient Maps: Another way of displaying gravity anomalies is in the form of horizontal gradient maps. The magnitude of the local horizontal gradient may be computed for Bouguer or isostatic anomaly maps at points on a grid and contoured. For example, Sharpton et al. (1987) calculated horizontal gradients of a Bouguer gravity anomaly map of North America by fitting a first degree polynomial (plane) to 5 x 5 gravity values within a 25 km by 25 km window. The gradient value was assigned to the central grid point. The window was then moved 5 km and the procedure repeated. The concept of horizontal gradient may be easily appreciated by looking at it from a one-dimensional perspective (Fig. 21). Horizontal gradient is simply the change in gravity in a given distance (Fig. 21a). In Fig. 21b a series of 5 straight lines is fitted to a Bouguer gravity profile across a vertical geological contact. The horizontal distance over which they are fitted is constant. The horizontal gradient of each of these line segments is plotted as large dots, and these define a bell-shaped curve. The peak of the horizontal gradient curve is located over the contact. In map format, such peaks will be manifested as ridge-like features, and these should fall along or close to geological contacts associated with changes in density.

A utility of horizontal gradient maps is that they enhance short-wavelength features, while filtering out long wavelength signals. In Bouguer anomaly maps, the latter might produce a progressive change in colour (for colour-contoured maps) across a region, thereby resulting in different ranges of colours for shorter wavelength anomalies spread throughout the region. Visual comparison of the latter anomalies or tracing a single belt of such anomalies could be more difficult. However, in horizontal gradient maps the datum is constant across a region, i.e. zero mGal/km, and visual comparisons are facilitated. It should be recognized that horizontal gradient maps do not contain anomalies in the sense of Bouguer or isostatic maps. Rather they contain a series of linear or curvilinear ridge-like features. Importantly, the axes of the ridges trace steep geological contacts across which there are significant changes in density. As a result, horizontal gradient maps are very useful for mapping structural trends. A grey-tone horizontal gradient map derived from a Bouguer gravity map (Fig. 22) of a section of the Trans-Hudson Orogen, largely buried under Phanerozoic sediments of the Interior Platform, appears as Figure 23. A complementary vertical gradient map of the same area is shown in Figure 24. All of these maps are portrayed in contour format in Figure 25. Three ridge-like features of the contoured horizontal gradient map (Fig. 25b), labelled A, B and C and highlighted with dots, are particularly noticeable. On the Bouguer map (Fig. 25a), the same dots coincide with linear belts of relatively abrupt change in the gravity field. The horizontal gradient feature A is interpreted to mark the western limit of the orogen in this region (Thomas et al., 1987). A comparison of Figures 25a and 25b indicates that the gradient map tends to bring certain features into focus. Features A, B and

C are good examples, for although they are present on the Bouguer map of Figure 25a, they are more noticeable on the gradient map (Fig. 25b).

Vertical Gradient Maps: Another by-product of Bouguer gravity maps is the vertical gradient map, a type of map that is, perhaps, more commonly associated with aeromagnetic surveys. In such surveys, the gradient may be calculated from direct measurements of the total magnetic field made by two magnetometers placed about 2 to 3 m apart and arranged vertically with respect to one another. In gravity surveys, the field is usually measured at one position only, by a gravity meter sitting on a tripod at a height above ground surface that is usually no more than a few tens of centimetres. Thus, the vertical gradient of the gravity field is usually obtained using a theoretical approach, rather than the direct measurement approach used in some aeromagnetic surveys. This theoretical approach is used also to calculate the magnetic vertical gradient when only one magnetometer is used in aeromagnetic surveys.

Whereas the concept of vertical gradient at a single point is easily visualized, it is perhaps more difficult to appreciate: (1) how the vertical gradient relates to the actual measured field, (2) how it is expressed in a map or profile, and (3) its geological significance. Such aspects of vertical gradients may be better understood through examination of Figure 26, which shows two gravity profiles across a body having a positive density contrast. One profile represents the gravity field computed at ground level and the other is the field computed at a height of 2.5 km (the large separation is utilized in order that a difference between the two curves is clearly discernible). The vertical gradient, in this case, is derived by subtracting the ground profile from that calculated at 2.5 km elevation, dividing the difference by 2.5 and reversing the sign. The reversal of sign follows a convention adopted in the calculation of magnetic vertical gradients, designed to produce positive gradient values over magnetic bodies (Hood and Teskey, 1989).

The vertical gradient signature associated with the body consists of a dominant, central positive component and flanking, subordinate negative components. The negative values arise from the fact that, at points outside the body (in a lateral sense), the vertical component of gravitational attraction of the body measured at height is greater than that measured at ground level. The reverse is true over the body. A characteristic feature of gradient anomalies is that they are narrower than their counterparts in the measured field. Thus, vertical gradient maps provide greater resolution than do maps of the measured field, with vertical gradient anomalies related to near-surface geological features tending to be emphasized at the expense of those related to deeper ones. Another useful feature of gradient maps is that the zero contour coincides with vertical contacts between geological bodies. In Figure 26 the zero value of the vertical gradient falls near, but not exactly at the contacts. This results from the large difference in the heights at which the two profiles were computed. As the difference becomes smaller, the zero value moves closer towards the contact. In practice, the vertical gradient is not computed in the simplistic manner used for the demonstration provided by Figure 26, but rather is computed with more sophisticated mathematical operators.

A vertical gravity gradient map for part of the Trans-Hudson Orogen is shown in Figures 24 and 25c. The dots centred on the linear horizontal gradient features shown in Figure 25b, when transferred to Figure 25c fall along the zero contour, supporting the existence of steep geological contacts in these locations.

Density Maps: The subject of density maps is included under the general heading of "Gravity Maps", because density maps are a derived product of gravity maps. Gravity anomalies are

directly related to variations in density of the crust, and short wavelength anomalies often reflect density variations observed at the Earth's surface. Such variations can be mapped using gravity maps. Furthermore, if density can be calibrated with geology, by extension it should be possible to produce pseudogeological maps. The derivation of density from gravity is illustrated for a gravity profile using an approach developed by Cordell and McCafferty (1989). Gravity fields vary smoothly and continuously, whereas variations in density are usually discontinuous, in the sense that values can change abruptly at geological boundaries. Cordell and McCafferty (1989) proceeded to derive density from gravity by first transforming a smoothly varying gravity profile into a profile consisting of discrete vertical and horizontal segments. This was achieved by moving a window across the gravity profile and increasing, decreasing or unchanging the value of the profile in the centre of the window, depending on the algebraic sign of local curvature of the profile determined at the central point. The new profile, so obtained, was then subjected to the same process, and the process repeated until a profile comprised entirely of vertical and horizontal segments was produced (Fig. 27). The final profile is called the terrace function, since it resembles terraces cut into the sides of hills (analogous to positive anomalies).

The amplitude range of the terrace function is constrained to be identical to that of the original gravity profile, and the function itself is in units of milligals. In Figure 27, the geological model from which the original gravity profile was computed comprises a series of blocks of identical thickness having upper and lower surfaces at 0.3 and 2 km depth, respectively. With only two exceptions (identified with arrows in Fig. 27), the block boundaries coincide exactly with vertical segments of the terrace function. By considering the terrace function to be proportional to density within the sheet of blocks, it is possible to estimate density from the function. However, it must be emphasized that this estimation requires an assumption about the thickness of the sheet.

Magnetic Maps

Total Field Magnetic Maps: Magnetic data are commonly portrayed as coloured total field maps. These are produced by gridding the data and assigning a particular colour to each grid cell, based on the magnetic value for the cell. Such maps allow a ready appreciation of patterns and of relatively strongly and weakly magnetized areas, magnetic expressions of which are commonly referred to as highs and lows, respectively. In some cases, the maps may be enhanced by separating colour intervals with contour lines. Broome (1991) discusses various aspects relating to the display of aeromagnetic data. One of them concerns division of the total range of anomaly values (known also as the dynamic range) into an appropriate number of intervals, a subject discussed previously under the heading "Range and Contour Interval of Data, and Sensitivity of Measurements". A simple method of dividing the range is to divide it into equal intervals. This is called linear equalization, and it can result in an effective image, particularly when the populations of grid cells within intervals are similar. However, if the populations for some intervals are very large (i.e. the interval covers a large area of the map), detail within those intervals may be lacking. The problem can be circumvented by dividing the dynamic range using a process known as histogram equalization. A mathematical operator is applied to the data that divides the range into a number of intervals within which the populations of grid cells are identical. A result of this process is that the ranges of individual intervals are not necessarily the same. Noticeably, intervals at the uppermost and lowermost ends of the dynamic range are relatively expanded. Whereas coloured maps are most popular, maps consisting of grey tones may also be considered.

Broome (1991) points out that in working with coloured maps, the human eye has a tendency to divide the image into areas having different colours. This may not always be desirable, and the use of grey-tone maps offers a perspective that could provide information not as obvious in a coloured rendition. An example of a grey-tone total field magnetic map, covering a region of the Trans-Hudson Orogen, is presented as Figure 28.

Shaded Relief Magnetic Maps: Sometimes the intensity and spatial distribution of magnetic variations within a region are such that a total field image may appear to be somewhat muted, containing little information. Such images can be enhanced using a technique known as shaded relief. A good description of this technique, which enhances small, low amplitude features is provided by Broome (1991). The process simulates the effects of light directed on the three-dimensional surface defined by the grid of magnetic anomaly values. The intensity of light reflected back from a slope on the surface will vary according to the steepness of the slope. The proportion of illuminating light reflected back is known as the reflectance, and attains a maximum for slopes that are perpendicular to the direction of the light. The overall effect is one of areas of varying brightness and areas of shadow, an effect very similar to that created by the sun shining over a range of hills. The light direction and its inclination from the horizontal can be varied, thereby providing different images of the same data set. Depending on the direction and inclination, certain features may be enhanced or suppressed. Generally magnetic features are enhanced when the light direction is oriented at right angles to them. The value of shaded relief maps is demonstrated in Figures 29 and 30, which are magnetic maps of an area within the Slave Province. Linear short wavelength anomalies related to the MacKenzie dykes are emphasized by light directed at right angles to their trend (Fig 29), but are suppressed when the light direction is parallel to the trend (Fig. 30).

Vertical Gradient Maps: The vertical gradient of potential fields has been discussed previously in the section dealing with gravity maps. The vertical gradient is often measured in aeromagnetic surveys, but it may also be calculated from measurements made using a single magnetometer. Hood and Teskey (1989) list the following advantages of magnetic vertical gradient maps over magnetic total field maps:

- Closely spaced geological units are better resolved (because vertical gradient anomalies are narrower).
- Vertical gradient anomalies produced by near-surface geological features are emphasized relative to those associated with deeper features (regional-scale anomalies tend to be removed).
- Vertical contacts are delineated directly by the zero contour at high magnetic latitudes.
- Regional magnetic gradients and diurnal variations of the Earth's magnetic field are eliminated.

Vertical (or steep) contacts are delineated by the zero contour at high magnetic latitudes, because the inclination of the Earth's field is also steep at high latitudes (the zero contour of the vertical gradient of gravity falls at or close to vertical or steep contacts at all latitudes, because the gravity field is everywhere directed vertically). An example of a magnetic vertical gradient map, covering a portion of the Trans-Hudson Orogen, is shown in Figure 31.

Contoured Magnetic Maps: In the past, images of the magnetic field were commonly presented in the form of contour lines. A disadvantage of such maps is that they can not always be readily evaluated, particularly in cases where the density of contours is high and the pattern of anomalies is complex, since it may be difficult to distinguish highs from lows. Nevertheless, contoured representations can provide effective illustrations and are still widely used.

Magnetic Susceptibility Maps: Just as density maps can be derived from gravity maps, magnetic susceptibility maps (or more correctly, **apparent** magnetic susceptibility maps) can be derived from magnetic maps using similar techniques. An outline of a process used to obtain susceptibility maps is provided by Broome (1991).

For more information on the portrayal of aeromagnetic data the reader is referred to Broome (1991).

INTERPRETATION OF POTENTIAL FIELD ANOMALIES

Before entering into discussion of various facets of interpretation, the differing nature of gravity and magnetic anomalies is examined. In magnetic terminology, gravity anomalies may be considered to be produced by monopolar sources, whereas magnetic anomalies result from bipolar sources. For a specific body, therefore, a gravity anomaly is an expression of a single entity, namely the density contrast between the body and its surroundings. It will be positive or negative depending on the sign of the contrast. The magnetic anomaly for the same body is an expression of two entities, a positive pole and a negative pole, whose effects are combined to produce the anomaly. For this reason, when a magnetic anomaly is observed in profile, part of the profile may have negative values relative to the zero background, and part will have positive values. If the magnetization is entirely induced and the Earth's field is steeply dipping, as it is throughout Canada, the positive component of the body's magnetization will dominate.

Another difference between gravity and magnetic anomalies arises because of differences in direction of the respective potential field vectors, i.e. direction of the attracting force. The force of gravity is always vertical, therefore the gravity anomaly produced by a symmetrical body, such as a right rectangular prism, will also be symmetrical, and the peak of the anomaly will sit above the centre of the body. If the Earth's magnetic field in an area were vertical, the magnetic anomaly would also be symmetrical, because the negative pole in a body would lie vertically above the positive pole. However, the Earth's magnetic field is vertical only at the magnetic poles themselves. Everywhere else it is inclined, and thus positive and negative poles will also adopt an inclined attitude relative to one another, as illustrated in Figure 32. Because the direction of the magnetic field is the direction in which a positive pole would move, the Earth's field produces the distribution of poles as shown, which generates a secondary field depicted by the indicated pattern of lines of force (Milsom, 1989). The upper, negative pole is closer to the surface and produces a relatively large positive component, whereas the deeper, positive pole produces a smaller negative effect. The positive pole is offset horizontally with respect to the negative, and thus the peaks of the respective anomalies will likewise be offset. If the secondary field is small and the total field is measured in the direction of the Earth's field, no anomalous component of the field will be detected near A and C (where the secondary lines of force are roughly perpendicular to the primary field), and the anomaly will peak near B where the directions of the secondary and

primary fields are the same. This results in a slight offset of the peak of the resultant anomaly towards the south.

In Canada, the Earth's field is inclined at angles ranging from about 70° to 90° from the horizontal, so it is not unusual to observe a small negative anomaly on the north side of positive anomalies. It is important to recognize that these are not necessarily related to bodies with low or no magnetization or even to reversed remanent magnetizations. Such negative anomalies may simply originate from the same body producing the more prominent high. The problem of negative "artifacts" is worse in southern latitudes where inclination values are lower. Baranov (1957) presented a method for eliminating such artifacts by a process which has come to be known as reduction to the pole (magnetic inclination at the magnetic pole being 90°). By a mathematical process using links between magnetic and gravitational potentials, total field magnetic anomalies are transformed into simpler anomalies called "pseudo-gravimetric anomalies". These are really magnetic anomalies computed on the assumption that the magnetization vector is vertical. They are simpler to interpret than total field anomalies, since they are located vertically with respect to the magnetized bodies (i.e. their peaks are not displaced laterally from the body), and are not influenced by the inclination of the Earth's field, nor by the direction of the magnetization (Baranov, 1957). An example of a total field magnetic anomaly reduced to the pole is shown in Figure 33.

There are factors other than those just discussed, which may add to the complexity of the sources of magnetic anomalies. These include declination direction, geometry of the magnetized body and remanent magnetizations.

Regional-Residual Separation:

The mapping capabilities of potential field maps has been outlined already. To recap, calibration of anomalies and different levels of the potential field using control areas of exposed geology, together with measurements of physical rock properties, allows geology to be extrapolated into regions of little or no exposure. This is a utility of the entire pattern of gravity or magnetic anomalies. Sometimes, however, there may be an interest in a specific anomaly on a map, and sometimes this anomaly is superposed on a gradient or is interfered with by another anomaly. Therefore, one of the primary tasks of an interpreter may be to isolate an anomaly of interest from the rest of the field. This process is commonly referred to as regional-residual separation, the isolated anomaly being the residual anomaly. The "regional component" more often than not extends over a great distance, hence the name, but frequently it may be represented by a relatively local signature. A simple example of a local anomaly superposed on a regional gradient is shown in profile format in Figure 34. In this, a negative anomaly produced by a granite body intruded into intermediate gneiss is superposed on a gradient related to a sloping interface between this gneiss and underlying denser mafic gneiss. The anomaly due to the granite can be isolated by subtracting the observed anomaly from the true regional. The residual anomaly is thus obtained and has similar background levels to either side. If the granite were the focus of interest it could be modelled without concern for the source of the gradient. It should be noted that the true regional sits above the observed profile for a considerable distance from the edges of the granite. This a "tailing" effect, since an anomaly does not return to background level abruptly near the limits of the causative body. An inexperienced interpreter not familiar with this characteristic might select the interpreted regional in the figure, resulting in a residual anomaly whose amplitude

would be too small. Estimation of regional anomalies or base levels for magnetic anomalies is more difficult, because of the bipolar nature of magnetism, which causes a single body to produce positive and negative components.

An example of regional-residual separation for an area, rather than for a profile is shown in Figures 35 and 36. Near Agricola Lake, in the Slave Province, a small positive anomaly related to a sulphide deposit (Boyd et al., 1975) is superposed on a gradient (Fig. 35). The trend of the gradient (the regional in this case) in the area under the anomaly has been estimated by extending contours from one side of the positive and linking them with equivalent contours on the other side. The regional is subtracted from the observed anomaly where the two sets of contours intersect, and the resultant values are contoured to produce a positive, 0.5 mGal amplitude, residual anomaly (Fig. 36). The indicated position of the zero contour is probably too close to the centre of the anomaly, because of uncertainty related to the "tailing" effect discussed above.

The preceding two examples are relatively simple, and are examples of "graphical" separation of anomalies. In nature things may be much more complicated. There are many mathematical approaches to separating regional and residual anomalies. One such approach involving polynomial regression has been discussed and is illustrated in Figures 18 and 20.

Depth Estimates

The shape of a potential field anomaly can be used to make estimates of the depth to the source. This may be useful information in the early assessment of geophysical data, before detailed modelling of the anomalies is undertaken. For gravity anomalies (Bott and Smith, 1958) provide the following expressions for maximum depths of three-dimensional and two-dimensional bodies:

3D body: maximum depth = 0.86 (total anomaly / maximum horizontal gradient)

2D body: maximum depth = 0.65 (total anomaly / maximum horizontal gradient)

These expressions may not be particularly accurate, depending on the geometry of the source (Telford et al., 1982). However, they provide exact depths to a point source and an infinite line source, respectively.

In the case of an anomaly due to a vertical contact, sometimes referred to as a step anomaly, where the step is buried to a depth D and has a thickness T (Fig. 37), the maximum depth to the top of the step = 0.32 (total anomaly / maximum horizontal gradient).

The amplitude of a gravity anomaly generated by a body can be readily estimated using the formula for an infinite slab, mentioned already with respect to the Bouguer correction. The gravity effect of a slab is 41.9ρ mGal/km, where ρ is the density of the slab in g/cm^3. Simply multiply the thickness of the body, in kilometres, by 41.9ρ to obtain the amplitude. The accuracy of the estimation will depend on how well the shape of the body is approximated by a slab.

There are many simple approaches to estimating the depths to the tops of magnetic bodies based on the shapes of magnetic anomalies. These depths are generally accurate to within 20% of the true depth (Milsom, 1989). Two are featured in Figure 38. For approximately tabular and abruptly truncated bodies, the depth to the top surface is roughly equal to the horizontal extent (D) of the "straight" part of the flank of the anomaly; in theory the flank is never absolutely straight, but the eye can detect a segment that is approximately straight. Another method known

as Peter's rule, requires that a tangent (= line of maximum slope) be drawn on the profile at its steepest point. Lines having half the slope of this tangent are then constructed and moved to upper and lower positions that are tangential to the profile. The horizontal distance between these positions is equal to 1.6 D, where D = depth to top of the body. Milsom (1989) notes that model studies indicate that the true depth factor lies between about 1.2 and 2, but that values close to the intermediate value of 1.6 are common.

Quantitative Modelling of Anomalies

One of the most valuable assets of potential field data is that they can be modelled to provide quantitative information on shapes and sizes of geological bodies. The process commences by placing simple bodies in appropriate positions and assigning them density contrasts or magnetic susceptibilities. The shapes are then varied, and possibly the rock properties as well, until a model curve matches closely the observed curve. All available constraints, such as measured rock properties, surface geological contacts, drill hole intersections, and seismic boundaries, should be incorporated into the initial model. The more controls the better, since they will help reduce the ambiguity of the model. Usually, surface geological contacts and rock properties are available, whereas information at depth is not. Where constraints are lacking, many different models may satisfy the same anomaly. Ambiguity is an inherent weakness of potential field modelling, as clearly demonstrated in Figure. 39, adapted from Skeels (1947). It shows that virtually the same gravity anomaly is produced by any one of several configurations of a boundary placed at various depths, across which the density contrast is 0.2 g/cm^3.

Commonly, geophysical interpreters select a profile crossing an anomaly and use modelling software that treats geological bodies as horizontal two-dimensional (2D) or two-and-a-half-dimensional (2.5) prisms of polygonal cross-section to attain a match to the profile. 2.5D modelling (Fig. 40) has the advantage over 2D modelling in that the strike length of the body can be specified, as opposed to being infinite. Both 2D and 2.5D modelling satisfy the requirements of many geological situations, since geological units are commonly very much longer (strike direction) than wide. The 2.5D approach is particularly useful when the ratio of strike length to width becomes less than about three to one. Ideally, for some software packages, the profile selected for modelling should cross geological strike at right angles and be centred with respect to the length of the body. Other packages have the facility to accommodate profiles that cross at angles other than 90°, and may be positioned anywhere along the body.

Modelling with 2.5D software provides good results for many geological situations, but occasionally approximation of a body using a 2.5D prism is not suitable. In such cases, 3D approximations using a number of right rectangular prisms or horizontal sheets provide a truer representation of the body shape.

POTENTIAL FIELD SIGNATURES OF SULPHIDE DEPOSITS

Physical Properties of Volcanogenic Massive Sulphide Deposits

Sulphide deposits invariably have density and magnetic properties that differ significantly from those of their host rocks. Hence there is considerable potential for discovery of the deposits using

gravity and magnetic exploration methods. A table of densities and magnetic susceptibilities for sulphide minerals and other minerals found in the ore environment is presented as Table 5.

Table 5 - Ore Mineral Density (g/cm^3) & Magnetic Susceptibility (10^{-3} SI)

Mineral	Density	Susceptibility
Chalcopyrite	4.20	0.4
Pyrite	5.02	5
Pyrrhotite	4.62	3200
Sphalerite	4.00	0.8
Galena	7.50	-0.03
Magnetite	5.18	5700
Hematite	5.26	40

All values from Hunt et al. (1995)

Any exploration method should be applied with due consideration of genetic models, since they could influence the kinds of approaches adopted in a geophysical exploration strategy. A brief examination of genetic models for sulphide deposits follows. Volcanic massive sulphide (VMS) deposits are widely accepted as forming from the discharge of hydrothermal solutions onto the seafloor, commonly near plate margins (e.g. Lydon, 1984). Modern examples, such as those formed at mid-ocean ridges, have been extensively documented (e.g. Hannington et al., 1995). Host rocks adjacent to VMS deposits are usually of volcanic origin, and include lavas, pyroclastics and volcaniclastics, but sedimentary rocks, such as shales and greywackes, having no volcanic association, are not uncommon (Lydon, 1984). Typically, VMS deposits take the form of a concordant lens that is underlain by a discordant stockwork or stringer zone comprising vein-type sulphide mineralization located in a pipe of hydrothermally altered rock. Lenses vary in shape from steep-sided cones to tabular sheets, which appear to have been associated with topographic highs and depressions, respectively. The contact between the lens and stringer zone is generally gradational, but the upper contact with hanging wall rocks is usually very sharp. A cross-section of an idealized VMS deposit is shown in Figure 41.

The most common sulphide mineral in VMS deposits is pyrite, which is accompanied by subordinate pyrrhotite, chalcopyrite, sphalerite and galena (Lydon, 1984). Magnetite, hematite and cassiterite are common non-sulphide metallic minerals. Densities of these minerals range from 4.0 to 7.5 g/cm^3 (Table 5), indicating that these minerals, singularly or in combination, will have a large density contrast with respect to densities of host rocks, some typical values of which (2.70 - 2.84 g/cm^3 for felsic volcanics and sediments) are listed in Table 6. Barite, a gangue mineral sometimes associated with sulphides, has a high density of 4.5 g/cm^3. In most cases, the magnetic susceptibilities of the ore or ore-related minerals of Table 5 are also considerably larger than those of host rocks. These distinctions in rock properties clearly mean that significant gravity and magnetic anomalies should be associated with sulphide deposits, thereby allowing direct detection of ore bodies through gravity and magnetic exploration. Theoretical potential field anomalies for a pyrrhotite-rich sulphide body having the form of a vertical sheet 20 m thick and extending to 300 m depth from the surface is shown in Figure 42.

Table 6 - Density (g/cm^3) & Magnetic Susceptibility (10^{-3} SI) Host Rocks to Sulphide Deposits, Bathurst Mining Camp		
Rock Type	Density	Susceptibility
Argillite, quartz wacke, siltstone (K)	2.74	1.1
Felsic volcanoclastics (K)	2.80	4.1
Crystal tuff (B)	2.84	0.1
Quartz eye schist (B)	2.81	0.4
Rhyolite, grey tuff (H)	2.70	0.3
Argillite, argillaceous sediments (C)	2.82	0.5
Acid tuff, rhyolite porphyry (C)	2.73	0.3
Interbedded siltstone & greywacke (W)	2.76	0.4
Siltstone (W)	2.81	0.6
Felsic schist & rhyolite (W)	2.73	0.2
Mafic tuffs, volcanoclastics (K)	2.91	30.0
Basalt (C)	2.82	0.5
Basalt (C)	2.89	41.0
Gabbro (C)	2.90	1.3
Gabbro (C)	2.94	0.6
Deposits: B, Brunswick No. 12; C, Canoe Landing Lake; H, Heath Steele; K, Key Anacon; W, Willett		

Gravity Signatures of Sulphide Deposits

A search of the literature indicates that one of the largest gravity anomalies associated with a sulphide deposit occurred over the Brunswick No. 6 deposit in the Bathurst mining camp, which was mined out after producing about 12 million tonnes (1 tonne is a metric ton = 1000 kilograms). A figure from Slichter (1955), reproduced as Figure 43, shows a positive anomaly, apparently superposed on a gentle eastward decreasing gradient, attaining about 4.5 mGal above background levels on the east side. Iron formation contributes to the anomaly, but the sulphide contribution dominates, having an amplitude of almost 4 mGal. The large size reflects essentially two characteristics of the body: (1) it was exposed at surface, and (2) it was relatively wide. It attained a width of about 75 m at surface, which increased to over 100 m at a depth of about 100 m, and from there it gradually wedged out, terminating at a depth of about 250 m. Thus width, down-dip extent, and depth of burial are the principal controls on anomaly amplitude, given a constant density contrast. Strike-length can also be an important factor, if it is relatively small, but once a critical length has been achieved, it becomes less significant. Therefore, there is not necessarily a relationship between tonnage and gravity anomaly amplitude, since an extremely long, relatively thin ore body could generate an anomaly having a smaller amplitude than that produced by a shorter, wider body of lower tonnage.

Another example of a significant gravity anomaly associated with a sulphide deposit at surface, is the estimated 3 mGal amplitude signal over the Mine Gallen body in the Abitibi Belt (Fig. 44). Pemberton (1989) describes the deposit as being 8 million tons, consisting of 3% zinc and containing gold and silver, and having a strike length of 275 m, a maximum width of 120 m and a depth of 150 m. Watkinson et al. (1990) note that the deposit comprises mainly pyrite with local

sphalerite content attaining 20%. In the section shown in Figure 44, the sulphide body is about 100 m wide at surface and is buried under some 5 to 10 m of overburden.

The effect of burying the geological section of the Brunswick No. 6 deposit at various depths up to 100 m deep is illustrated in Figure 43. At 100 m depth, the composite anomaly, ignoring the effect of the local gradient, has been reduced to roughly one-third of the amplitude for zero depth. Because of this reduction, the signature is smoother and less prominent, and probably would be less likely to be identified as a favourable target for follow-up investigations. A graph illustrating the effect of burial for an ore body 100 m wide, having a vertical extent of 250 m and a strike-length of 500 m, is presented in Figure 45. At 20 m depth, the amplitude of the gravity anomaly is already reduced to 80% of the anomaly for zero depth of burial, and at depths of 50 m and 100 m, it is reduced to 60% and 39%, respectively. A complementary graph for the effect of burial on a magnetic anomaly is included in the figure.

The host rocks to the Brunswick No. 6 deposit are identified simply as sediments and volcanics by Slichter (1955). In detail, the volcanics include mainly rhyolitic and felsic varieties and the sediments include quartz wackes, shales (schist) and tuffaceous components (Lentz, 1994). Densities of similar rock types in the Brunswick mining camp determined by the author are presented in Table 6 and are less than 2.85 g/cm^3. Slichter (1955) indicates a mean density for sediments and volcanics combined to be higher at 2.90 g/cm^3. Whatever the true density is, the distribution of rock types (Lentz, 1994) suggests that densities surrounding the sulphide body should not vary significantly. This is substantiated by the gravity profile, which is fairly symmetrical, apart from a slight tilt down to the east (Fig. 43). The only interference in the signal is caused by the iron formation, but in this case the sulphide anomaly is so strong that it does not pose a problem for exploration.

Geological "noise" can, however, distort or mask a signal related to a sulphide deposit. A good example is the signature over the Brunswick No. 12 deposit, the largest in the Bathurst mining camp, with past production and reserves totalling almost 150 million tonnes. The ore horizon attains a strike length of more than 1200 m, and in the section shown in Figure 46 has a similar depth extent, dipping steeply at 75°. The gravity field west of the body is between 2 and 4 mGal higher than it is to the east. This results from the considerable thickness of basaltic rocks on the west, in conjunction with their relatively high density of 2.90 g/cm^3, which compares with densities of 2.74-2.75 g/cm^3 for most sediments on the east side. From an exploration viewpoint, this is a complication, since the gravity expression of the ore body, which would take the form of a reasonably symmetrical high with an amplitude of about 3.5 mGal, is masked by a step-like anomaly. Only the eastern flank of the high is apparent, though a local peak rising about 0.8 mGal above background values to the immediate west marks the ore body. This would probably be flagged for further consideration in an exploration program.

Because of factors such as depth of burial and geological "noise" in the gravity signal, discrete anomalies having amplitudes as large as several mGal, such as the Bathurst No. 6 example, are probably quite rare. The explorationist must therefore give careful consideration to anomalies that are small as a few tenths of a mGal. The importance of such relatively small anomalies is demonstrated by the example of the Neves-Corvo sulphide deposits in Portugal. These deposits, lying at depths between 300 and 700 m, are estimated to exceed 250 million tonnes (Leca, 1990). An anomaly having an amplitude of 0.4 - 0.6 mGal associated with the deposits near Neves played a key role in their discovery (Leca, 1990). Not all such small anomalies signify such large deposits. In the Bathurst camp, for example, small anomalies of about 0.25 and 0.3 mGal are

associated with the Key Anacon No. 2 zone and CNE deposits, respectively. These have estimated tonnages of ~1.1 million tonnes (Irrinki, 1992) and ~208,000 tonnes (Whaley, 1992), respectively.

Gravity surveys are usually applied when favourable areas for detailed exploration are outlined on the basis of other methodologies, e.g. geochemical surveys. They are extremely useful as a follow-up tool for evaluating geochemical and electromagnetic (EM) anomalies. Strong EM anomalies may sometimes reflect graphitic horizons or even superficial deposits. Gaucher (1983) concludes that gravity is the only "objective" screening method that can be applied to the numerous EM conductors that exist, with the expectation of discovering most major sulphide bodies Gravity surveys are sometimes conducted on a regional basis to obtain systematic coverage. This is an approach commonly followed in the Iberian Pyrite Belt of Spain and Portugal, where there are at least 20 sulphide deposits larger than 100 million tonnes (Castelo Branco, personal communication 1996). Surveys are conducted on grids having cell dimensions of the order of a few hundred metres, e.g. 300 by 100 m, 200 by 200 m, 100 by 100 m. These grid sizes are appropriate for delineating anomalies associated with large deposits, for which the expected amplitude should be greater than about 0.5 mGal. Las Cruces deposit, in Spain, has an amplitude of 2.5 mGal, quite large when one considers that it is buried under about 150 m of younger sediments.

Gravity Estimation of Mass of Ore Reserves

Gravity has a unique utility in the evaluation of ore deposits, namely the estimation of reserves through the application of Gauss' theorem in potential theory. Unlike ambiguity associated with interpretation of the *distribution* of mass associated with a gravity anomaly, the *magnitude* of mass excess (excess is the product of the volume of the anomalous mass and the difference in density between the mass and the material which envelopes it) may be uniquely determined. A brief discussion based on Hammer (1945) follows. The total flux of force of attraction over any closed surface in a gravitational field of force equals $4\pi G$ times the total mass (M) enclosed by the surface:

$$\iint_s g_n dS = 4\pi GM....(1)$$

where g_n equals the inward component of gravitational attraction normal to the element (dS) of the surface, G equals the gravitational constant and M equals the total mass enclosed by the surface. The special case of Gauss' theorem applied to determination of mass is illustrated in Figure 47a, the closed surface enclosing a mass (M) being represented by a hemisphere. The diametral plane represents the Earth's surface.

In the case of a single point mass (M) positioned within a finite distance of the origin, integration of the normal component of gravitational attraction (g_n) over the infinite plane P equals $2\pi GM$, independant of the location of the mass.

$$\iint_P g_n dS = 2\pi GM....(2)$$

Likewise the integral over the infinite half sphere, S/2, equals $2\pi GM$.

$$\iint_{S/2} g_n dS = 2\pi GM....(3)$$

The sum of these two integrals is $4\pi GM$, and while the theory has been developed for a point mass, it applies to any finite body. For geophysical purposes, it is the integration over the plane P (equation 2), representing the surface of the Earth, that is of interest. If Δg is a local gravity anomaly, equation 2 may be rewritten as a practical formula for determining the anomalous mass producing the anomaly:

$$\Delta M = 1/2\pi G \iint_P \Delta g dS \ldots (4)$$

where Δg is the value of the gravity anomaly, and integration is to be carried out over the horizontal extent of the anomaly. This means that the size of the anomalous mass is determined by the total "volume" under the gravity anomaly (Fig. 47b). If the anomalous mass has a density of D_1 and is enclosed in rock of density D_2, the expression to the right of the equals sign in equation 4 must be multiplied by $D_1/(D_1 - D_2)$. With reference to Fig. 47b, it is important to note that incorrect selection of the datum, or zero value, of the anomaly can lead to significant error in estimating the volume. The "tails" of the anomaly actually extend far beyond the obvious part of the anomaly where the gradients are relatively steep. A datum has been incorrectly placed in the figure to illustrate the differences in "volume" under the curve, when different datums are used.

Estimation of the volume under an anomaly can be achieved by superposing a grid of points on the anomaly in map view. An example is shown in Figure 48, where the size of a grid cell is 40 m by 40 m. The volume is obtained by estimating the amplitude (Δg) of the gravity anomaly at all grid points, multiplying each one by the area (ΔS) of the grid cell, and summing the products. Once the volume is estimated, the total anomalous mass (M) may be calculated in metric (= 1000 kilograms), long (= 2240 pounds) or short (= 2000 pounds) tons by multiplying the volumes by 23.85, 2.18 (Parasnis, 1973) or 2.44 (Telford et al., 1982), respectively. These calculations may be expressed as the following formulae, derived from equation 4:

- $M = 23.85\ \Sigma(\Delta g \times \Delta s)$ metric tons (units: Δg, mGal; Δs, m^2).
- $M = 2.18\ \Sigma(\Delta g \times \Delta s)$ long tons (units: Δg, mGal; Δs, ft^2).
- $M = 2.44\ \Sigma(\Delta g \times \Delta s)$ short tons (units: Δg, mGal; Δs, ft^2).

Note that, as mentioned above, total anomalous mass is the difference between the actual ore body mass and a mass of host rock of identical shape. The mass of the ore body, however, is computed by multiplying the above expressions by the density of the ore body divided by the density of the ore body minus the density of host rock.

Magnetic Signatures of Sulphide Deposits

Of the sulphide minerals themselves, pyrrhotite has a large magnetic susceptibility (3200×10^{-3} SI - Table 5) and can be expected to produce prominent magnetic anomalies. Pyrite has a susceptibility of 5×10^{-3} SI, which is significantly larger than susceptibilities (0.1 to 1.1×10^{-3} SI - Table 6) of many sedimentary and volcanic units in the vicinity of several deposits in the Bathurst mining camp. According to Lydon (1984) pyrite is by far the most common sulphide mineral in a sulphide lens (Fig. 41). Thus, discernible positive signatures should be associated with deposits of significant size, and should provide pointers to any associated chalcopyrite, sphalerite or galena.

Chalcopyrite and sphalerite have susceptibilities (Table 5) differing little from those of the selected sedimentary and volcanic hosts, and probably would not generate a good signal. Galena has a very small negative susceptibility (Table 5), and also would not normally be expected to influence the magnetic field. Lydon (1984) observes that magnetite and hematite are two common non-sulphide metallic minerals occurring in sulphide lenses. The association of VMS deposits and magnetite, coupled with the large susceptibility of magnetite (5700 x 10^{-3} SI - Table 5), provides another "remote" sensor for sulphide species via the large anomalies expected to be produced by the magnetite. Magnetite tends to be concentrated in the core of the stockwork zone and central, basal part of the overlying sulphide lens (Lydon, 1984). Hematite, although having a much smaller susceptibility (40 x 10^{-3} SI - Table 5) than magnetite, has good potential to produce sizable positive signals.

The Ansil Cu-Zn-Au-Ag sulphide deposit in the Abitibi Belt is a good example of a deposit containing abundant magnetite, formed in response to late stage hydrothermal alteration (Fig. 49). The deposit includes a lens composed of sphalerite, pyrite, pyrrhotite and chalcopyrite, and a stockwork system extending hundreds of metres above and below the lens (Galley et al., 1995); the hanging wall stockwork is not present in the illustrated section. The late stage hydrothermal event produced a footwall magnetite stockwork vein system and was responsible for the replacement of some 300,000 tonnes of massive sulphide by magnetite. Disseminated magnetite is present in the immediate hanging wall.

Examples of magnetic anomalies across the Heath Steele C Zone and Stratmat Main Zone sulphide deposits in the Bathurst mining camp are shown in Figures 50 and 51, respectively. The magnetic high over the Heath Steele deposit is related to pyrrhotite, magnetite and ilmenite, and that over the Stratmat deposit to pyrrhotite. Both deposits contain, in addition, pyrite, sphalerite, galena and chalcopyrite.

A complicating factor in assessing positive magnetic anomalies in the search for sulphide deposits is a group of anomalies that may be produced by mafic volcanic rocks and gabbroic intrusions. Basalt, for example, may be relatively non-magnetic or strongly magnetic. In the Bathurst mining camp, for example, both types are observed near the Canoe Landing Lake deposit, the magnetic variety having a mean susceptibility as high as 41 x 10^{-3} SI (Table 6). Gabbro can likewise have large susceptibilities, although the examples of Table 6 have weak susceptibilities.

Not all magnetic signatures associated with sulphide deposits are necessarily positive. Deposits containing pyrrhotite, in particular, can give rise to negative anomalies . In a study of pyrrhotite-bearing rocks in the United Kingdom, Thomson et al. (1991) concluded that pyrrhotite commonly has intense remanent magnetizations and high Koenigsberger (Q) ratios, properties thought to explain associated large anomalies that frequently indicate reversed magnetizations (negative anomalies). They concluded further that pyrrhotite-rich rocks typically have Q ratios of around 10, indicating that magnetic anomalies related to pyrrhotite-bearing ore bodies will usually be caused by remanent magnetization. A good example of a negative anomaly ascribed to a body of pyrrhotite-bearing gneisses having a reversed magnetization direction (inclination = -80°) of presumed Tertiary age is shown in Figure 52; this example is from Germany. The gneisses themselves are Paleozoic, but the Tertiary magnetization is attributed to a thermal event that may have created a new magnetization in the syngenetic pyrrhotite of the Paleozoic gneiss (Pucher, 1994).

Some pyrrhotites acquire a remanent magnetization through a process of self-reversal of magnetization in the sense that the magnetization is reversed with respect to the direction of the applied field. Bina and Daly (1994) offer the following explanation for the self-reversal process in monoclinic pyrrhotite (Fe_7S_8). Partial oxidation of pyrrhotite grains in a magnetic field at temperatures greater than the Curie temperature (Tc) of the mineral produces fine-grained magnetite at the surface of the grain (Fig. 53), which acquires a chemical remanent magnetization (CRM) in the direction of the field. If the pyrrhotite grain is sufficiently large so that it does not become completely oxidized, when it cools in a zero field, on attaining Tc of pyrrhotite it would acquire a thermal remanent magnetization (TRM) in the interactive field of the CRM of the magnetite. The TRM direction would oppose that of the CRM. Depending on their relative proportions, a total reversed remanent magnetization could be obtained at room temperature. If the initial pyrrhotite is hexagonal, a layer below the outer magnetite layer may be changed into monoclinic pyrrhotite, which then acquires the reversed TRM (Fig. 53). Both phases may exist after partial oxidation.

Reversed remanent magnetizations are not the only cause of negative magnetic anomalies over sulphide deposits. Sometimes the host rocks may be more magnetic than the deposit. Such appears to be the case for the Mine Gallen sulphide deposit in the Abitibi Belt. A magnetic profile crossing the deposit, presented by Pemberton (1989), contains a local low of about 200 nT amplitude (Fig. 44). No comment is made on this relationship, but is assumed that the sulphide body, which comprises mainly pyrite with local sphalerite content attaining 20% (Watkinson et al., 1990), has relatively low magnetic susceptibilities compared to those of enveloping mainly felsic volcanic rocks and granodiorite.

Pathfinder Magnetic Signatures

Anomalies produced as a result of the sulphide-forming process, but which are not related directly to the ore deposit itself, can provide an indirect indication of the possible presence of sulphide deposits. Two kinds of these anomalies are examined in the context of a genetic model for sulphide formation.

Magnetic Anomalies Related to Iron Formations: Large (1977) proposed that metal-bearing hydrothermal solutions moving upward through oceanic crust (volcanics and sediments) on to the sea floor will undergo chemical changes during mineralization, largely controlled by the degree and rate of mixing with sea water. Temperature, pH, oxygen fugacity and total sulphur content are critical parameters. Grant (1985b) describes the paragenesis for minerals in the Fe-S-O system and for chalcopyrite, sphalerite and galena, with reference to an oxygen fugacity (fO_2)-temperature plot adapted from Large (1977), reproduced here with minor modification as Figure 54. A hot hydrothermal solution on rising in a volcanic vent mixes with downward-percolating sea water, undergoes a sudden decrease in pH and temperature; the temperature of the mixture is in the range 250°C-300°C. These changes and the availability of sulphur induces the precipitation of metals. The paragenesis for the cooling path A in Figure 54 is as follows. The first mineral to form is pyrrhotite, followed by magnetite. Then chalcopyrite and pyrite form, followed by sphalerite, chalcopyrite and pyrite, with or without galena. These minerals are formed within or close to the vent producing the typical polymetallic sulphide deposit as shown in Figure 41, which has the characteristic bottom to top Fe-Cu-Zn (± Pb) zoning. If the sea water contained more

sulphur or the pH was significantly lower than assumed, the pyrrhotite-magnetite boundary would move up, and no magnetite would be deposited within the vent. This might account for the lack of magnetite in the Kidd Creek deposit (Grant, 1985b). In this context, compared to modern oceans, the Archean ocean may have been relatively enriched in reduced sulphide species (Large, 1977).

As the hydrothermal solutions travel away from the vent, their temperature continues to drop, and by the time it is less than about 200°C, the cooling path A (Fig. 54) has moved into the field of magnetite or pyrite. These minerals may be precipitated over a broad region away from the vent, forming a blanket of iron-rich sediments. They are often cherty and are referred to as iron formations or exhalites. The mineral field will depend on pH and sulphur content. At this stage, the solutions continue to carry some dissolved Zn or Pb, but not very much Cu (Grant, 1985b). Zn and Pb may be carried to distal anoxic regions of the sea floor where they are precipitated as banded sulphide deposits. According to this genetic model, the iron formations represent a marker horizon linking proximal and distal sulphide deposits (Fig. 55). They have been recognized throughout the world in geological settings ranging in age from the Archean (Noranda mining camp) to the present (Red Sea) (Grant, 1985b).

Importantly, they may be associated with strong magnetic signatures, which provide desirable targets for exploration. Good examples are positive anomalies associated with iron formations in the Brunswick and Heath Steele belts of the Bathurst mining camp. A magnetic susceptibility log for drill core containing iron formation from hole 5175 on the property of the Brunswick No. 12 deposit is shown in Figure 56. The response of iron formations and chloritic iron formations is variable. The lower, thicker layer of iron formation is characterized by high susceptibilities that are generally $>175 \times 10^{-3}$ SI and range up to 3700×10^{-3} SI. This is not surprising considering that the unit comprises mainly layered magnetite-chert. The upper layer consisting of layered siderite-chert and intermixed siderite-chert and magnetite-chert has yielded generally low susceptibilities. This probably reflects a preponderance of siderite-chert. A single value $>525 \times 10^{-3}$ SI can be attributed to magnetite-chert. The upper layer of chloritic iron formation is also characterized by relatively low susceptibilities ($<10 \times 10^{-3}$ SI), whereas the lower unit produces values between about 10 and 90×10^{-3} SI. The lack of strong susceptibility signatures can be tied to the mainly chloritic-sideritic nature of these units. Magnetic susceptibilities of sulphides in Brunswick No. 12 hole 5175 are generally on the order of only a few tens $\times 10^{-3}$ SI at most. The sulphide minerals are mainly pyrite and sphalerite.

Magnetic Anomalies Associated with Hydrothermal Alteration Zones: Hydrothermal alteration of the host rocks is strongly developed in stockwork zones underlying massive sulphide deposits, typically consisting of an inner chloritized core surrounded by a sericitized mantle (Fig. 41) (Lydon, 1984). The chloritic core is characterized by major additions of iron and magnesium, and by the loss of calcium, sodium and silicon. Potassium also tends to be depleted in the core, but is enriched in the sericitic zone, which seems to represent a zone of transition between fresh host rock and the chloritic core. Hanging wall alteration has been observed above some deposits (Lydon, 1984).

Alteration is not necessarily confined to the margins of the sulphide deposit. It is observed to extend laterally over a wide area below the favourable horizon in several mining areas (Lydon, 1984). Examples up to several hundreds metres thick and several kilometres long are cited. Govett (1989), discussing geochemical anomalies, refers to aureoles that extend 500 m or more vertically in a stratigraphic sense, and up to 2 km laterally. Thus alteration occurs on a regional

scale and offers a much larger target than the ore body itself. As far as magnetic detection of these alteration zones is concerned, one must ask the question "Are the geochemical changes with their attendant enrichment or depletion of elements manifested in mineralogical changes leading to the enrichment or depletion of magnetic minerals?". Grant (1985b) draws attention to the possibility of detecting alteration zones by high resolution magnetic surveys, suggesting that they "can often be perceived as areas of abnormally suppressed magnetic activity", but gives no details. A search of the literature has so far failed to uncover many detailed descriptions of mineralogical changes in the alteration zones that might affect their magnetization in a significant manner.

One exception is an example of an anomaly related to alteration in the vicinity of the Agrokipia ore bodies hosted by ophiolitic rock of the Troodos Massif, Cyprus (Johnson et al., 1982). An intense magnetic low in the vertical magnetic field, located to one side of the Agrokipia 'A' ore body, has an amplitude of about 5000 nT below local background (Fig. 57). It is "approximately twice the size of the original sulphide deposit" (Johnson et al., 1982). Assuming this to refer to horizontal dimensions, it is noted that the maximum width of the anomaly is about 250 m. The ore body itself is described as being surrounded by a magnetic high on two sides, but this anomaly is not included in the figure since it was defined by measurements of the total field. The anomaly is attributed to intense hydrothermal alteration of basaltic lavas, which have been demagnetized by alteration of silicates to clay, silica and chlorite, and by replacement of iron-titanium oxides by pyrite.

Tivey et al. (1993) and Wooldridge et al. (1992) have described areas of relatively low magnetic field from several sites on mid-oceanic ridges. They conclude that many lows are related in large part to hydrothermal alteration of oceanic crust. Within the TAG hydrothermal field on the Mid-Atlantic Ridge, a magnetic low coinciding with an active sulphide mound ($\approx$200 m diameter) is attributed to intense hydrothermal activity within a vent system feeding the growth of the mound (Tivey et al., 1993). Associated alteration is believed to have destroyed any original magnetic minerals in the basaltic oceanic crust, magnetite being replaced by non-magnetic sphene. Tivey et al. (1993) also address the source of a broader magnetic low, covering an area of roughly 2 by 8 km. Their preferred explanation is that it reflects a deeper thermal and alteration zone controlled by a hydrothermal system that may be related to late-stage intrusive bodies. The respective contributions of thermal demagnetization and hydrothermally induced magnetization are impossible to estimate. If the latter is significant and survives with age, and the occurrence of anomalies over ophiolites (Johnson et al., 1982) demonstrates that this is possible, then such related magnetic signatures provide preferred targets for exploration. Because such magnetic lows are related to demagnetization effects in modern seafloor (and ophiolitic rocks), it might be expected that such fossil signatures will be associated more commonly with the Cu-Zn type of sulphide deposit, for which the most common regional footwall rock type is mafic volcanic rocks (Lydon, 1984) They would not be expected for the Zn-Pb-Cu type of deposit, floored by mainly felsic volcanic rocks and fine-grained sediments.

SUMMARY

This report has touched on a number of topics in introducing the reader to some of the fundamental concepts regarding the understanding and interpretation of gravity and magnetic maps, and their utility in the exploration for massive sulphide deposits. Further information may be obtained from the cited references, several of which are recommended as essential reading.

These include: Breiner (1981), a concise account of the basics of measurement and processing of magnetic data, Earth's magnetic field, magnetization of geological bodies and simple interpretation of anomalies; Grant (1985a), an excellent overview of magnetite in igneous, sedimentary and metamorphic rocks; Grant (1985b), a must for explorationists - a succinct examination of magnetite and ore environments; Reynolds et al. (1990), a review that includes a description of magnetic minerals in igneous, metamorphic and sedimentary rocks, magnetization and ore deposits, magnetization related to exploration for hydrocarbons and sandstone-hosted uranium deposits; Clark and Emerson (1991), a summary of magnetic susceptibilities and remanent magnetizations in rocks. Finally, for those wishing to explore the subject of gravity and magnetic interpretation in more detail, a set of notes published by the Canadian Geophysical Union (Goodacre and Keating, 1996) is highly recommended. This complements the material presented herein.

ACKNOWLEDGEMENTS

I am very grateful to several colleagues at the Geological Survey of Canada for various forms of assistance: Al Galley and John Lydon for information on sulphide deposits and digital graphics files, Warner Miles for data processing and digital images, Azad Rafeek for digital drafting and Wayne Goodfellow for continued support of the geophysical component of EXTECH II program. Thanks are due also to Diane Jobin of Geomatics Canada for gravity data and images, and to Graham Ascough of Noranda Exploration Co. Ltd. for geophysical profiles and geological sections. Finally, I thank Alan Goodacre and Ian Jonasson of the Geological Survey of Canada for their care and patience in reviewing these notes, and for the helpful ensuing comments.

BIBLIOGRAPHY

Baranov, V. 1957. A new method for interpretation of aeromagnetic maps: pseudo-gravimetric anomalies. Geophysics, v. 22, 359-382.

Bible, J. L. 1962. Terrain correction tables for gravity. Geophysics, v. 27, 715-718.

Bina, M. and Daly, L. 1994. Mineralogical change and self-reversed magnetizations in pyrrhotite resulting from partial oxidation; geophysical implications. Physics of the Earth and Planetary Interiors, v. 85, 83-99.

Bott, M.H.P. and Smith, R.A. 1958. The estimation of the limiting depth of gravitating bodies. Geophysical Prospecting, v. 6, 1-10.

Boyd, J.B., Gibb, R.A., and Thomas, M.D. 1975. A gravity investigation within the Agricola Lake geochemical anomaly, District of Mackenzie. Geological Survey of Canada, Paper 75-1, Part A, 193-198 (check for final).

Breiner, S. 1981. Applications for portable magnetometers. Chapter 5 In Practical Geophysics for the Exploration Geologist, Compiled by R. Van Blaricom. Northwest Mining Association, Spokane, 205-237.

Broome, J. 1991. Display and enhancement of aeromagnetic data with examples from Guysborough County, Nova Scotia. Chapter 11 In Interpretation of Gravity and Magnetic Anomalies for Non-Specialists. Canadian Geophysical Union, 255-291.

Carmichael, R.S. 1982. Magnetic properties of minerals and rocks. Chapter 2 In Handbook of Physical Properties of Rocks. Edited by R.S. Carmichael. CRC Press Inc., Boca Raton, Florida, 229-287.

Clark, D.A. 1983. Comments on magnetic properties. Bulletin of the Australian Society of Exploration Geophysicists, v. 14, 49-62.

Clark, D.A. and Emerson, D.W. 1991. Notes on rock magnetization characteristics in applied geophysical studies. Exploration Geophysics, v. 22, 547-555.

Cordell, L. and McCafferty, A.E. 1989. A terracing operator for physical property mapping with potential field data. Geophysics, v. 54, 621-634.

Galley, A.G., Watkinson, D.H., Jonasson, I.R., and Riverin, G. 1995. The subsea-floor formation of volcanic-hosted massive sulfide: Evidence from the Ansil deposit, Rouyn-Noranda, Canada. Economic Geology, v. 90, 2006-2017.

Gaucher, E. 1983. Estimation of sulphide content of a potential orebody from surface observations and its role in optimising exploration programmes. Chapter 1 In Developments in

Geophysical Exploration Methods - 4, Edited by A.A. Fitch, Applied Science Publishers Ltd., London, 1-37.

Geodetic Reference System 1967. 1971. International Association of Geodesy, Special Report No. 3, 116 pp.

Goodacre, A. and Keating, P. (Editors). 1996. Notes based on Canadian Geophysical Union Short Course: Interpretation of Gravity and Magnetic Anomalies for Non-Specialists. Canadian Geophysical Union.

Govett, G.J.S. 1989. Paper 25. Bedrock geochemistry in mineral exploration. In Proceedings of Exploration '87, Third Decennial International Conference on Geophysical and Geochemical Exploration for Minerals and Groundwater. Edited by G.D. Garland. Ontario Geological Survey, Special Volume 3, 273-299.

Grant, F.S. 1985a. Aeromagnetics, geology and ore environments, I. Magnetite in igneous, sedimentary and metamorphic rocks: An overview. Geoexploration, v. 23, 303-333.

Grant, F.S. 1985b. Aeromagnetics, geology and ore environments, II. Magnetite and ore environments. Geoexploration, v. 23, 335-362.

Hammer, S. 1939. Terrain corrections for gravimeter stations. Geophysics, v. 4, 184-194.

Hammer, S. 1943. Note on the variation from equator to pole of the Earth's gravity. Geophysics, v. 8, 57-60.

Hammer, S. 1945. Estimating ore masses in gravity prospecting. Geophysics, v. 10, 50-62.

Hannington, M.D., Jonasson, I.R., Herzig, P.M., and Petersen, S. 1995. Physical and chemical processes of seafloor mineralization at mid-ocean ridges. In Seafloor Hydrothermal Systems, Physical, Chemical, Biological and Geological Interactions. Geophysical Monograph 91, American Geophysical Union, 115-157.

Hood, P. and McClure, D.J. 1965. Gradient measurements in ground magnetic surveying. Geophysics, v. 30, 403-410.

Hood, P. and Teskey, D.J. 1989. Aeromagnetic gradiometer program of the Geological Survey of Canada. Geophysics, v. 54, 1012-1022.

Hunt, C.P., Moskowitz, B.M., and Banerjee, S.K. 1995. Magnetic properties of rocks and minerals. In Rock Physics and Phase Relations, a Handbook of Physical Constants. AGU Reference Shelf 3. Edited by T.J. Ahrens. American Geophysical Union, 189-204.

Irrinki, R.R. 1992. Key Anacon sulfide deposit, Gloucester County, New Brunswick. Exploration and Mining Geology, v. 1, 121-129.

Johnson, H.P., Karsten, J.L., Vine, F.J., Smith, G.C., and Schonharting, G. 1982. A low-level magnetic survey over a massive sulfide ore body in the Troodos ophiolite complex, Cyprus. Marine Technology Society Journal, v. 16, 76-80.

Keckler, D. 1994. Surfer[R] for Windows, User's Guide. Golden Software Inc., Golden, Colorado.

Large, R.R. 1977. Chemical evolution and zonation of massive sulfide deposits in volcanic terrains. Economic Geology, v. 72, 549-572.

Leca, X. 1990. Discovery of concealed massive-sulphide bodies at Neves-Corvo, southern Portugal - a case history. Transactions of the Institution of Mining and Metallurgy (Section B,: Applied Earth Science), v. 99, B139-B152.

Lentz, D.R. 1994. A gamma-ray spectrometric study of the footwall felsic volcanic and sedimentary rocks around Brunswick No. 6 massive sulphide deposit, northern New Brunswick. In Current Research 1994-D, Geological Survey of Canada, 135-141.

Lydon, J.W. 1984. Volcanogenic massive sulphide deposits, Part 1: a descriptive model. Geoscience Canada, v. 11, 195-202.

Milsom, J. 1989. Field Geophysics. Geological Society of London Handbook. Open University Press, Milton Keynes, 182 pp.

Newitt, L.R. and Haines, G.V. 1990. Total intensity chart of Canada 1990.0. Geological Survey of Canada, Canadian Geophysical Atlas, Map 8, (1:10,000,000).

Parasnis, D.S. 1973. Mining Geophysics. Elsevier, Amsterdam, 395 pp.

Payne, M.A. 1981. SI and Gaussian CGS units, conversions and equations for use in geomagnetism. Physics of the Earth and Planetary Interiors, v. 26, P10-P16.

Pemberton, R.H. 1989. Paper 40. Geophysical response of some Canadian massive sulphide deposits. In Proceedings of Exploration '87, Third Decennial International Conference on Geophysical and Geochemical Exploration for Minerals and Groundwater. Edited by G.D. Garland. Ontario Geological Survey, Special Volume 3, 517-531.

Piper, J.D.A. 1987. Palaeomagnetism and the Continental Crust. Open University Press, Milton Keynes and Halsted Press, John Wiley and Sons, New York, 434 pp.

Pucher, R. 1994. Pyrrhotite-induced aeromagnetic anomalies in western Germany. Journal of Applied Geophysics, v. 32, 33-42.

Reynolds, R.L., Rosenbaum, J.G., Hudson, M.R., and Fishman, N.S. 1990. Rock magnetism, the distribution of magnetic minerals in the Earth's crust, and aeromagnetic anomalies. In Geologic

Applications of Modern Aeromagnetic Surveys. Edited by W.F. Hanna. U.S. Geological Survey Bulletin 1924, 24-45.

Sharpton, V.L., Grieve, R.A.F., Thomas, M.D., and Halpenny, J.F. 1987. Horizontal gravity gradient: An aid to the definition of crustal structure in North America. Geophysical Research Letters, v. 14, 808-811.

Shive, P.N. 1986. Suggestions for the use of SI units in magnetism. EOS, v. 67, p. 25.

Skeels, D.C. 1947. Ambiguity in gravity interpretation. Geophysics, v. 12, 43-56.

Slichter, L.B. 1955. Geophysics applied to prospecting for ores. Economic Geology Fiftieth Anniversary Volume, 1905-1955, Part II, 885-969.

Strangway, D.W. 1981. Magnetic properties of rocks and minerals. Chapter 10 In Physical Properties of Rocks and Minerals. Edited by Y.S. Touloukian, W.R. Judd, and R.F. Roy. McGraw-Hill/CINDAS Data Series on Material Properties, Volume II-2, McGraw-Hill Book Company, New York, 331-360.

Telford, W.M., Geldart, L.P., Sheriff, R.E., and Keys, D.A. 1982. Applied Geophysics, Cambridge University Press, 860 pp.

Thomas, M.D., Sharpton, V.L., and Grieve, R.A.F. 1987. Gravity patterns and Precambrian structure in the North American Central Plains. Geology, v. 15, 489-492.

Thomas, M.D., Tanczyk, E.I, Cioppa, M., and O'Dowd, D.V. 1991. Ground magnetic and rock magnetism studies near the Appalachian Dunnage-Gander terrane boundary, northern New Brunswick. In Current Research, Part D, Geological Survey of Canada, Paper 91-1D, 169-178.
Thompson, R. and Oldfield, F. 1986. Environmental Magnetism. Allen and Unwin, London, 227 pp.

Thomson, G.F., Cornwell, J.D., and Collinson, D.W. 1991. Magnetic characteristics of some pyrrhotite-bearing rocks in the United Kingdom. Geoexploration, v. 28, 23-41.

Tivey, M.A., Rona, P.A., and Schouten, H. 1993. Reduced crustal magnetization beneath the active sulfide mound, TAG hydrothermal field, Mid-Atlantic Ridge at 26° N. Earth and Planetary Science Letters, v. 115, 101-115.

Watkinson, D.H., McEwen, J., and Jonasson, I.R. 1990. Mine Gallen, Noranda, Quebec: Geology of an Archean massive sulphide mound. In The Northwestern Quebec Polymetallic Belt. Edited by M. Rive, P. Verpaelst, Y. Gagnon, J.M. Lulin, G. Riverin and A. Simar. Canadian Institute of Mining, Special Volume 43, 167-174.

Whaley, K.D.A. 1992. The Captain North Extension zinc-lead-silver deposit Bathurst District, New Brunswick. Exploration and Mining Geology, v. 1, 143-150.

Wooldridge, A.L., Harrison, C.G.A., Tivey, M.A., Rona, P.A., and Schouten, H. 1992. Magnetic modeling near selected areas of hydrothermal activity on the Mid-Atlantic and Gorda ridges. Journal of Geophysical Research, v. 97, 10911-10926.

FIGURE CAPTIONS

Fig. 1: Shape of Earth approximated by an ellipsoid. Polar and equatorial radii are indicated (not to scale). Polar and equatorial gravity fields are based on the formula for the theoretical value of gravity (reference). The difference between the two values (5.19 Gal) is slightly different from the 5.17 Gal value calculated much earlier by Hammer (1943), which is discussed in the text.

Fig. 2: Gravity survey on land comprising several observations (G_{obs}) reduced to Bouguer anomalies on a sea level datum by applying free air and Bouguer corrections, and subtracting the theoretical gravity value (G_t) on the geoid for that particular latitude.

Fig. 3: Earth's magnetic field schematically represented by lines of force as produced by a theoretical bar magnet.

Fig. 4: Vector diagram illustrating declination (D) and inclination (I) of Earth's magnetic field (F). H and V represent horizontal and vertical components of the field, respectively.

Fig. 5: Comparison of grey-tone Bouguer gravity anomaly (gravity stations represented by dots) and total magnetic field maps covering an area of the southern margin of the Trans-Hudson Orogen and adjacent Phanerozoic cover. Selected geological features are superposed. NFSZ, Needle Falls Shear Zone; WB, Wathaman Batholith; BRSB, Birch Rapids Straight Belt (part of Rottenstone Domain); GT, Guncoat Thrust; SSZ, Stanley Shear Zone; IC, Istwatikan Complex; HBD, Hunter Bay Dome; HSZ, Hartley Shear Zone. Heavy line marks southern margin of Canadian Shield. Dashed lines represent shear zones and faults.

Fig. 6: Comparison of data set comprising 21 x 21 values (white dots) contoured at intervals of (a) 0.5 and (b) 2.0 mGal. H and L designate gravity highs and lows, respectively.

Fig. 7: Simplified geological map of part of Flin Flon - Snow Lake Belt and its boundary with the South Flank of the Kisseynew Gneiss Belt. Bouguer gravity contours at 5 mGal intervals are superposed.

Fig. 8: Comparison of contoured gravity data in area of Canoe Landing Lake sulphide deposit, Bathurst mining camp, contoured automatically using grid cells measuring 100 m (a) and 10 m (b). A search radius of 1250 m was used in each case.

Fig. 9: Comparison of magnetic field measured at 305 m elevation and at ground level (after Thomas et al., 1991, Fig. 7); scales for the profiles are on the right and left, respectively. The ground profile is modelled with a number of magnetic bodies, whose induced magnetizations, indicated by the numbers within, are in units of 10^{-2} A/m.

Fig. 10: Classification of igneous rocks according to quartz content, ratio of alkali to total feldspar, feldspar composition and content and mafic mineral content. Volcanic equivalents of plutonic rocks are italicized.

Fig. 11: Influence of mafic mineral (olivine) content on the density of the anorthosite-troctolite series of plutonic rocks.

Fig. 12: Schematic illustration of effect of external magnetizing field (H) on a material having a susceptibility = k. M is the induced magnetization of the material, which equals kH.

Fig. 13: Ranges of ratios of remanent to induced magnetization, Koenigsberger ratio (Q), for various rock types (after Clark and Emerson, 1991, Fig. 6). The dark sections represent the ranges of the most commonly occurring Q values.

Fig. 14: Ternary phase diagram of iron and titanium oxides (after Clark and Emerson, 1991, Fig. 1).

Fig. 15: Ternary phase diagram of iron and titanium oxides illustrating the compositions of natural titanomagnetites and ilmenites in igneous rocks (after Piper, 1987, Fig. 2.2).

Fig. 16: Ranges of magnetic susceptibilities for various minerals and rock-types (modified from Clark and Emerson, 1991, Fig. 3). Distributions of susceptibilities are commonly bimodal; modal ranges are indicated by dark sections.

Fig. 17: Effect of isostatic compensation on Bouguer gravity profile related to two positive masses (+) in the crust. Upper panel shows a Bouguer profile reduced to sea level for a section of crust with a topographic load that is supported by the strength of the crust. Lower panel shows the corresponding profile when the topographic load is supported by an isostatically-compensating crustal root.

Fig. 18: Bouguer gravity map of area in southwestern Alberta (contour interval 5 mGal). Dashed contours represent the regional component of the Bouguer gravity field (contour interval 5 mGal) determined by polynomial regression.

Fig. 19: Isostatic gravity map of area in southwestern Alberta (contour interval 5 mGal).

Fig. 20: Residual Bouguer gravity anomaly map of area in southwestern Alberta (contour interval 5 mGal).

Fig. 21: **(a)** Bouguer gravity profile across a vertical geological boundary. The horizontal gradient of a section of the profile is defined as change in gravity (X) divided by the distance (Y) over which the change takes place.

(b) Plot of horizontal gradient corresponding to Bouguer profile based on gradient values computed for 5 sections of the profile.

Fig. 22: Grey-tone Bouguer gravity anomaly map of part of the Trans-Hudson Orogen. Each grey tone represents 5 mGal. Contour lines are added at 10 mGal intervals.

Fig. 23: Grey-tone horizontal gradient of Bouguer gravity anomaly map of part of the Trans-Hudson Orogen.

Fig. 24: Grey-tone vertical gradient of Bouguer gravity anomaly map of part of the Trans-Hudson Orogen. The zero value contour, which theoretically coincides with steep boundaries is added.

Fig. 25: **(a)** Bouguer gravity anomaly map of part of the Trans-Hudson Orogen (contour interval 10 mGal). Contours with values < -40 mGal are dashed; values≥ -40 mGal are solid.

(b) Horizontal gradient of Bouguer gravity anomaly (contour interval 0.5 mGal/km).

(c) Vertical gradient of Bouguer gravity anomaly (contour interval 0.4 mGal/km). Contours with values less than zero are dashed; other contours are solid.

The large dots in all figures are based on dots originally placed on linear horizontal gradient features A, B and C in **(b)**.

Fig. 26: Schematic representation of derivation of vertical gradient from gravity curves computed at ground level and at 2.5 km elevation.

Fig. 27: Gravity profile corresponding to geological section, and the terrace function derived from it.(after Cordell and McCafferty, 1989, Fig. 2). The sheet-like geological section extends between 0.3 and 2 km depth and comprises several discrete blocks. Densities of blocks in g/cm^3 are indicated.

Fig. 28: Grey-tone total magnetic field anomaly map of part of the Trans-Hudson Orogen.

Fig. 29: Shaded relief aeromagnetic map of part of the Slave Province produced by illumination directed along 245°.

Fig. 30: Shaded relief aeromagnetic map of part of the Slave Province produced by illumination directed along 155°.

Fig. 31: Vertical gradient of the total magnetic field map for part of the Trans-Hudson Orogen.

Fig. 32: Pattern of lines of force around a body magnetized by the Earth's field, distribution of positive and negative magnetizations and the resulting magnetic profile (after Milsom, 1989, Fig. 3.8).

Fig. 33: Example of total field magnetic anomaly over a vertical prism of infinite length, before (left) and after (right) being reduced to the pole (pseudo-gravimetric anomaly) (after Baranov, 1957, Fig. 7).

Fig. 34: Example of local anomaly related to granite body superposed on regional gradient caused by sloping interface between gneiss units.

Fig. 35: Contoured gravity map showing small positive anomaly superposed on a linear belt of "regional" gradient, whose position under the positive anomaly has been interpolated. Contour interval 0.1 mGal.

Fig. 36: Residual gravity anomaly derived from Figure 35.

Fig. 37: Gravity anomaly across a vertical contact (step).

Fig. 38: Two methods for estimating the depth to the top of a magnetic body (after Milsom, 1989, Figs. 3.9 and 3.10).

Fig. 39: Demonstration of the ambiguity inherent in gravity modelling (after Skeels 1947, Fig. 1). Relief on each of the seven boundaries produces a close match (to within 0.1 mGal) with the gravity profile. The density contrast across the boundaries is the same in all cases (0.2 g/cm^3).

Fig. 40: Illustration of horizontal polygonal prism used to approximate geological bodies in modelling studies.

Fig. 41: Idealized cross section through volcanogenic massive sulphide deposit (after Lydon, 1984, Fig. 2).

Fig. 42: Gravity and magnetic signatures calculated for a theoretical vertical, pyrrhotite-rich ore body in the Bathurst mining camp, 20 m wide, 300 m deep and 300 m strike-length. The magnetic signature is computed at a flight elevation of 50 m. Host rocks are assumed to have a density of 2.8 g/cm^3 and to be non-magnetic. The indicated rock properties are based on the author's work in the camp.

Fig. 43: Observed gravity profile, geological section and densities for the Brunswick No. 6 sulphide deposit (after Slichter, 1955). Model gravity curves for different depths of burial to the top surface of the section are indicated. These curves incorporate a component simulating a gentle gradient that decreases eastward.

Fig. 44: Gravity and magnetic signatures over the Mine Gallen ore body (after Pemberton, 1989, Fig. 40.7).

Fig. 45: Graph of amplitude of anomaly (gravity and magnetic) as a percentage of the amplitude observed for zero depth of burial, versus depth of burial for a vertical tabular ore body. The density contrast between ore and host rocks is 1.4 g/cm^3. The magnetization of the ore body is 6.2 A/m, based on a field strength of 55,800 nT and a susceptibility of 140×10^{-3} SI. A magnetic inclination and declination of 72° and 339°, respectively, were used in the computations. The host rocks are assumed to be non-magnetic.

Fig. 46: Geological section and observed and model gravity profiles across the Brunswick No. 12 sulphide deposit. Densities for the geological units are in g/cm^3. Figure is courtesy of Graham Ascough, Noranda Exploration Co. Ltd.

Fig. 47: Modification of figures (Figs. 2 and 3) from Hammer (1945) relating to estimation of mass of ore bodies from their gravity signature.

(a) Special case of Gauss' theorem in which the diametral plane of a hemisphere enclosing a point mass (M) is analogous to the surface of the Earth.

(b) Schematic illustration of "volume" under an anomaly using a profile presentation. Figure also illustrates how errors in estimation of volume can arise from the incorrect selection of the background field or datum. Three formulae for the estimation of mass (M) are given.

Fig. 48: Map of gravity anomaly over the Udden sulphide deposit, Sweden, with superposed 40 m grid (dots) (modified from Parasnis, 1973, Fig. 100A).

Fig. 49: Cross section of Ansil sulphide deposit, Abitibi belt (modified from Galley et al., 1995, Fig. 3).

Fig. 50: Magnetic profile across the Heath Steele C Zone sulphide deposit. Profile and geological section provided by Graham Ascough, Noranda Exploration Co. Ltd., Bathurst.

Fig. 51: Magnetic profile across the Stratmat Main Zone sulphide deposit, provided by Graham Ascough, Noranda Exploration Co. Ltd., Bathurst.

Fig. 52: Example of reversed magnetization related to pyrrhotite-bearing gneiss, Germany (modified from Pucher, 1994, Fig. 7).

Fig. 53: Schematic cross section of hexagonal pyrrhotite grain showing development of surface layer of magnetite by partial oxidation, which acquires a chemical remanent magnetization (CRM) in the direction of the applied field. A layer of monoclinic pyrrhotite may be formed underneath, having a lower Fe/S ratio, that carries a reversed thermoremanent magnetization in the interactive field of the CRM (after Bina and Daly, 1994, Fig. 13).

Fig. 54: Paragenesis of minerals in the Fe-S-O system with respect to oxygen fugacity (fO_2) versus temperature (after Grant, 1985b, Fig. 3, adapted from Fig. 12 of Large, 1977).

Fig. 55: Schematic cross section illustrating connection between proximal ores, exhalites and distal ores on the oceanic floor (after Grant, 1985b, Fig. 6, adapted from Fig. 13 of Large, 1977).

Fig. 56: Density and magnetic susceptibility logs of core from Brunswick No. 12 hole 5175, Bathurst mining camp.

Fig. 57: Profiles of magnetic anomaly over sulphide ore bodies hosted by ophiolitic rocks of the Troodos Massif (after Johnson et al., 1982, Fig. 2). Positions of A and B are projected onto the section.

TABLES

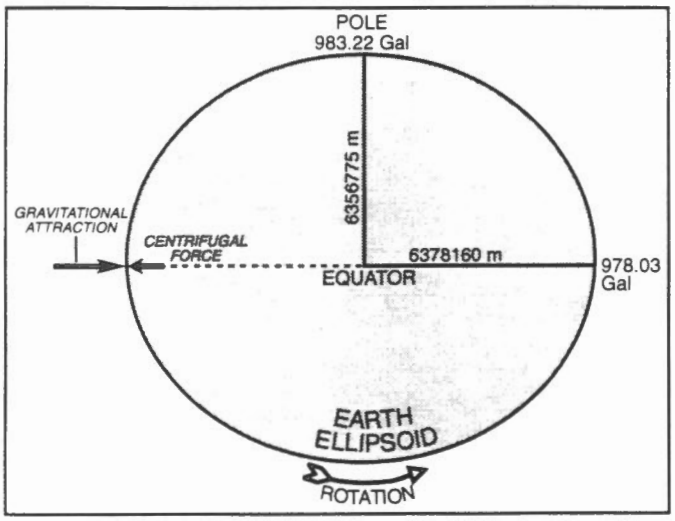

FIGURE 1

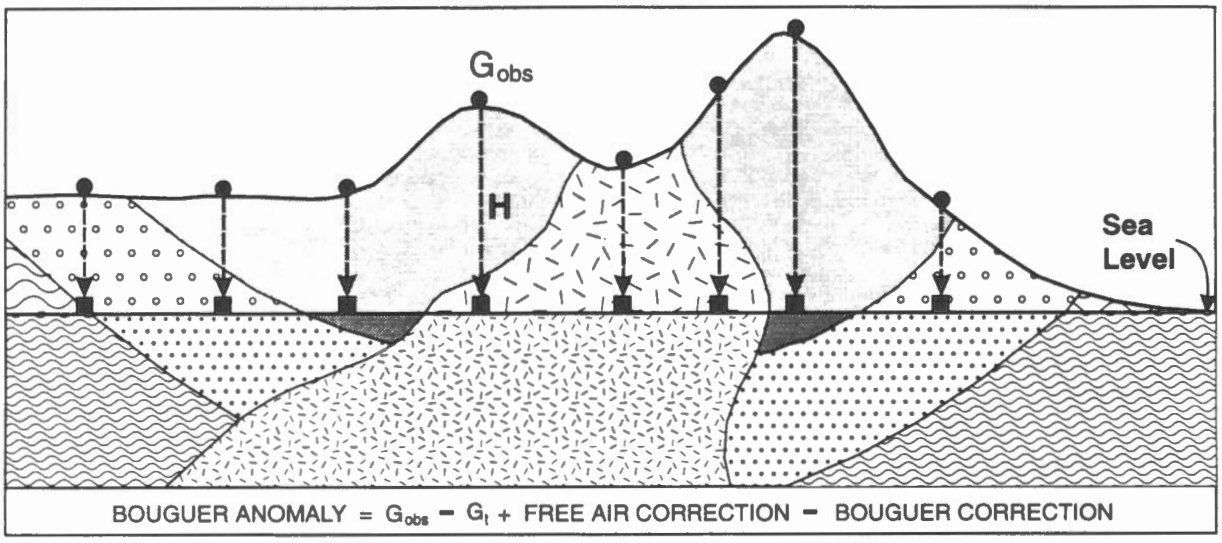

FIGURE 2

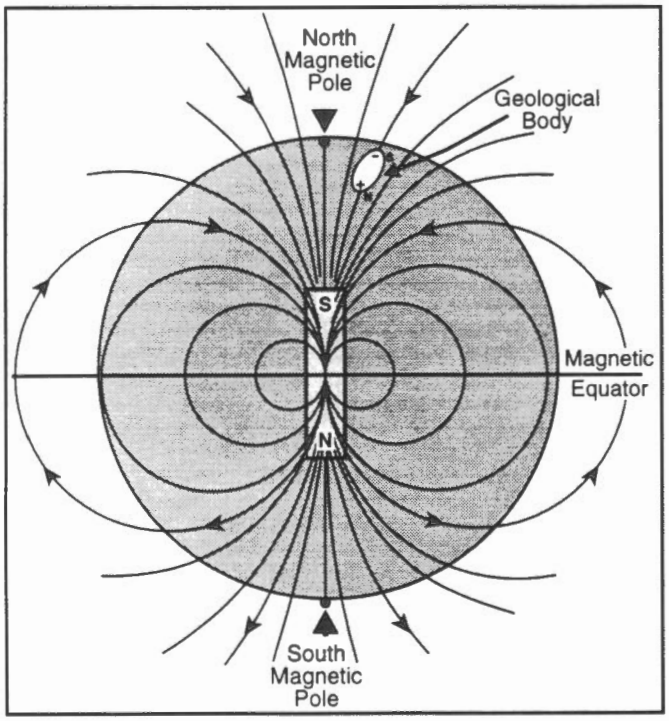

FIGURE 3

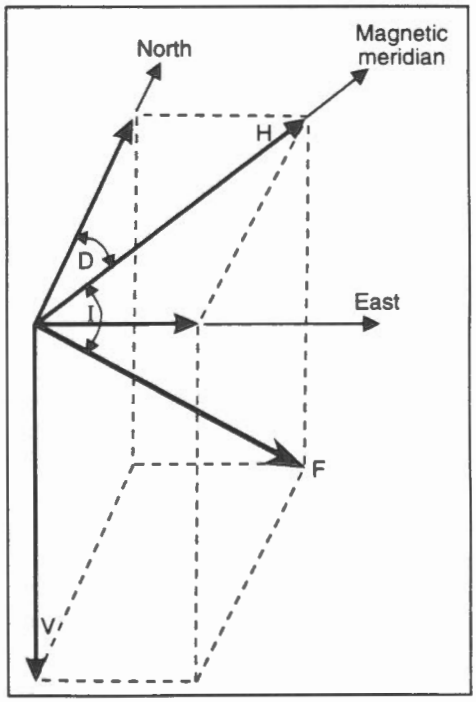

FIGURE 4

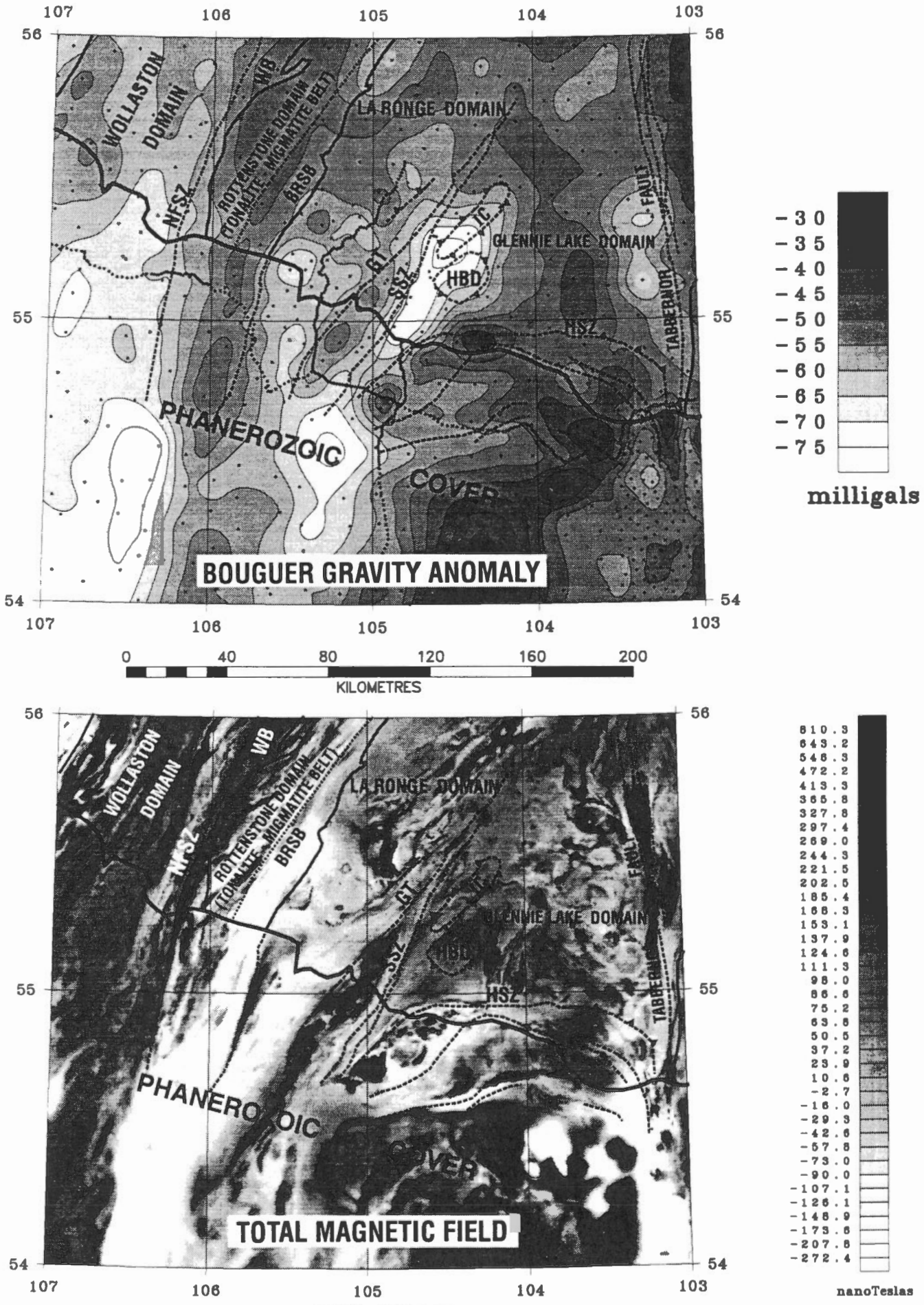
107
106
105
104
103
56
55
54
WOLLASTON DOMAIN
WB
ROTTENSTONE DOMAIN (TONALITE-MIGMATITE BELT)
BRSB
LA RONGE DOMAIN
NFSZ
GT
SSZ
IC
GLENNIE LAKE DOMAIN
HBD
HSZ
TABBERNOR FAULT
PHANEROZOIC COVER
BOUGUER GRAVITY ANOMALY
-30
-35
-40
-45
-50
-55
-60
-65
-70
-75
milligals
0
40
80
120
160
200
KILOMETRES
TOTAL MAGNETIC FIELD
810.3
643.2
546.3
472.2
413.3
365.8
327.8
297.4
269.0
244.3
221.5
202.5
185.4
168.3
153.1
137.9
124.6
111.3
98.0
86.6
75.2
63.8
50.5
37.2
23.9
10.6
-2.7
-16.0
-29.3
-42.6
-57.8
-73.0
-90.0
-107.1
-126.1
-148.9
-173.6
-207.8
-272.4
nanoTeslas

FIGURE 5

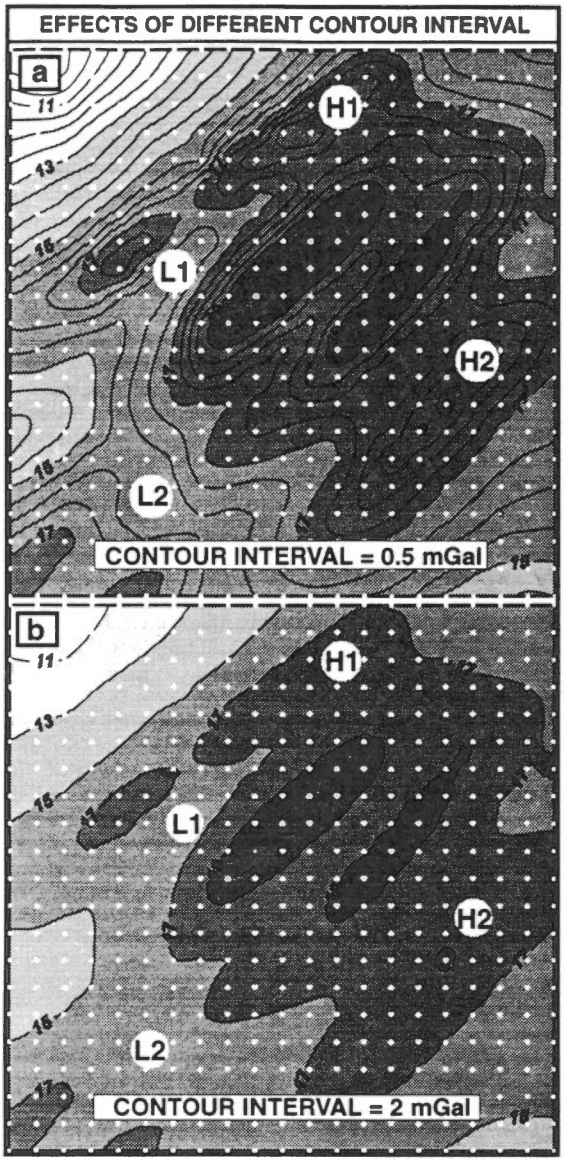

FIGURE 6

FIGURE 7

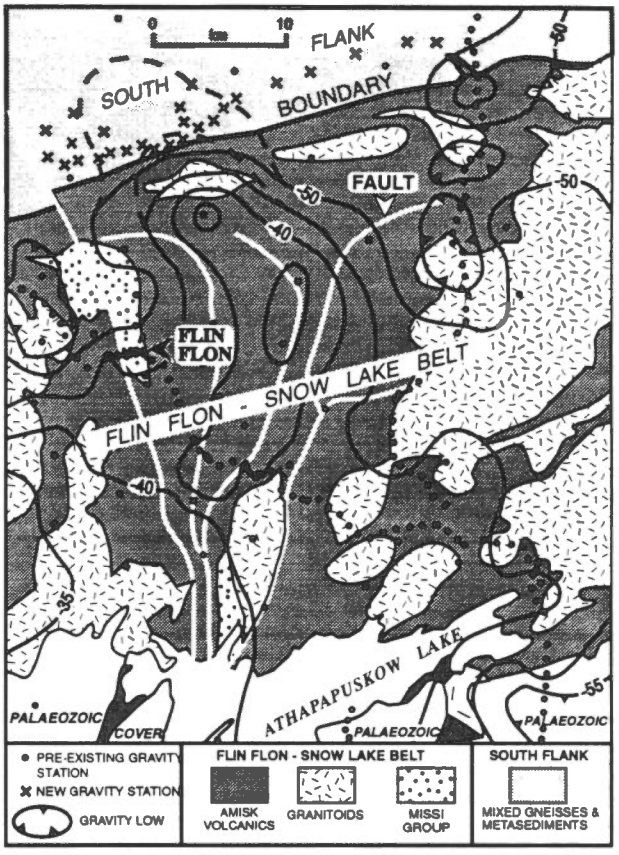

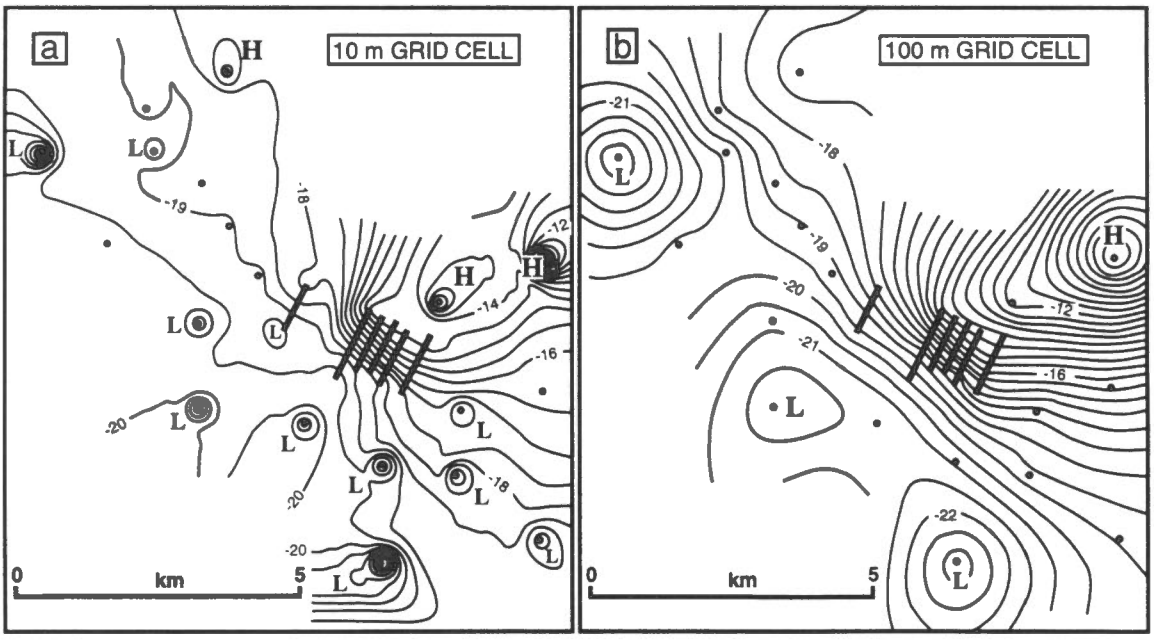

FIGURE 8

FIGURE 9

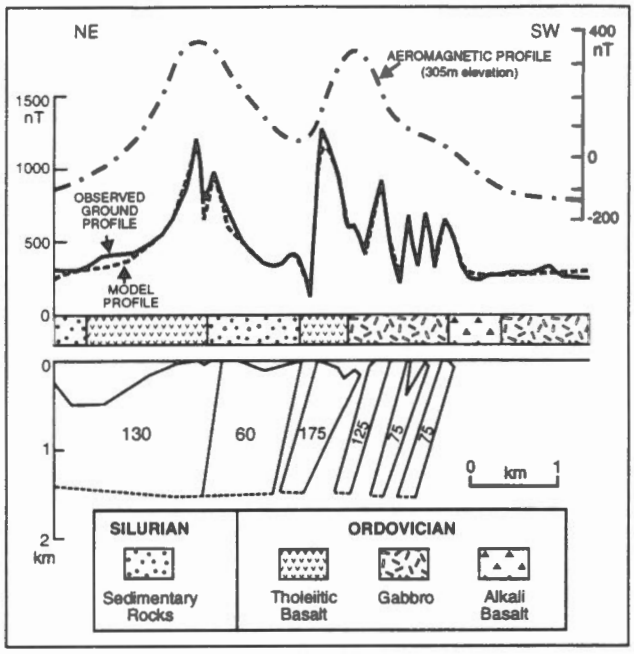

FIGURE 11

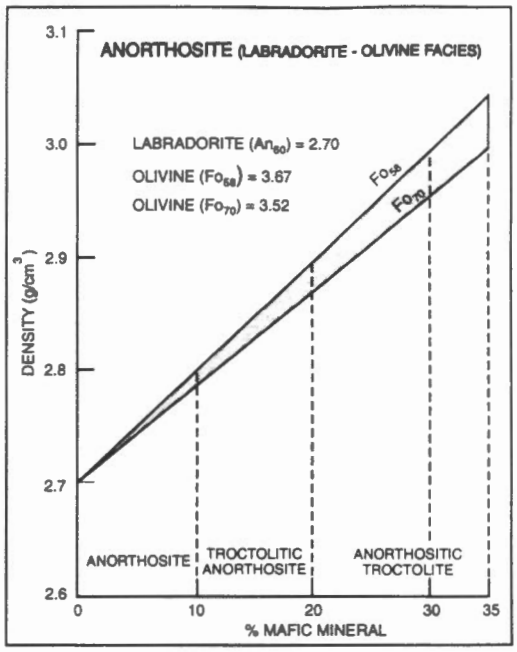

FIGURE 10

% QUARTZ	RATIO K FELDS TO TOTAL FELDSPAR	> 10% FELDSPAR			< 10% FELD.
		PLAGIOCLASE COMPOSITION			
		ALBITE AN_0 - AN_{10}	OLIGOCLASE AN_{10} - AN_{30}	ANDESINE AN_{30} - AN_{50}	LABRADORITE ETC. AN_{50} - AN_{100}	
> 10%	> 2/3	GRANITE *RHYOLITE*			
	1/3 - 2/3	QUARTZ MONZONITE (ADAMELLITE) *QUARTZ LATITE*			
	< 1/3	GRANODIORITE *QUARTZ LATITE*		QTZ DIORITE (TONALITE) *DACITE*	QTZ GABBRO *QTZ BASALT*	
< 10%	> 2/3	SYENITE *TRACHYTE*				PERIDOTITE PYROXENITE HORNBLENDE
	1/3 - 2/3	MONZONITE *LATITE*				
	< 1/3	SYENODIORITE *LATITE*		DIORITE *LATITE*	GABBRO *BASALT*	
		0 - 10		10 - 40	40 - 70	70 - 100
		% MAFIC MINERALS				

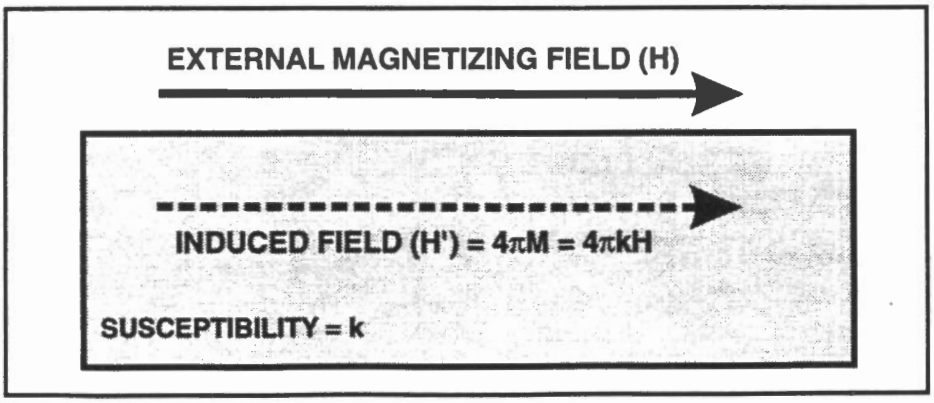

FIGURE 12

FIGURE 13

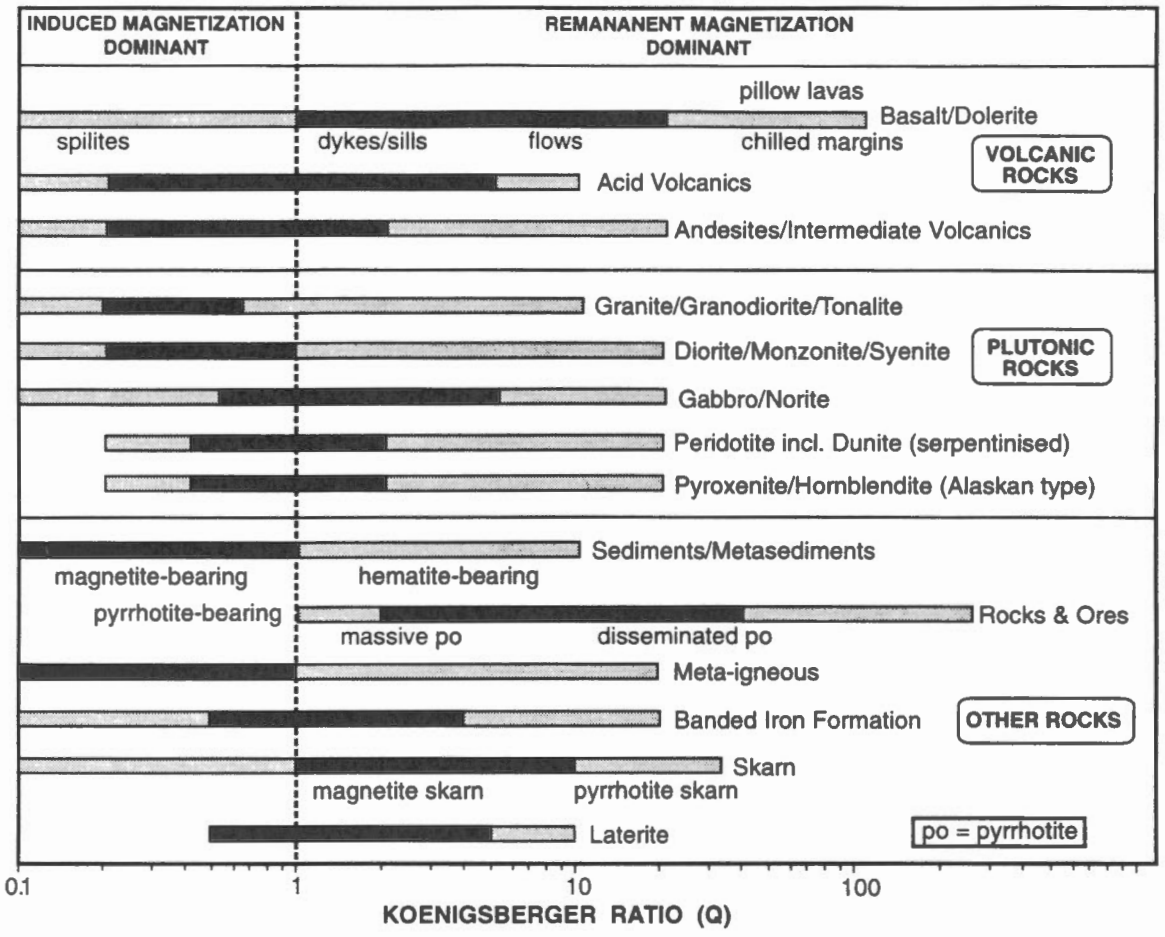

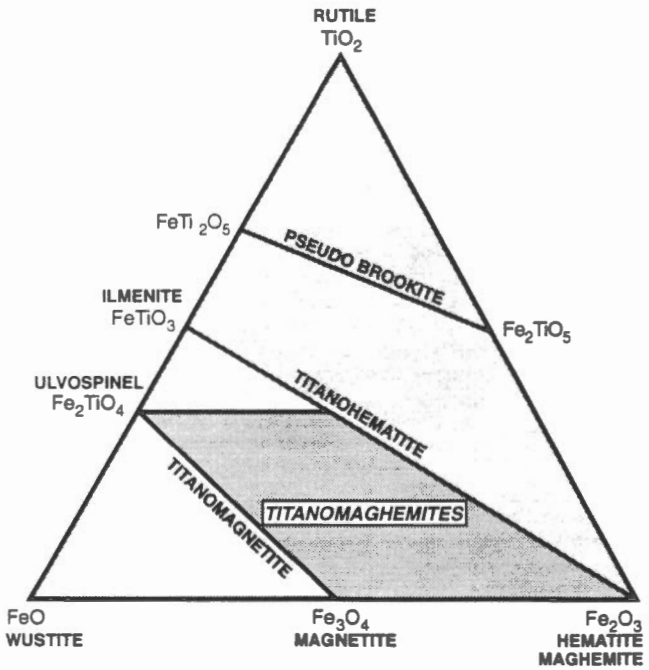

FIGURE 14

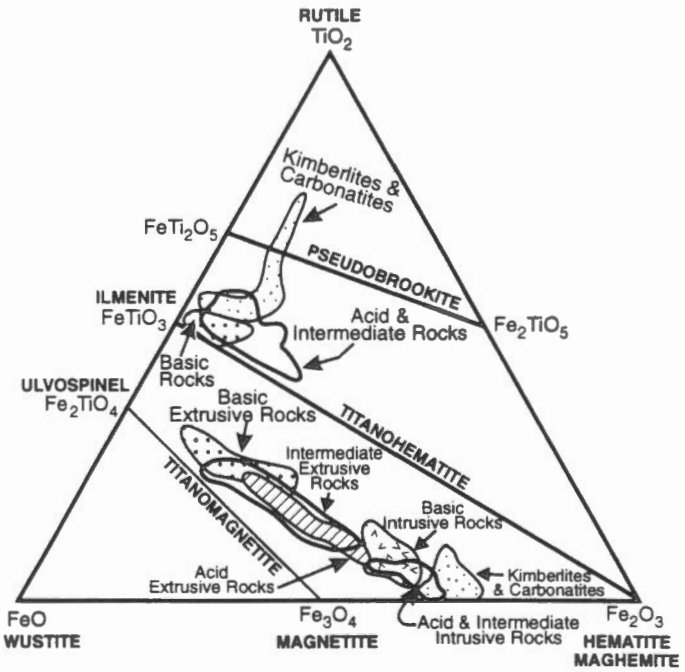

FIGURE 15

FIGURE 16

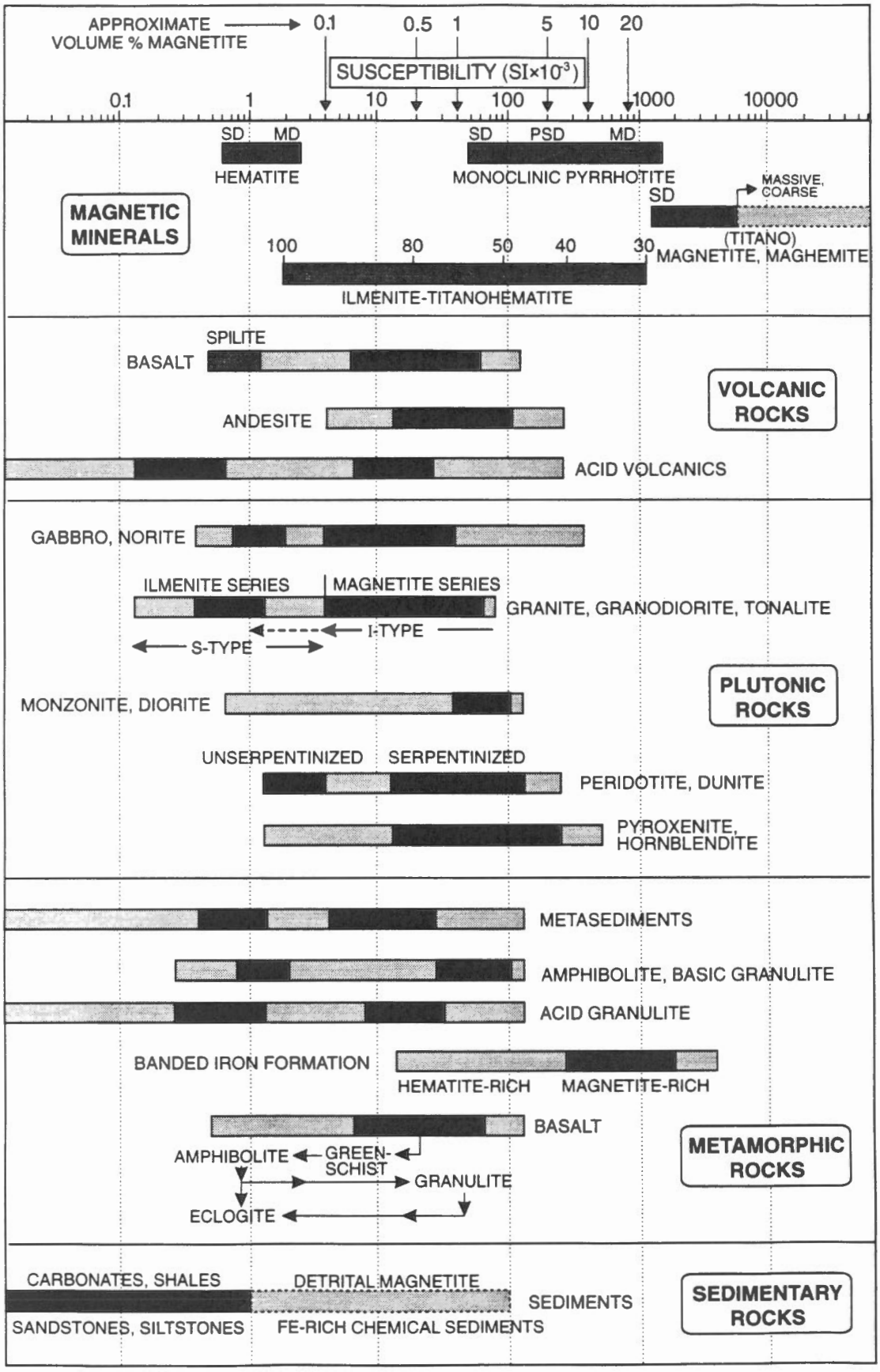
APPROXIMATE VOLUME % MAGNETITE
0.1
0.5
1
5
10
20
SUSCEPTIBILITY (SI×10³)
0.1
1
10
100
1000
10000
SD
MD
HEMATITE
SD
PSD
MD
MONOCLINIC PYRRHOTITE
SD
MASSIVE, COARSE
(TITANO) MAGNETITE, MAGHEMITE
MAGNETIC MINERALS
100
80
50
40
30
ILMENITE-TITANOHEMATITE
SPILITE
BASALT
ANDESITE
VOLCANIC ROCKS
ACID VOLCANICS
GABBRO, NORITE
ILMENITE SERIES
MAGNETITE SERIES
GRANITE, GRANODIORITE, TONALITE
I-TYPE
S-TYPE
PLUTONIC ROCKS
MONZONITE, DIORITE
UNSERPENTINIZED
SERPENTINIZED
PERIDOTITE, DUNITE
PYROXENITE, HORNBLENDITE
METASEDIMENTS
AMPHIBOLITE, BASIC GRANULITE
ACID GRANULITE
BANDED IRON FORMATION
HEMATITE-RICH
MAGNETITE-RICH
BASALT
AMPHIBOLITE
GREEN-SCHIST
GRANULITE
ECLOGITE
METAMORPHIC ROCKS
CARBONATES, SHALES
DETRITAL MAGNETITE
SEDIMENTS
SANDSTONES, SILTSTONES
FE-RICH CHEMICAL SEDIMENTS
SEDIMENTARY ROCKS

FIGURE 17

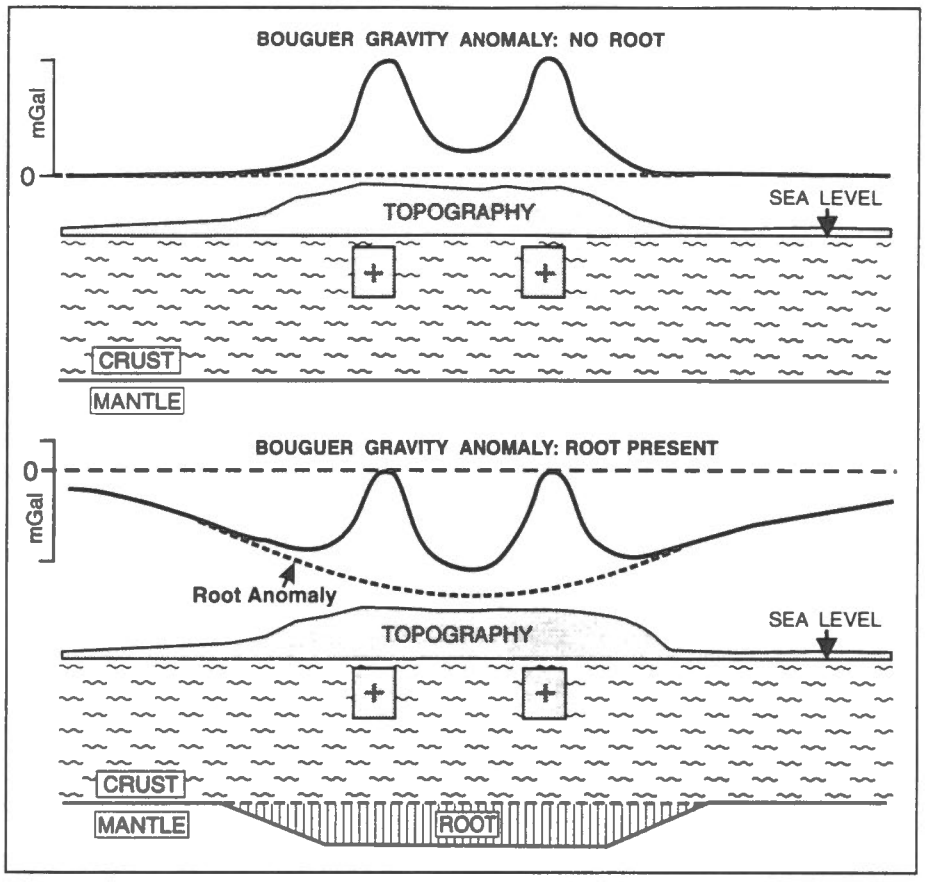

FIGURE 18

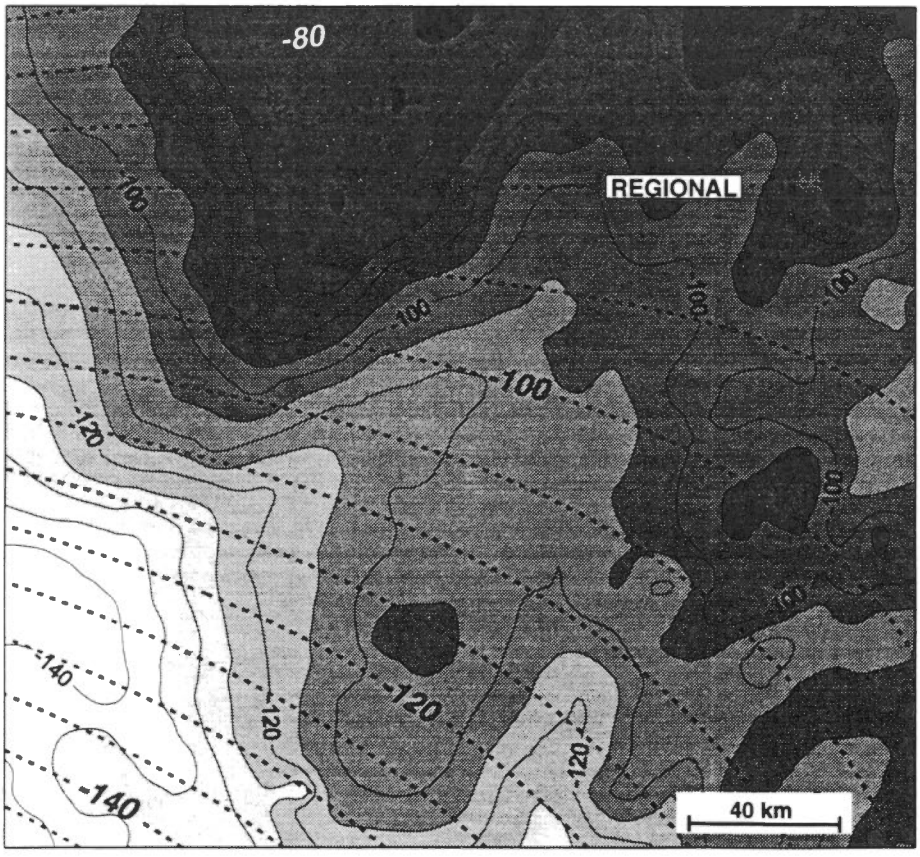

FIGURE 19

ISOSTATIC GRAVITY ANOMALY MAP

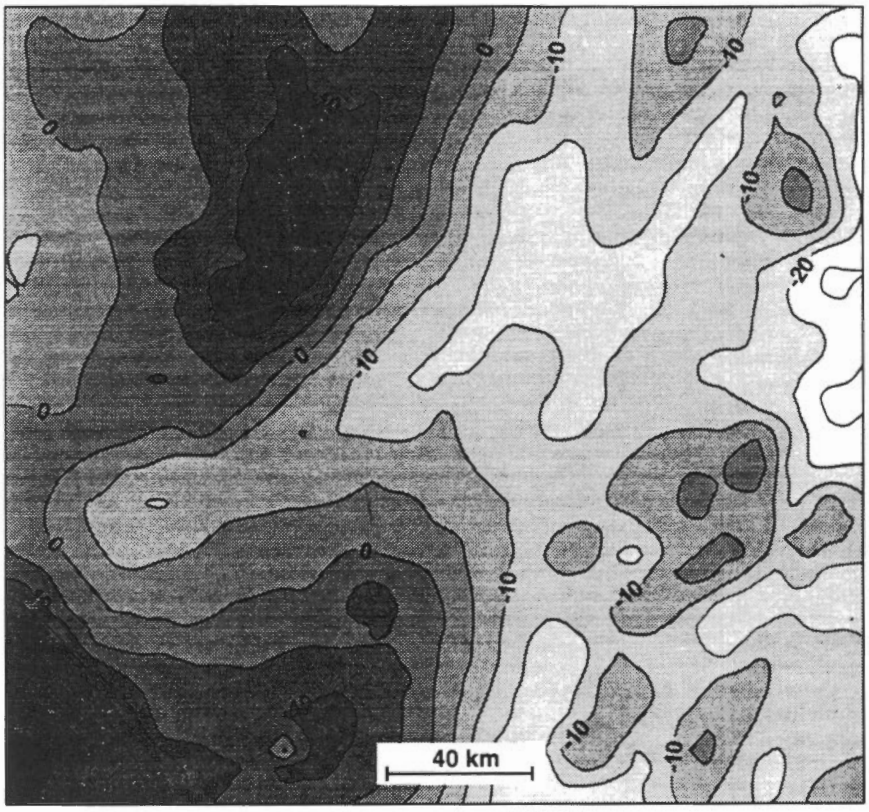

FIGURE 20

RESIDUAL BOUGUER ANOMALY MAP

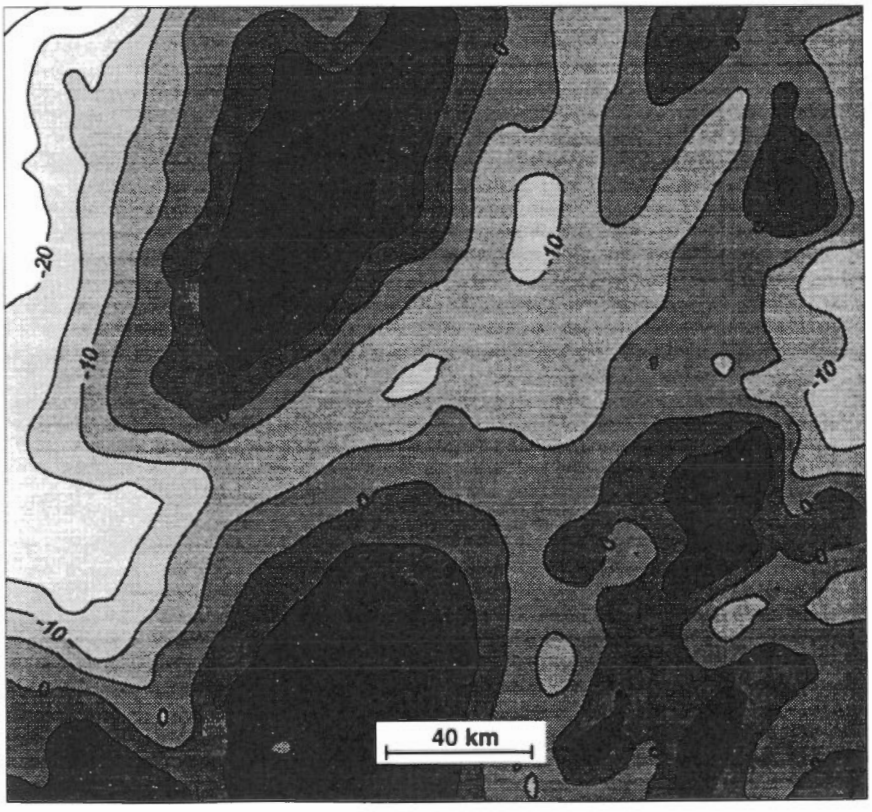

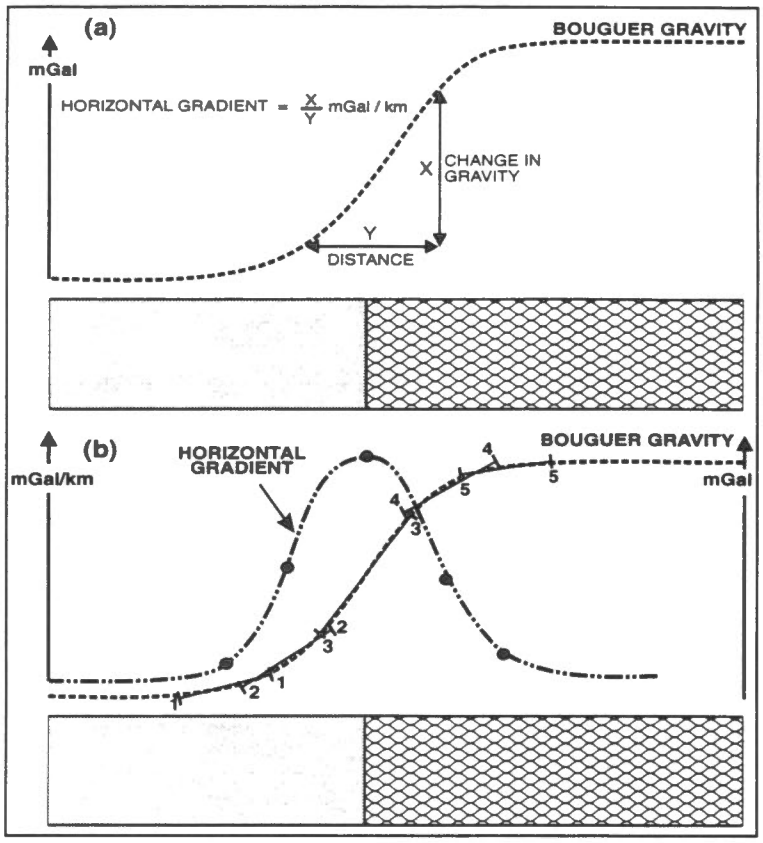

FIGURE 21

FIGURE 22

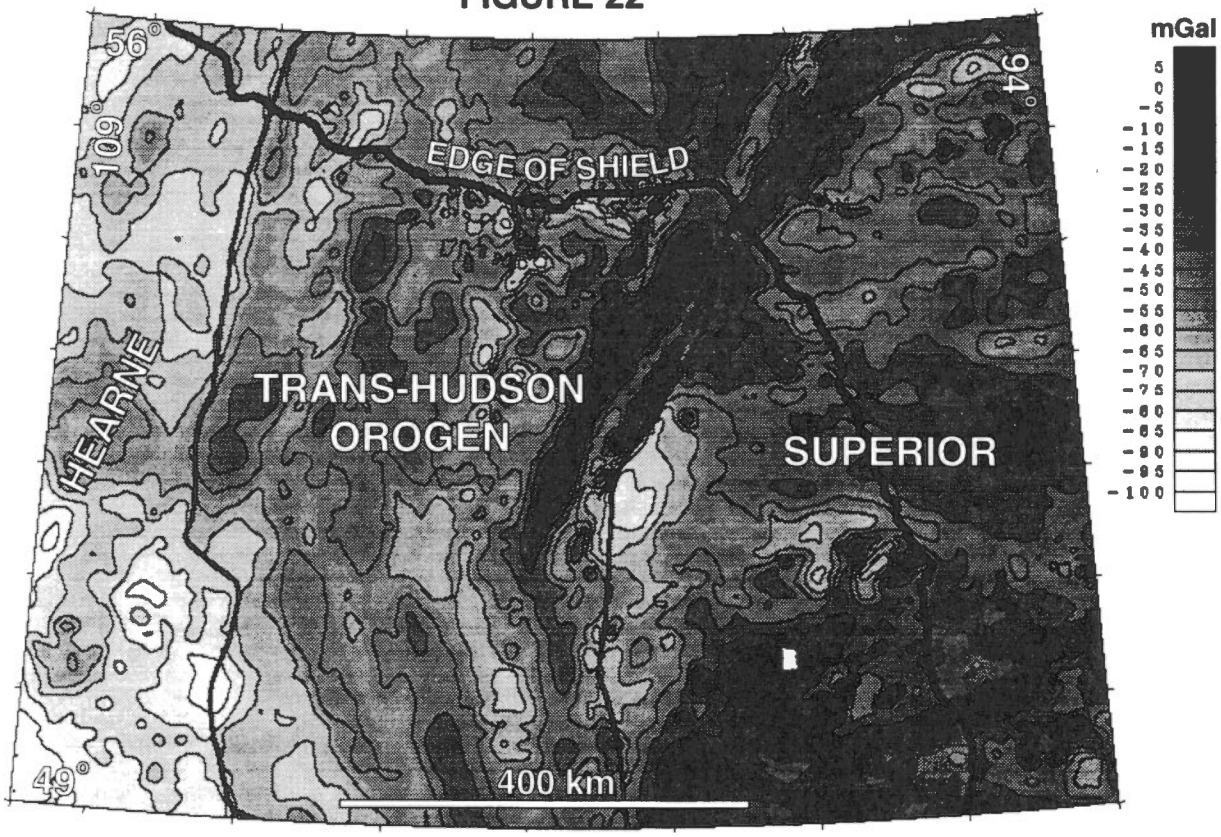

FIGURE 23

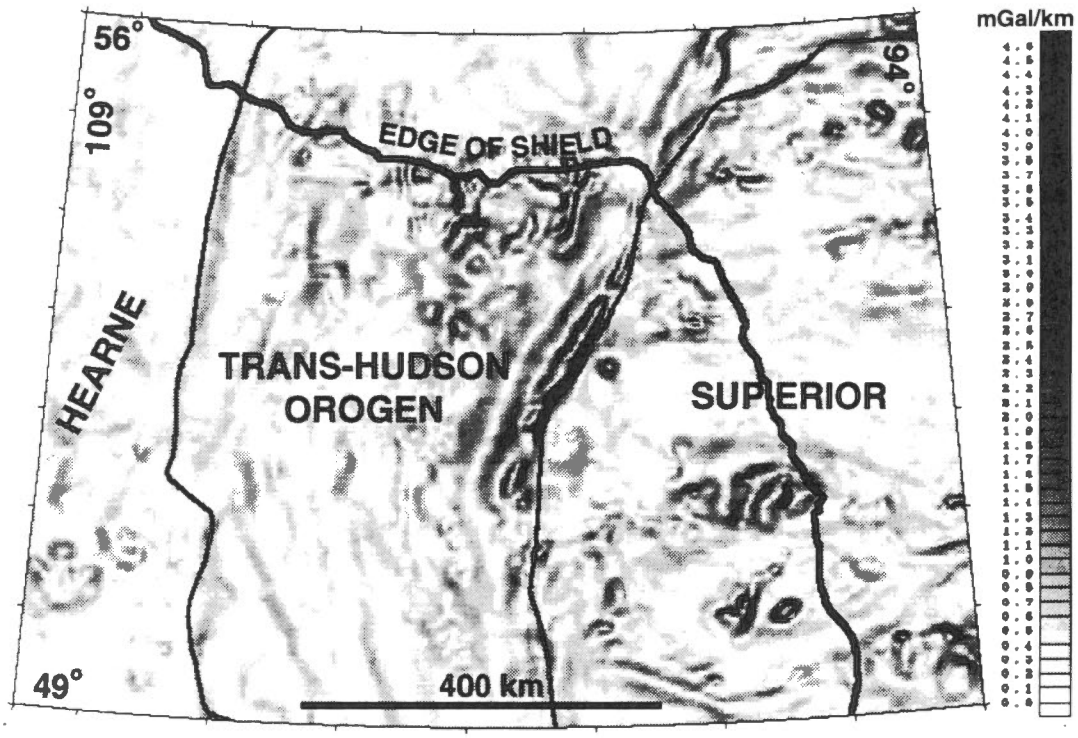

FIGURE 24

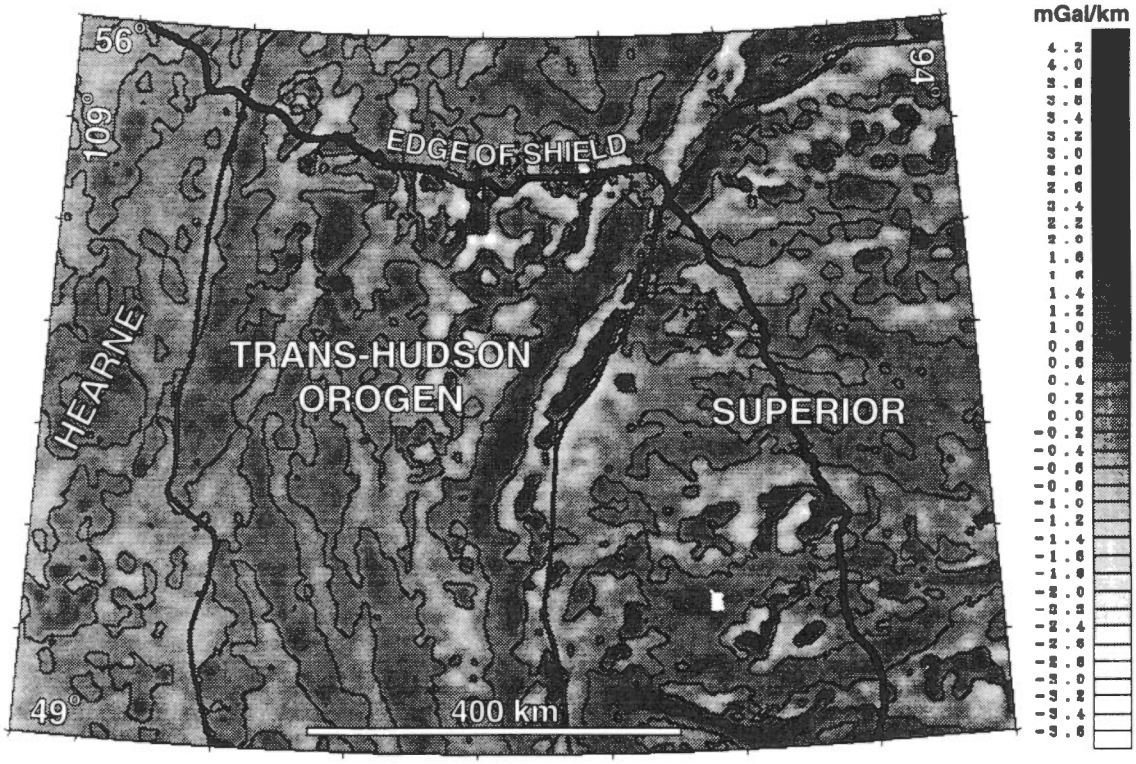

FIGURE 25

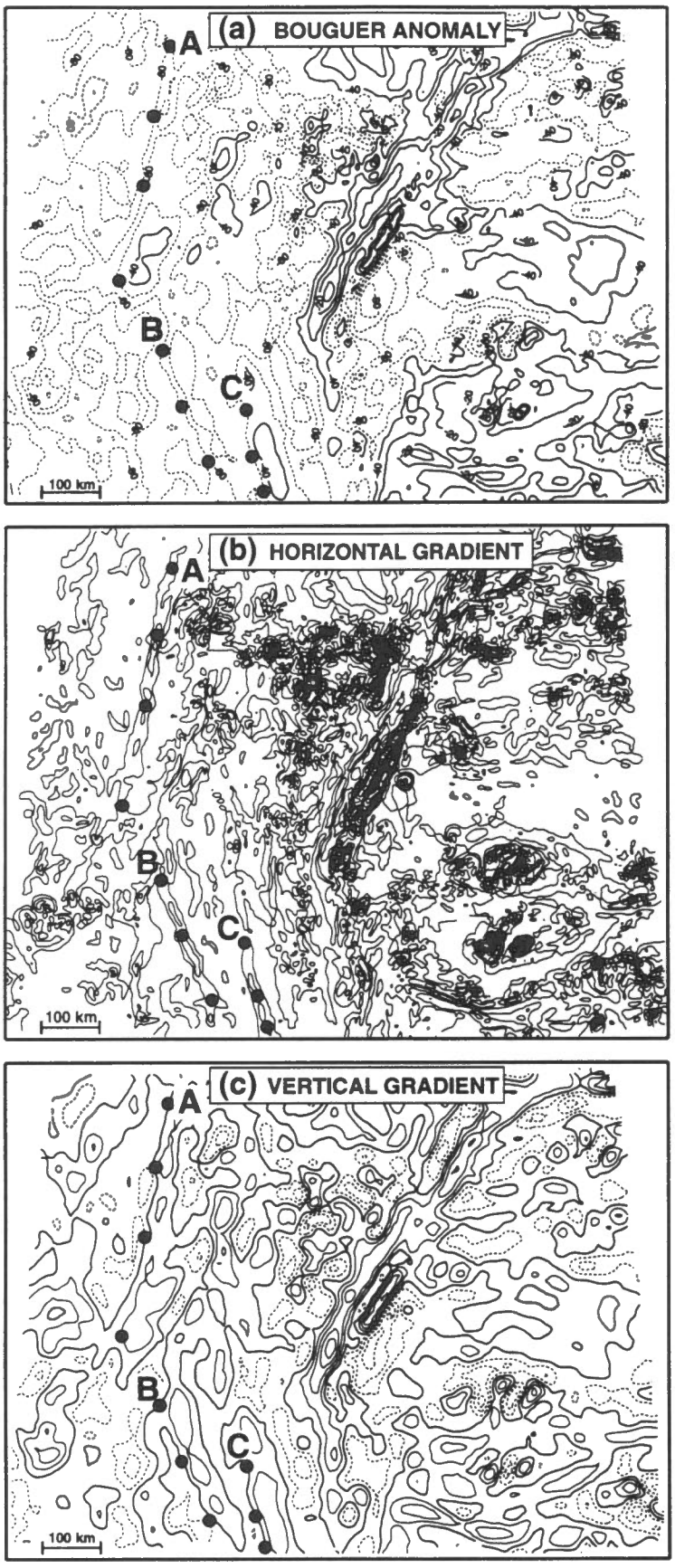

FIGURE 26

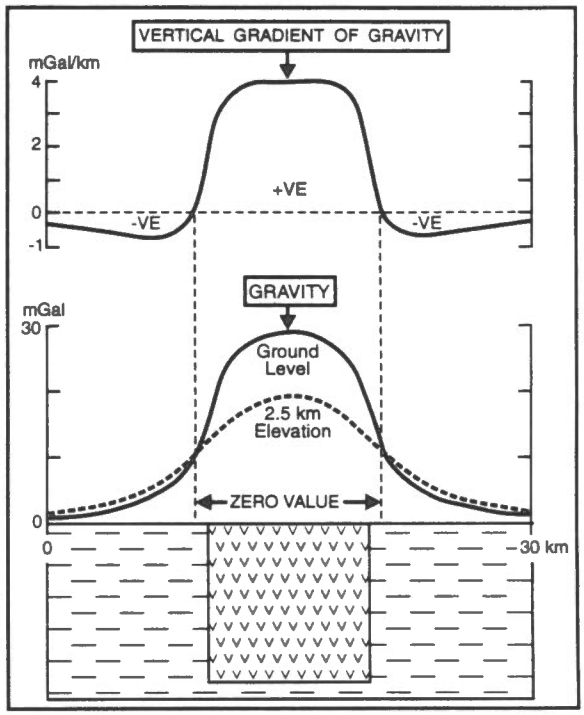

FIGURE 27

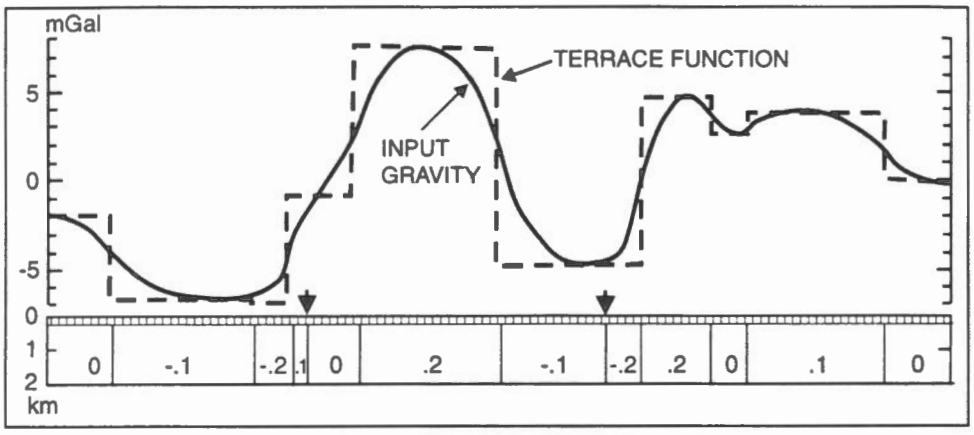

FIGURE 28

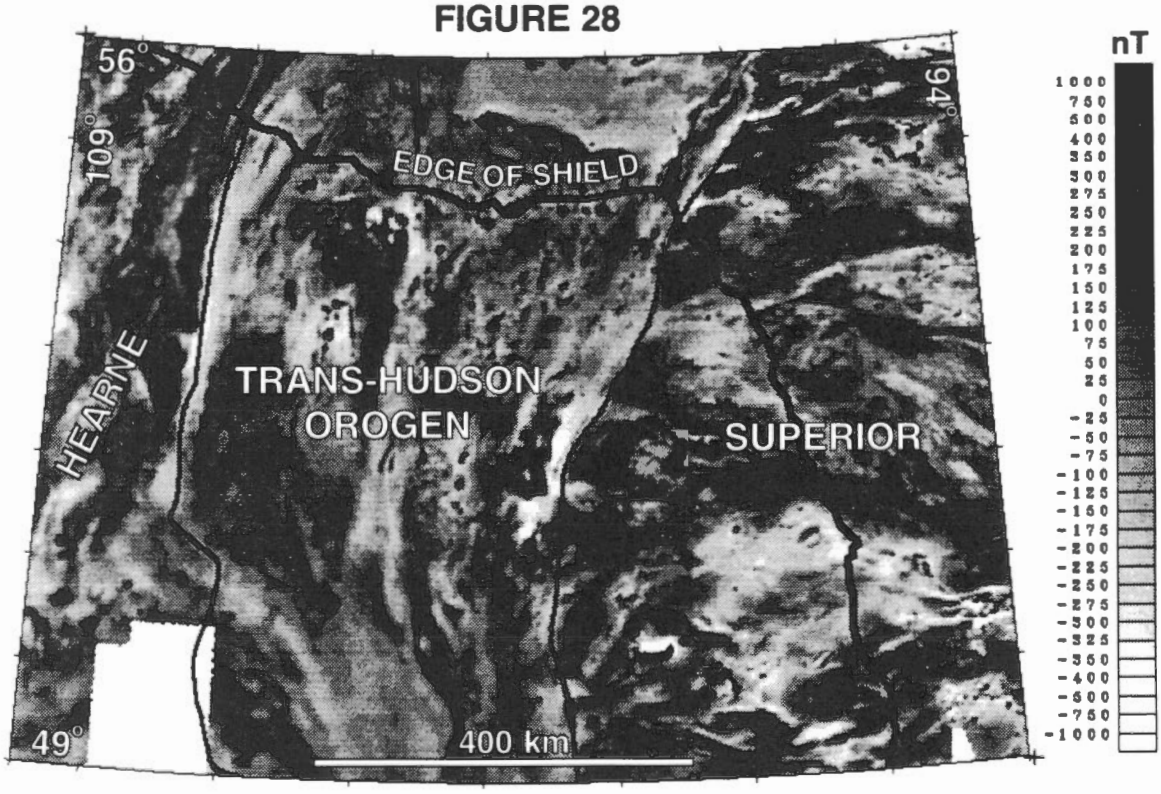

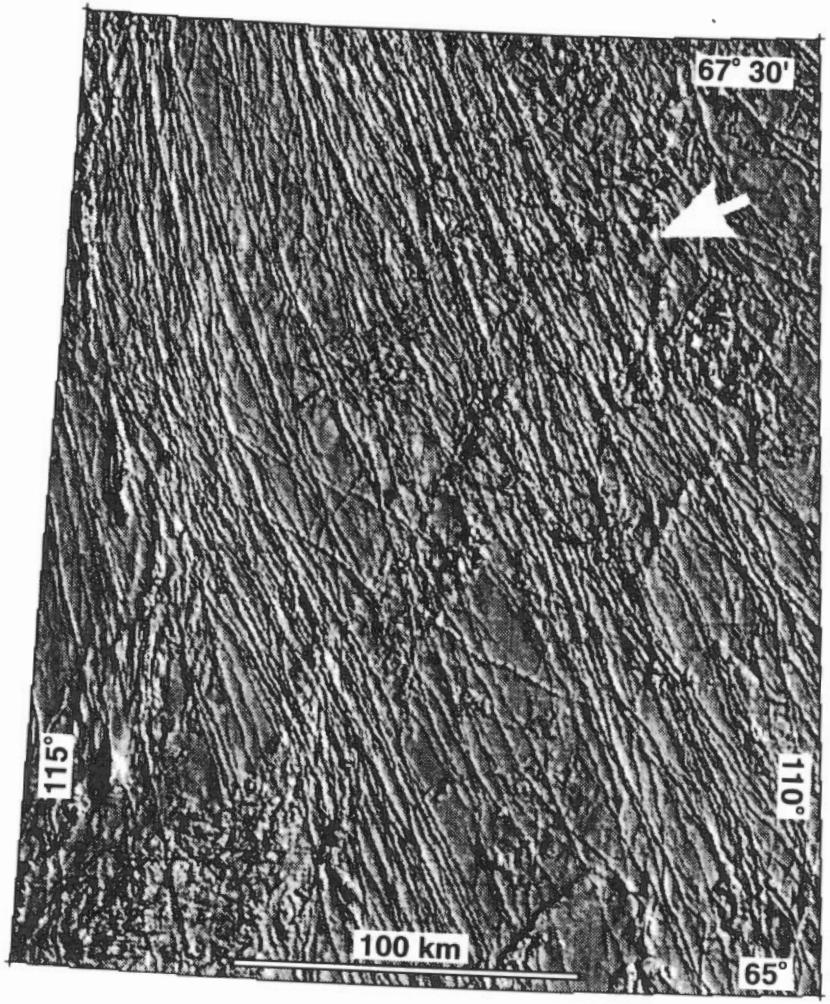

FIGURE 29

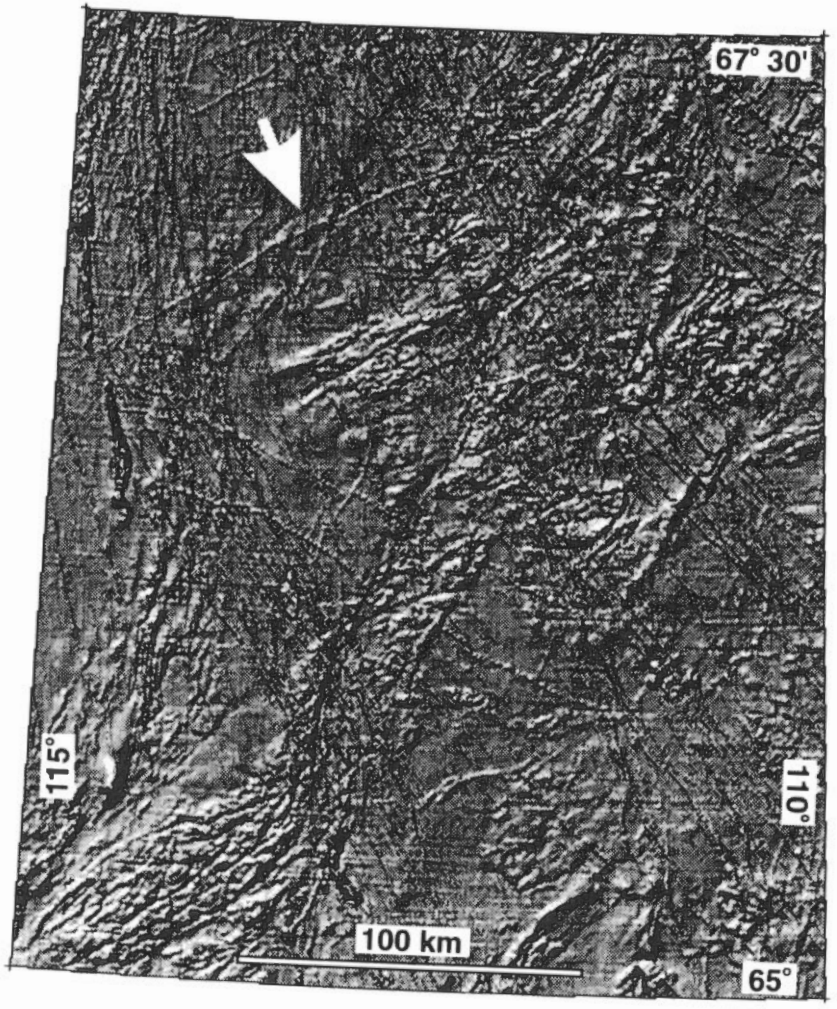

FIGURE 30

FIGURE 31

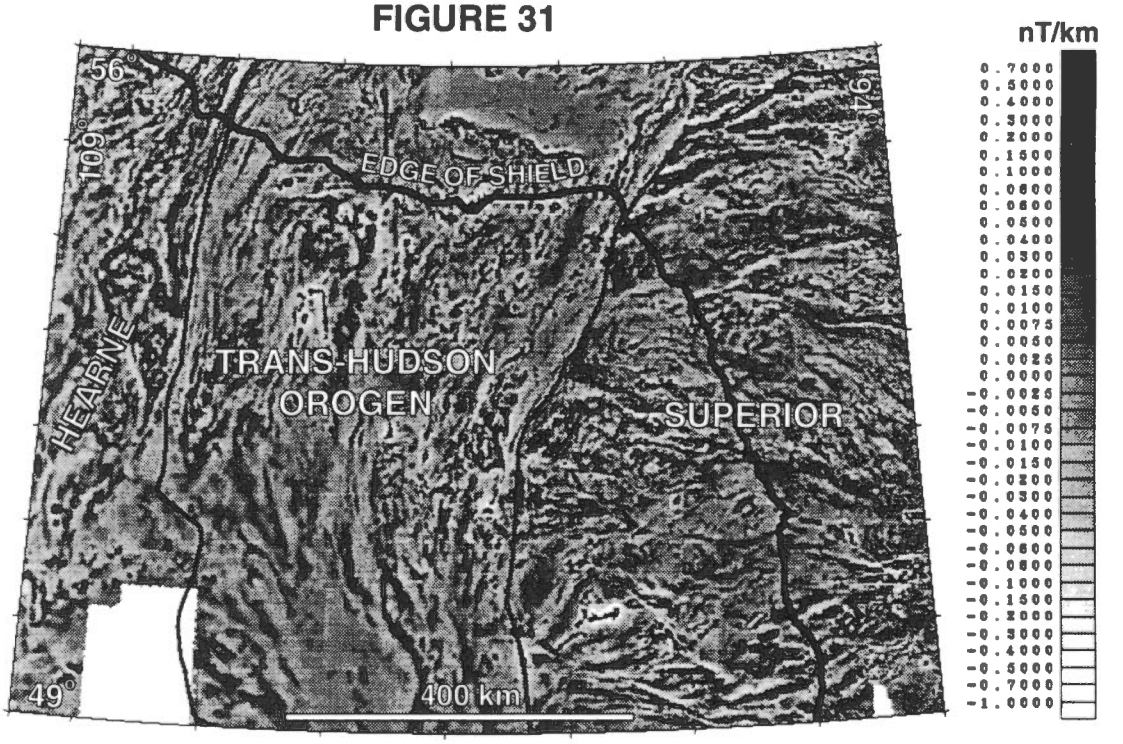

FIGURE 32

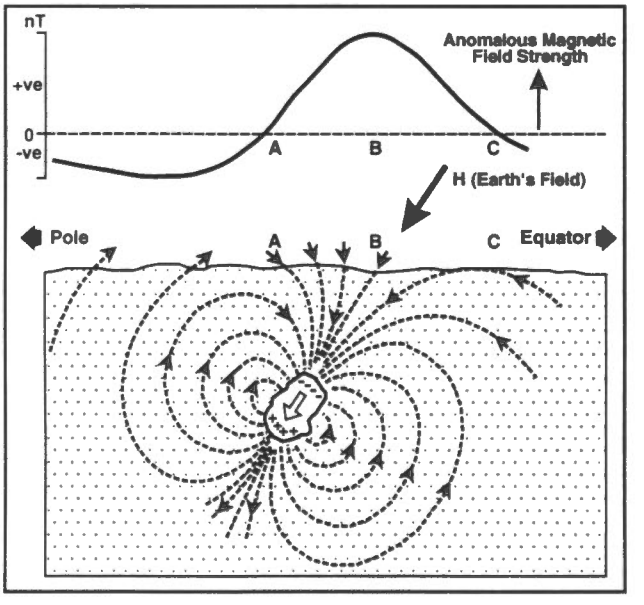

FIGURE 33

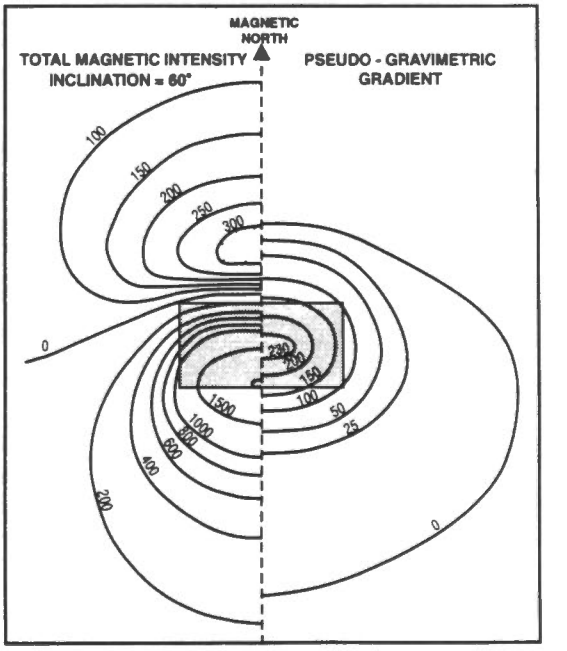

FIGURE 34

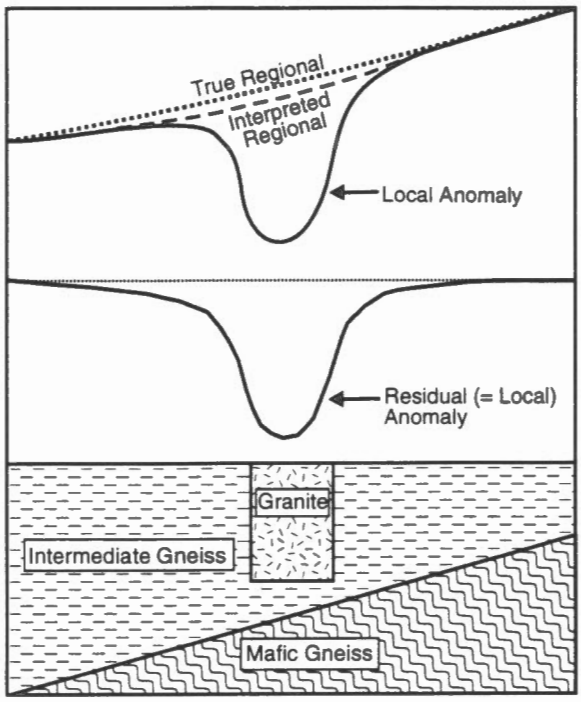

FIGURE 35

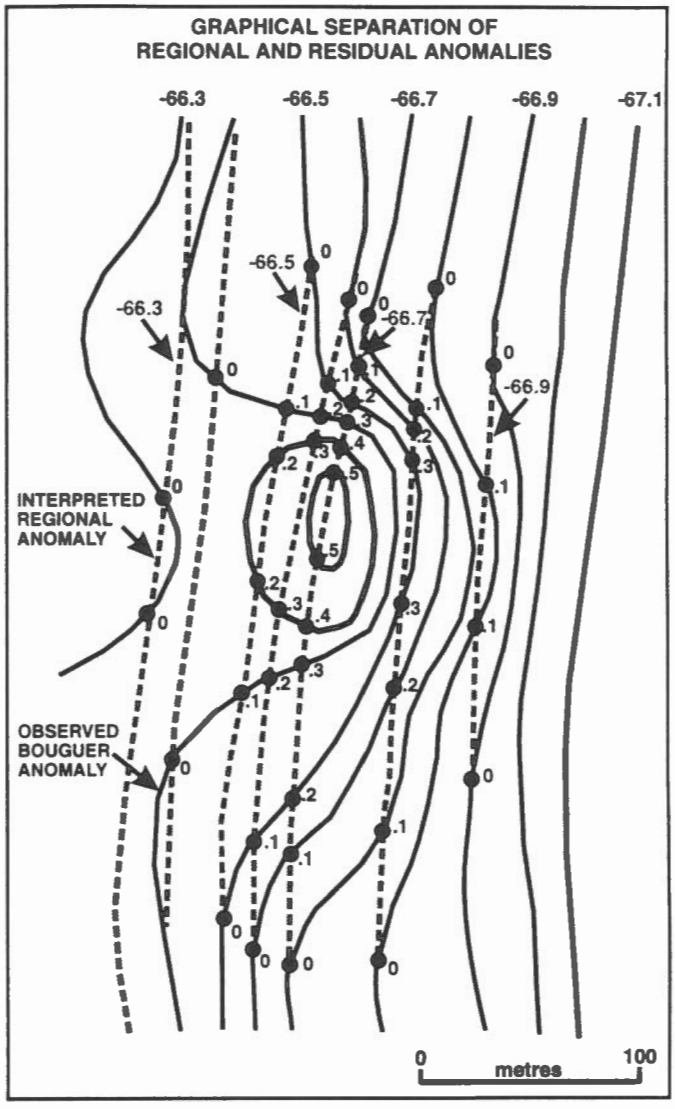

FIGURE 36

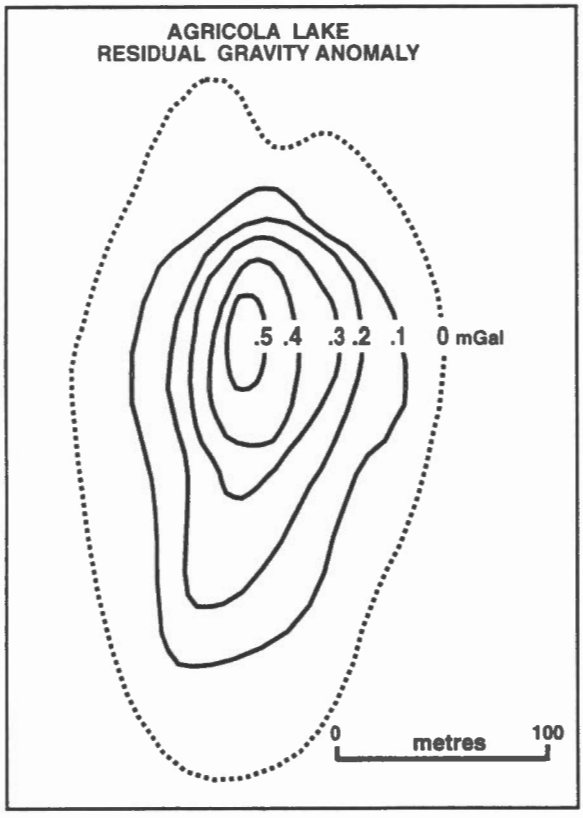

FIGURE 37

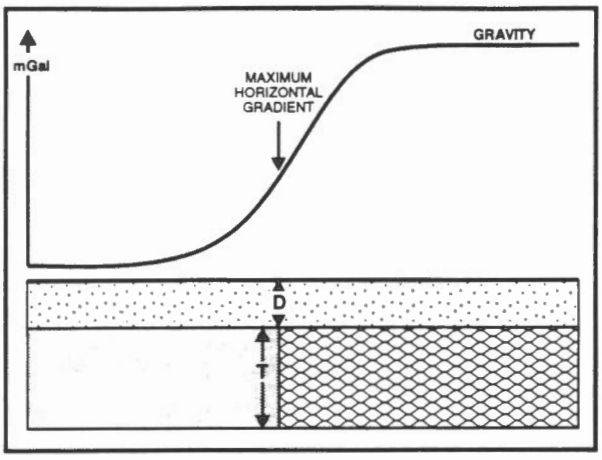

FIGURE 38

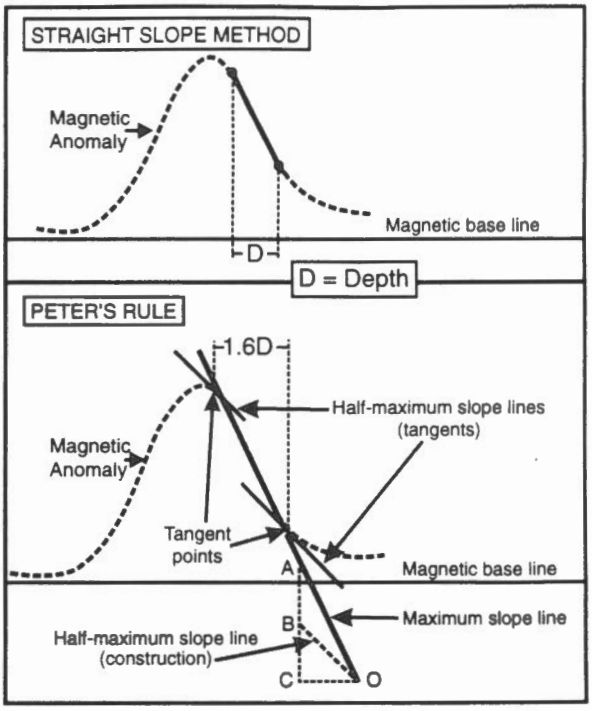

FIGURE 39

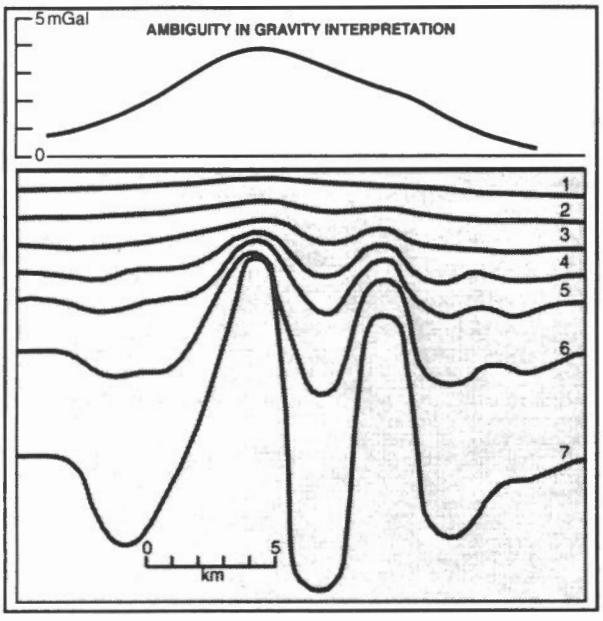

FIGURE 40

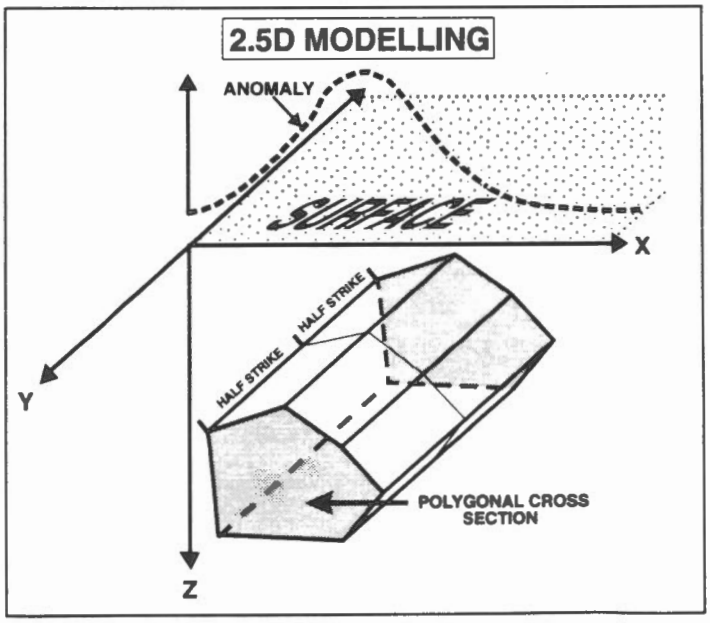

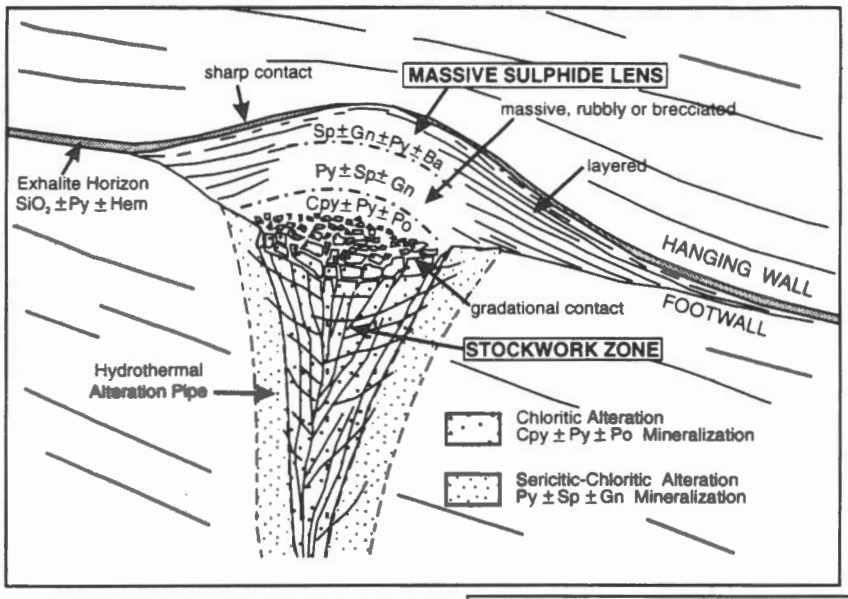

FIGURE 41

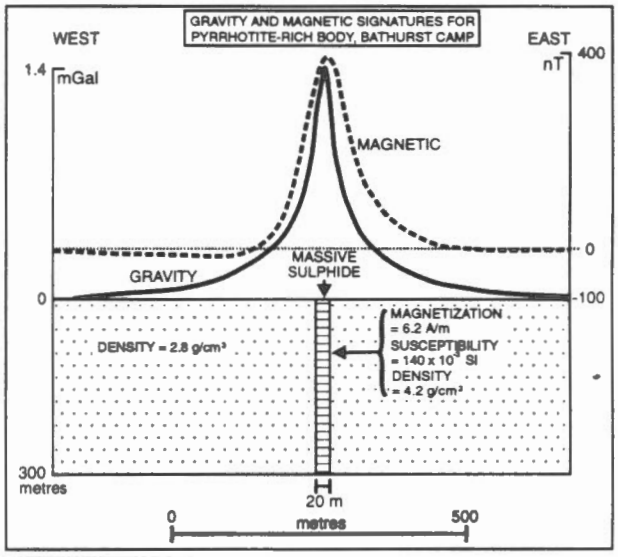

FIGURE 42

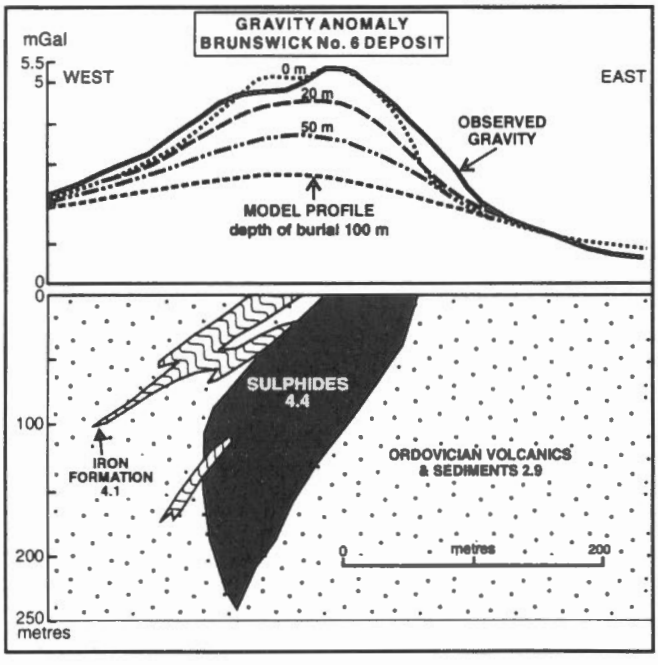

FIGURE 43

FIGURE 44

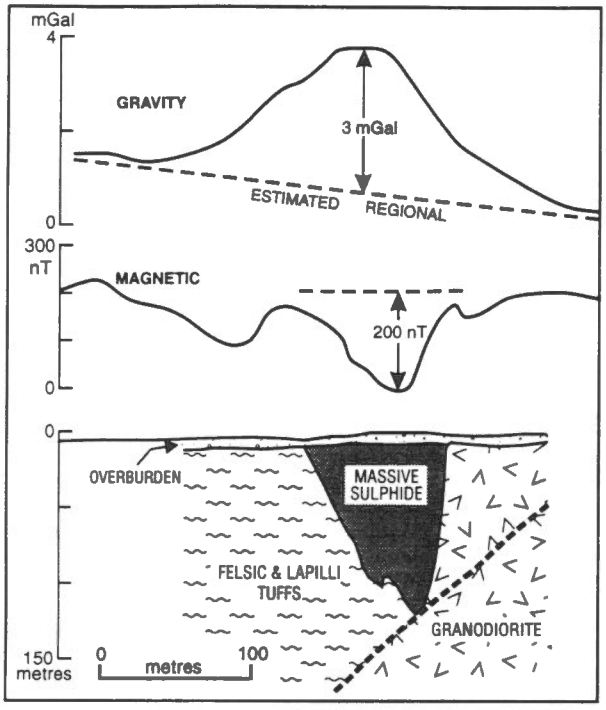

FIGURE 45

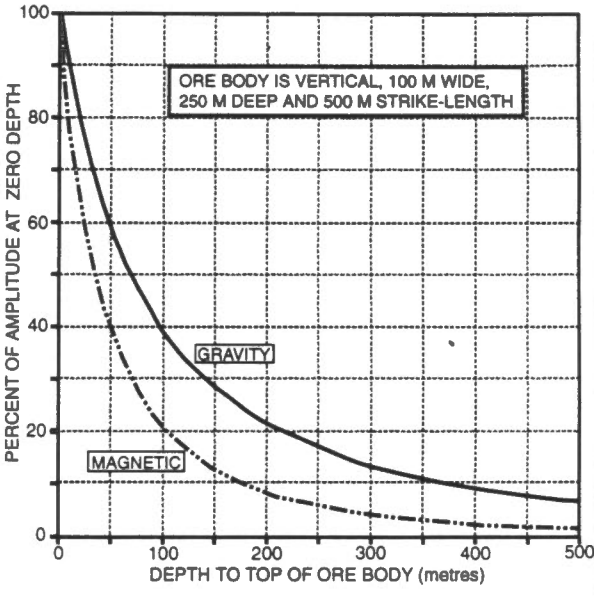

FIGURE 46

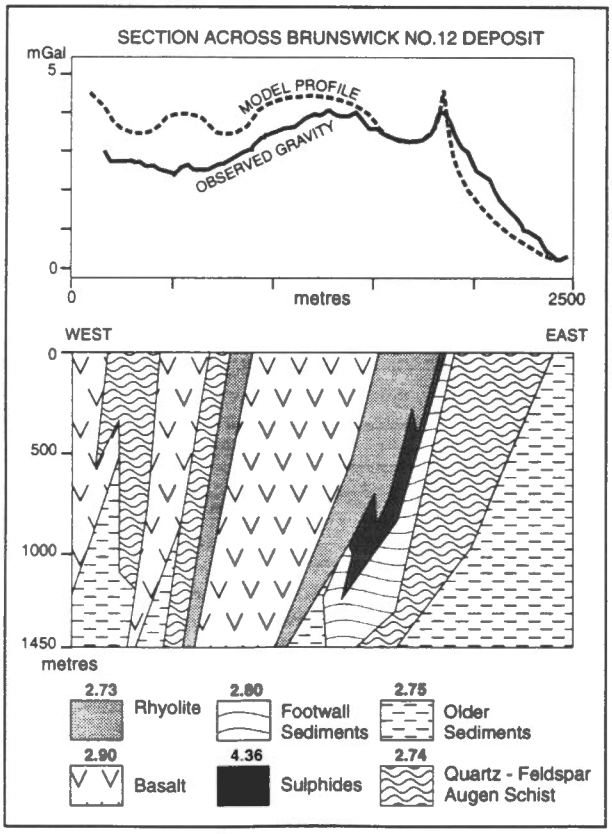

FIGURE 47

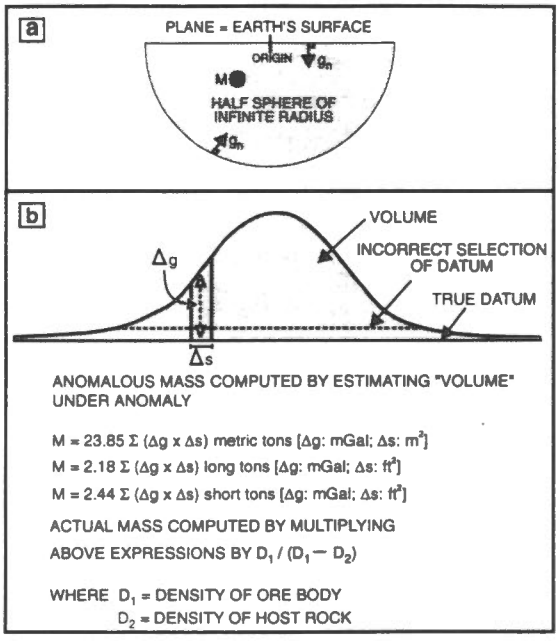

FIGURE 48

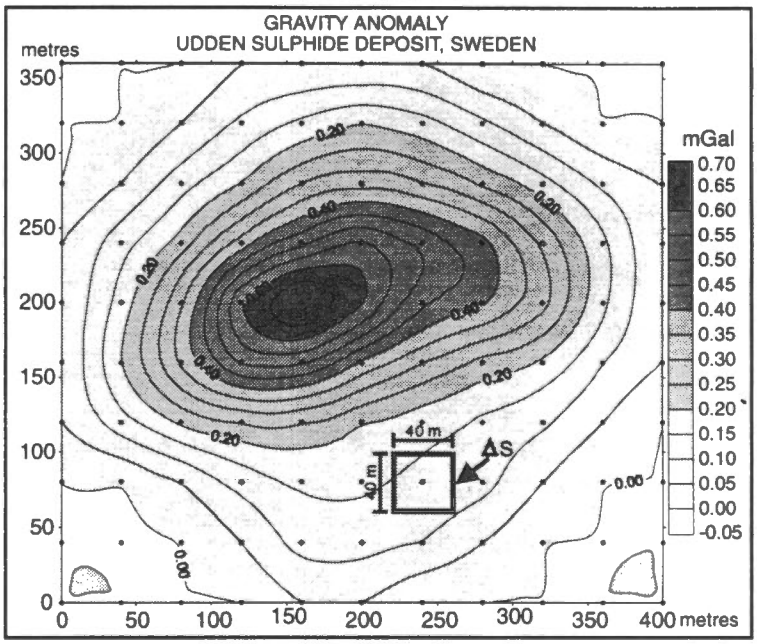

FIGURE 49

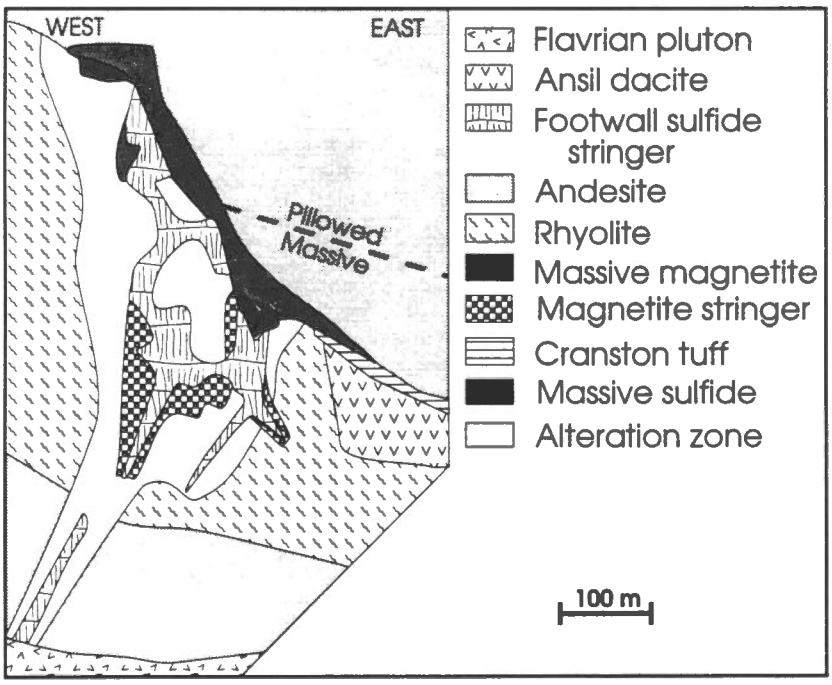

FIGURE 50

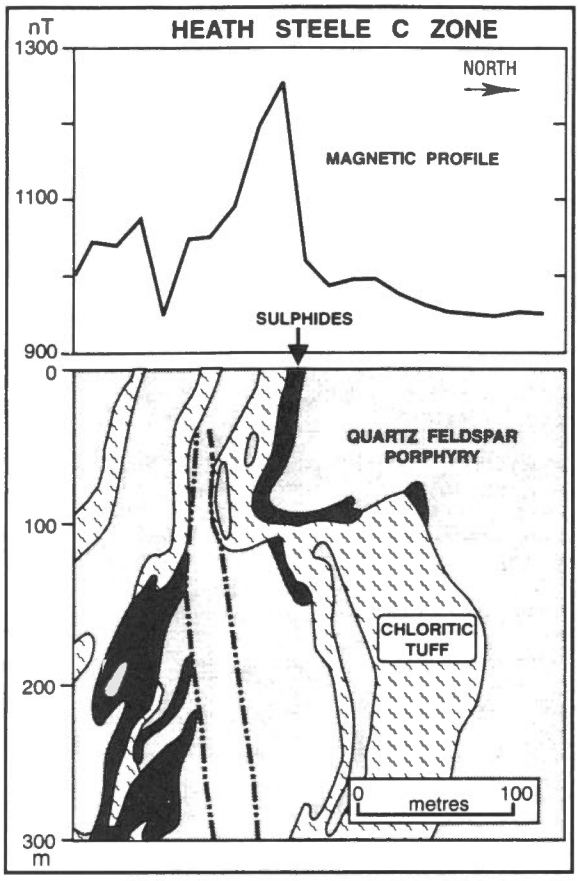

FIGURE 51

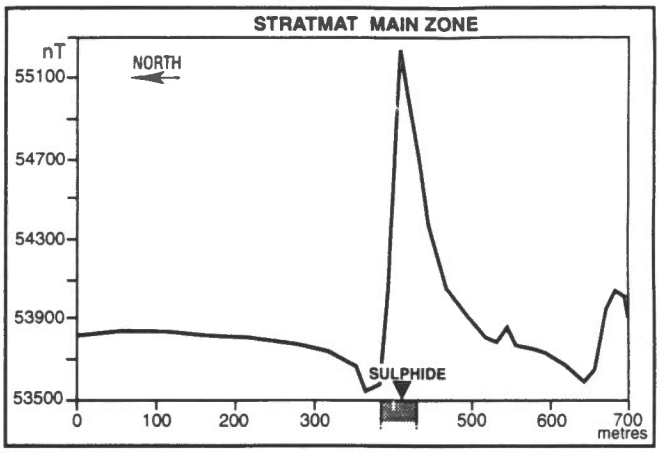

FIGURE 53

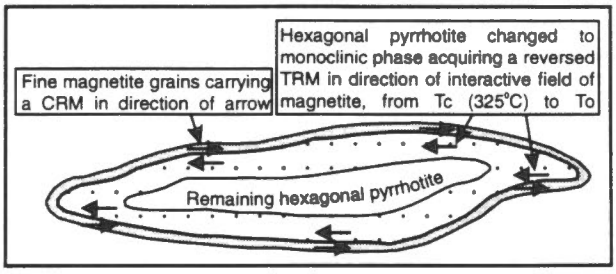

FIGURE 52

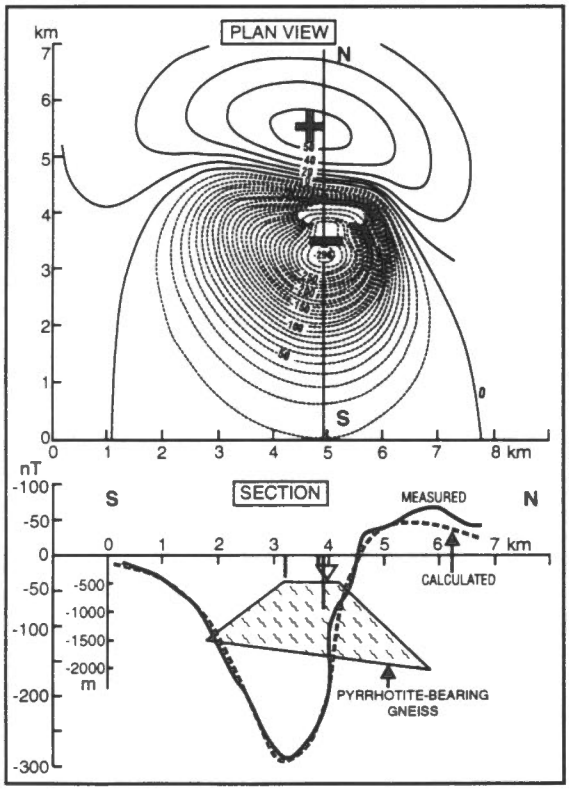

FIGURE 54

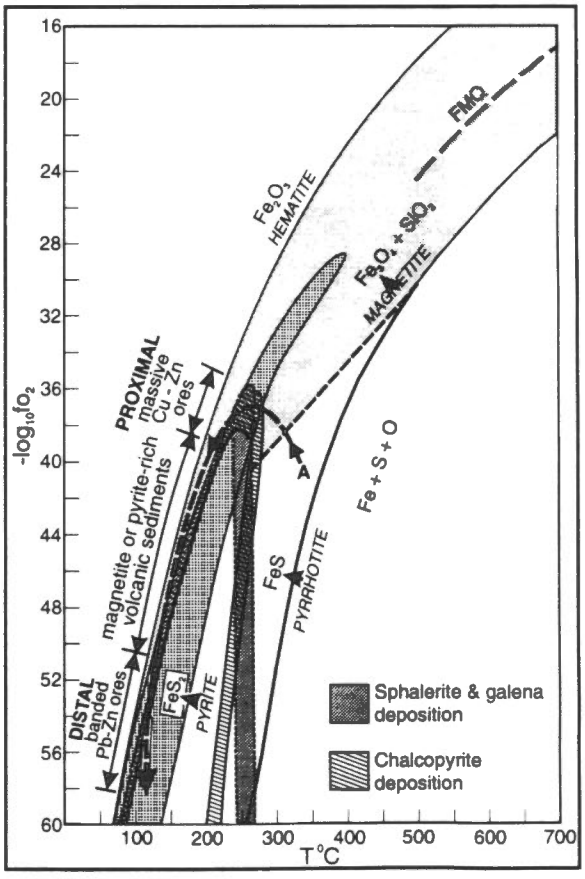

FIGURE 55

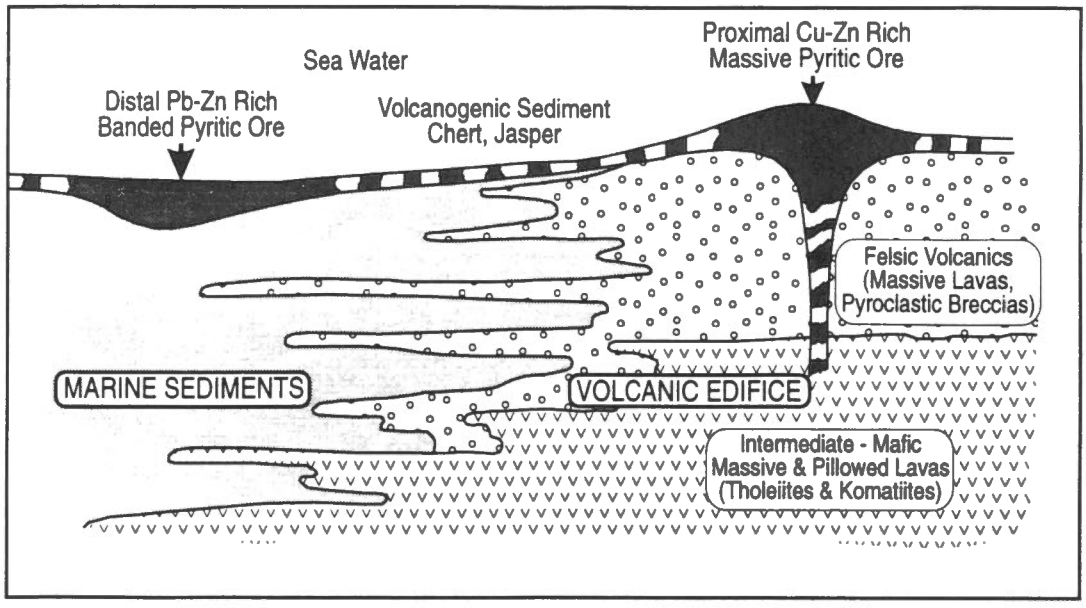

FIGURE 56

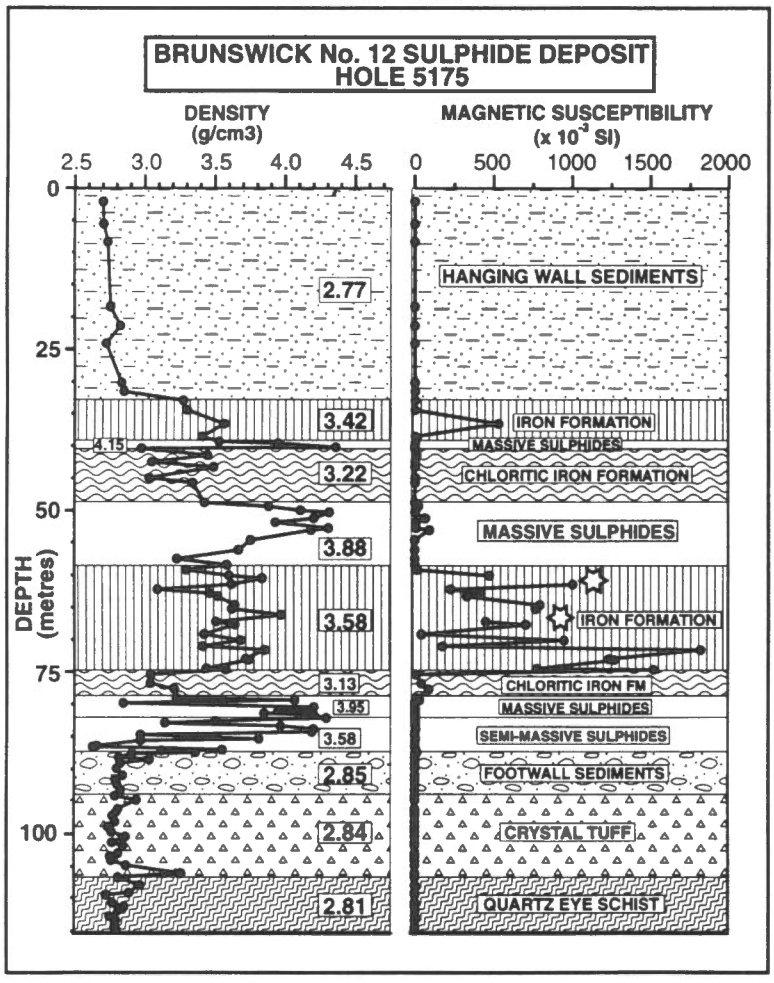

FIGURE 57